UNIVERSITA' degli STUDI di TRIESTE

XXVI Ciclo del Dottorato di Ricerca in Scienze e Tecnologie Chimiche e Farmaceutiche

PhD in Chemical and Pharmaceutical Sciences and Technologies

Three-dimensional devices based on biopolymers and carbon nanotubes for tissue regeneration

Settore scientifico-disciplinare CHIM/06

PhD student
Michela Cok

PhD School Director
Chiar.mo Prof. Mauro Stener

Thesis supervisor
Chiar.mo Prof. Maurizio Prato

Thesis co-supervisor
Dott.ssa Susanna Bosi

Academic year 2012/2013

Index

List of abbreviations

°C	Degree Celsius
µm	Micrometer
A	Ampere
a.a.	Amminoacid
AcOEt	Ethyl acetate
Alg	Sodium alginate
aq	Aqueous
Boc	Tert-buthylcarbonil
CH_2Cl_2	Dichloromethane
cm	Centimeters
CNSs	Carbon nanostructures
CNTs	Carbon nanotubes
f-CNTs	Functionalized carbon nanotubes
CS	Chitosan
DMF	Dimethylformamide
DRG	Dorsal root ganglia
ECM	Extracellular matrix
Et_2O	Diethyl ether
EtOH	Ethanol
HAp	Hydroxyapatite
HA	Hyaluronic acid
H_2O	Water

H_2SO_4	Sulfuric acid
HCl	Hydrochloric acid
HNO_3	Nitric acid
ISISA	Ice segregation induced self assembly
LbL	Layer by layer
MeOH	Methanol
min	Minutes
mm	Millimeter
MWNTs	Multi-walled carbon nanotubes
SWNTs	Single-walled carbon nanotubes
N2	Nitrogen
nm	Nanometer
NMR	Nuclear magnetic resonance
PSCs	Spontaneous synaptic currents
PDMS	Polydimethyl siloxane
R	Resistance
r.t.	Room temperature
SEM	Scanning electron microscopy
TEM	Transmission electron microscopy
TGA	Thermogravimetric analysis
T_2	Transverse relaxation time
UV-vis-NIR	Ultraviolet-visible-near-infrared
ρ	Resistivity
Ω	Ohm

Abstract

Carbon Nanostructures (CNSs) have been receiving increasing attention during the last years for their unique physical and chemical characteristics that made these structures good candidate for their use for neurological and tissue engineering applications. Although the current scientific data have shown conflicting results about potential nano-toxicity of CNSs, many studies are pointing out the biocompatibility of several forms of CNSs (especially in functionalized form) and their ability to support growth and proliferation of cells like neurons and osteoblasts. For these reasons, the field of tissue engineering is more and more attracted by the design and fabrication of materials or devices based on conductive nanomaterials. Carbon nanotubes (CNTs), for example, have been widely used in many fields due to their electronic, mechanical and chemical characteristics. They possess important characteristics such as flexibility, mechanical strength and electrical conductivity. Initially, the use of CNTs in biological systems was limited due to their poor solubility and the presence of toxic metallic impurities. More recently, the developments in the study of these nanostructures have improved the purity and biocompatibility of CNT materials. Concerning the biomedical applications, their use is becoming relevant in neuroscience research and tissue engineering. During this thesis work these two branches of the tissue engineering have been taken into account. Concerning the neuronal tissue regeneration, first of all the state of the art and the progress of the research activity have been presented and described. A special attention has been pointed on the results obtained by our group in collaboration with Prof.

Ballerini's in terms of effect of CNTs on the neural activity. In the chapter 4, the development of a f-CNTs-based biopolymeric device able to support and boost the growth and the communication of complex nervous will be described. Also the role of CNTs in the bone tissue regeneration field has been investigated and the description of the results obtained during the last years has been reported. Regarding the experimental part of the work done during my PhD, in the chapter 5 will be described the screening investigation of the role of CNTs functionalized through different reaction in the polymeric matrix of a hydrogel system largely employed in this field in terms of mechanical properties and cellular toxicity. In the materials and methods chapter, a description of mechanical tests and the related theories is present (Rheology, compression test and low field NMR rhelaxometry). It has been useful to describe these techniques since these technique are not frequently employed in the "environment" of the Chemical and Pharmaceutical Sciences and technologies PhD school.

Riassunto

Nel corso degli ultimi anni, il campo delle nano strutture a base carboniosa ha ricevuto sempre più attenzione grazie alle loro peculiari caratteristiche chimiche e fisiche che le hanno rese buoni candidati per l'utilizzo nell'ambito biomedico. Nonostante dati scientifici contrastanti riguardo alla questione di potenziale tossicità, molti studi stanno invece dimostrando la biocompatibilità di diverse forme di nano strutture di carbonio (soprattutto dopo funzionalizzazione chimica) e la loro capacità di sostenere la crescita e la proliferazione di cellule e tessuti complessi. Per queste ragioni, il campo dell'ingegneria tissutale è sempre più attratto dalla progettazione e fabbricazione di materiali o dispositivi basati su nanomateriali conduttivi. I nanotubi di carbonio (CNTs), per esempio, vengono ampiamente studiati per l'applicazione in molti campi della ricerca grazie alle loro caratteristiche elettroniche, meccaniche e chimiche. Essi possiedono infatti caratteristiche importanti quali la flessibilità, resistenza meccanica e conducibilità elettrica. Inizialmente, l'impiego di nanotubi di carbonio in sistemi biologici è stato limitato a causa della loro scarsa solubilità e la presenza di impurità metalliche tossiche. I recenti sviluppi nello studio di queste nano-strutture hanno migliorato notevolmente la purezza e la biocompatibilità di questo materiale nano-strutturato. Per quanto riguarda le applicazioni biomediche, il loro uso sta diventando sempre più rilevante nella ricerca delle neuroscienze e dell'ingegneria tissutale. Durante questo lavoro di tesi sono stati presi in considerazione questi due rami dell'ingegneria tissutale. Per quanto riguarda la rigenerazione del tessuto neuronale, innanzitutto lo stato dell'arte e il

progresso dell'attività di ricerca sono stati presentati e descritti. Una particolare attenzione è stata puntata sui risultati ottenuti dal nostro gruppo in collaborazione con la Prof.ssa Ballerini in termini di effetto dei nano tubi di carbonio sull'attività neuronale. Nel capitolo 4 verrà descritto lo sviluppo di un dispositivo biopolimerico contenente nanotubi di carbonio funzionalizzati in grado di supportare e stimolare la crescita e la comunicazione di tessuti nervosi complessi. Anche il ruolo dei CNTs nel campo della rigenerazione ossea è stato preso in considerazione durante questo lavoro di tesi e la descrizione dei risultati ottenuti negli ultimi anni è stata riassunta e riportata. Per quanto riguarda la parte sperimentale del lavoro svolto durante il dottorato, nel capitolo 5 sarà descritto l'indagine di screening riguardante il ruolo di nano tubi di carbonio caratterizzati da differenti tipi di funzionalizzazione all'interno della matrice polimerica di un sistema idrogel largamente impiegato in questo campo in termini di proprietà meccaniche e tossicità cellulare. Nella sezione riguardante i materiali e i metodi impiegati, è stato approfondito l'aspetto legato alle tecniche di caratterizzazione meccanica dei materiali studiati (reologia, test di compressione meccanica e NMN a basso campo). Abbiamo ritenuto opportuno approfondire questi aspetti poiché nell'ambito della scuola di dottorato in Scienze e Tecnologie Chimiche e Farmaceutiche tali tecniche non sono spesso impiegate.

1. Carbon nanotubes

1.1 Carbon nanotubes structure and properties

Carbon Nanostructures (CNSs) have been receiving increasing attention during the last years for their unique physical and chemical characteristics that made these structures good candidate for their use in many biological fields[1]. Although the current scientific data have shown conflicting results about potential nano-toxicity of CNSs, many studies are pointing out the biocompatibility of several forms of CNSs (especially in functionalized form) and their ability for example to support growth and proliferation of cells like neurons and osteoblasts[2,3]. Carbon nanotubes (CNTs) have been noticed for the first time in 1976 and they have been proposed for biotechnological applications just in 1991[4,5]. During the last decades, CNTs have been widely studied in order to understand their peculiar characteristics. This material can be represented as a graphite sheet rolled up creating a cylinder of carbon atoms with the characteristic aromatic network (figure 1).

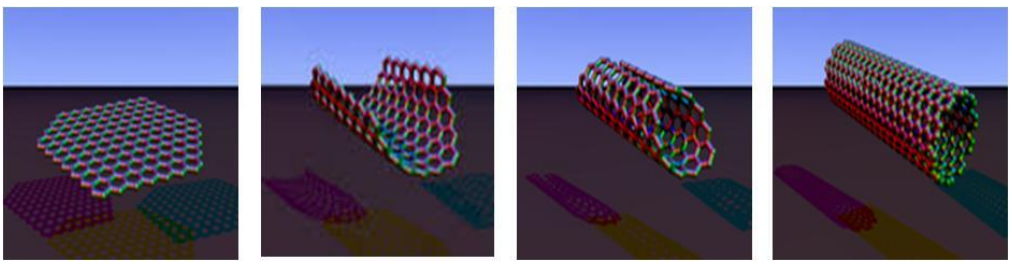

Figure 1. Schematic representation of a graphite sheet rolled up creating a carbon nanotube.

CNTs can be divided according to the number of concentric cylinders of graphite sheets. Therefore, CNTs can be gathered in two main groups called single walled nanotubes (SWNTs, Figure 2a) and multi walled nanotubes (MWNTs, Figure 2b)[6,7].

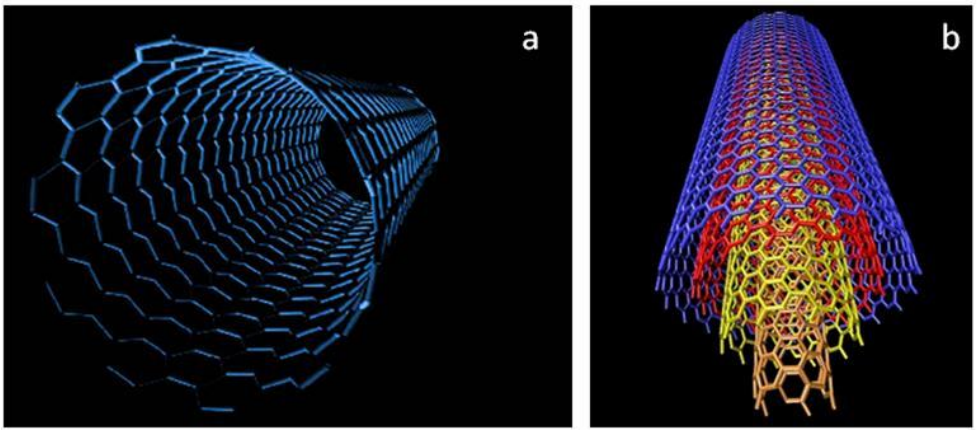

Figure 2. Structures of SWNTs (a) and MWNTs (b)

On the other hand, CNTs are also characterized by the chirality of the carbon network. Indeed the rolling up direction of the graphene sheet affects the electronic properties[8-10]. The different structures originated by the different directions are described through a chiral vector. Through this value θ it's possible to identify a huge variety of CNTs structures. The two extremes are the "zigzag" structure, where θ = 0° and m = 0, and the "armchair" structure, where θ = 30° and n = m ≠ 0. When 0° < θ < 30° CNTs are defined as chiral tubes (Figure 3). Armchair CNTs turn out to have metallic properties, while zigzag and chiral ones can have either metallic or semiconducting behaviours.

In general SWNTs are a mixture of metallic and semiconductive tubes, while MWNTs are mainly metallic conductive tubes.

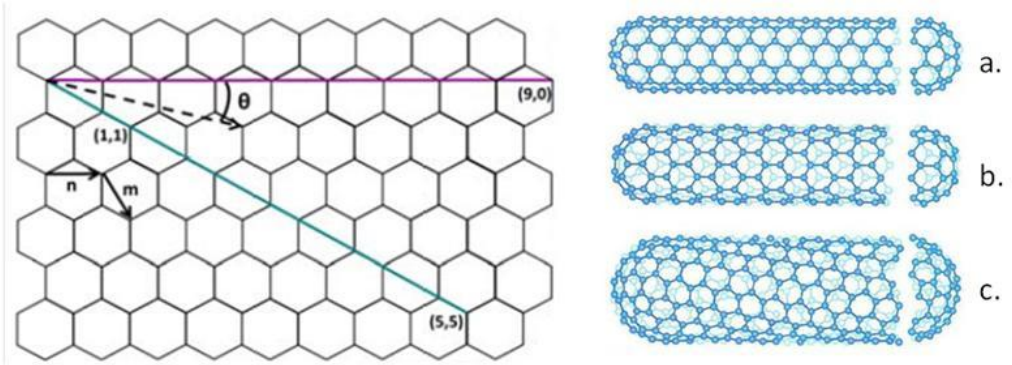

Figure 3. Gaphical explanation of the chiral vector θ of the aromatic sidewall of CNTs. The vector refers to the direction of rolling up of the graphene sheet (left). CNTs can be described by the couple of values (n,m). Structures of armchair (a), zigzag (b) and chiral (c) tubes (right).

The ballistic electronic transport in metallic SWCNTs and MWCNTs over long nanotube lengths enables the tubes to carry high currents with essentially no heating. Before the discovery of carbon nanotube, diamond was the best known thermal conductor. CNT have been proofed to have a thermal conductivity at least twice that of diamond at room temperature[11-13].

As anticipated, CNTs have raised considerable interest for their unique mechanical properties. The carbon-carbon bonds of graphene is probably the strongest bond ever known existing in nature. For this reason it is possible to affirm that CNTs manifest considerable mechanical properties in terms of tensile strenght and elastic modulus. An entire chapter on the description of this type of parameters will be reported later. On the other hand CNTs have

been found to have the capacity for changing their shape without irreversible atomic rearrangements[14-16].

Defects in nanomaterials drastically influence their optical, mechanical and thermal properties. The presence of defects brings benefits, for example the presence of defects on the aromatic networks allows us to easily functionalize the surface of the tubes. The possible defective structures can be splitted into four main groups: topological, where the introduction of ring sizes other than hexagons is involved; rehybridization, which refers to the ability of carbon atom to hybridize between sp^2 and sp^3 configuration; incomplete bonding defects, where vacancies or dislocations are present; doping, when other elements than carbon are involved in the structure. The presence of defects such as topological ones produces also a change in the helicity and in the electronic properties of CNTs. This is the typical situation when multiple pentagon-heptagon defects affect the hexagonal network (Figure 4)[17-19].

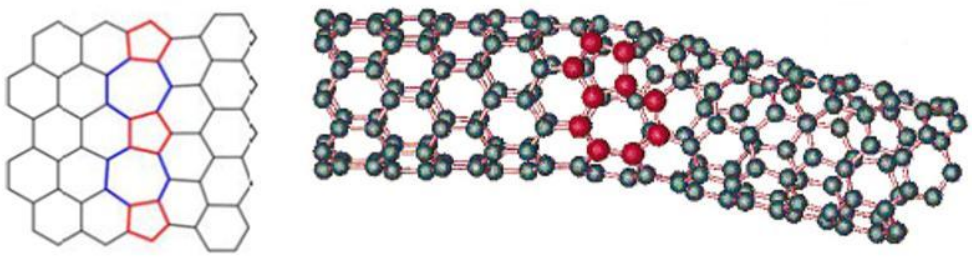

Figure 4. Example of pentagon-heptagon defects in the hexagonal network in the 2D layer (a) and the atomic structure resulting in the 3D shape of the CNTs (b).

The existence of a large number of variables that leads to the formation of different structures causes the lack of batch-to-batch reproducibility. This variability during the production processes is releated to lenght, the diameter, the chirality, the presence of impurities and the presence of defects. Impurities usually derive from the production precesses and they can be represented by metallic nanoparticles, carbonaceous material such as amorphous carbon.

CNTs can be produced through different synthetic techniques. The main ones are arc discharge, laser ablation and catalytic carbon vapour deposition. The first two techniques employ a high power energy in order o vaporize the solid state carbon (graphite) obtaining CNTs in presence of high temperature. The CCVD methodology allows us to obtain CNTs at lower temperatures (500-1000 °C) starting from the gaseous state of carbon precursors. This technique provides a better control in the growth of CNTs and low cost of the process allows the scale up in the industrial production[20,21].

1.2 Carbon nanotubes toxicity

Initially, the use of CNTs in biological systems was limited due to their poor solubility and the presence of toxic metallic impurities[22,23]. More recently, the developments in the study of these nanostructures have improved the purity and biocompatibility of CNT materials[24]. Regarding CNTs it is important to distinguish two different concepts about toxicity: the biocompatibility and the possible applications of CNTs-based systems in biomedical fields and on the other hand the problems related to the manipulation of the materials. Pristine MWNTs have been compared to asbestos, a carcinogenic silicate material that tends to aggregate. In case of inhalation, asbestos promotes the formation of reactive oxygen species initiating an inflammatory and a scavenging processes. The possibility for pristine CNTs to share the same carcinogenic mechanism is still under investigation despite CNTs are generally considered less toxic than asbestos fibers[25-27]. A lot of in vivo studies have been performed especially on the inhalation toxicity of CNTs but it is still not possible to reach a conclusion. In any case the use of precautions is necessary to prevent the assimilation of volatile particles.

In the literature there are a number of conflicting reports concerning the in vivo potential toxicity of CNTs: some investigations have reported toxic effects following the exposure of several cell types to both SWNTs and MWNTs, while others demonstrate very low or insignificant cellular responses[28]. This debate is mainly due to the fact that toxicity depends on factors like purity (metal content), surface modification (charge), dimensions (aspect ratio), layer number, degree of dispersion (aggregate formation) [29-31]. Other in vivo studies

focused on the toxicity and biodistribution of CNTs in the organism reveal that they are not confined in a specific area of the body. Macrophages are the first cells that interact with CNTs before the transit into the bloody and lymphatic systems[32,33]. The effects due to the migration of CNTs is still under investigation. It has been noticed for example the possibility of CNTs to generate the actine boundling, the reduction of cell proliferation and the chronically changing of the cellular functions[34]. It has been demonstrated that CNTs toxicity decreases after their functionalization with the consequent enhancement of the dispersibility. Appropriately functionalized CNTs are uptaken by B and T lymphocytes as well as macrophages in vitro, without affecting cell viability[35]. Furthermore the functionalization and the surface charge affect the binding of blood proteins and this could greatly alter their cellular interaction pathways and their metabolic fate and can reduce the cytotoxicity[36]. During studies in the neurological field, it has been observed that peptide or amino-functionalized CNTs does not affect both the neuronal survival and the electric activity[37-38]. Other experiments have shown for example that CNTs dispersed in biocompatible polymers can be gradually eliminated by the organism[25,39,40]. One of the most important result is the capability of CNTs to be digested by enzymes like peroxydases and the residual fragments to be fagocytosized and eliminated (*in vitro* studies)[41,42].

1.3 Carbon nanotubes functionalization

A big limitation releated to the employment of CNTs in the biomedical field is the poor dispersibility of the pristine material both in water and in organic solvents. To make the CNTs soluble and easy to manipulate a functionalization process is necessary[43,44]. Specific groups can be introduced on the tubes surfaces to decrease the inter-tubes interactions making them more soluble in certain solvents and creating anchor points for further chemical modifications. Two main strategies of functionalization can be considered: covalent or not-covalent approaches (Figure 5 a,b).

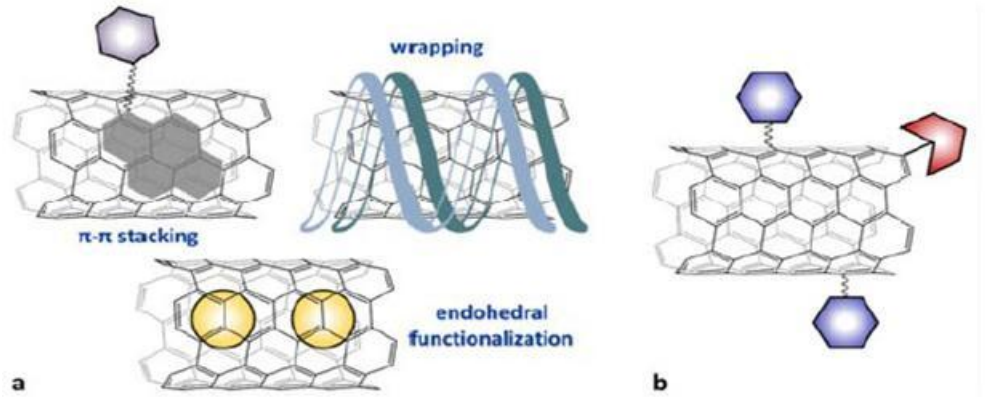

Figure 5. Non-covalent (a) and covalent (b) strategies for CNTs functionalization.

A non-covalent functionalization strategy is based on the interaction of small aromatic molecules such as pyrene or porphyrene, and the aromatic surface of CNTs creating a π-π stacking bond[45]. Another one is based on the wrapping of polymeric chains around the tubes[46]. This methodology can be useful to

associate biological macromolecules to the nanotubes, for example in case of DNA fragments[47] or lipids[48]. The last approach is the filling of the inner cavity of CNTs that can be considered an empty area for the storage of suitable molecules. For example it has been studied the possibility to fill the SWNTs cavity with fullerenes[49]. Through this non-covalent methodologies of functionalization the CNTs surface remains intact, however the electronic transition could be affected.

Concerning the covalent modifications of CNTs, the highly aromatic hexagonal network of sp^2-hybridized carbons in their sidewalls can be functionalized by taking advantage of the curvature of CNTs. It is necessary to consider that the extent of the curvature induces the weakening of the π conjugation. The presence of the curvature induces the pyramilization of the π-orbitals of the carbon atoms and consequently their misalignment within CNTs[50-51]. This peculiar structural conformation makes the CNTs sidewall reactive towards chemical functionalizations. On the other hand, also the presence of sidewall defects locally increases the chemical reactivity of the surface (Figure 6).

While non-covalent functionalizations not necessary affect the electronic and mechanical properties of CNTs, the covalent approach influences a lot the characteristics in point generating sp^3 carbon sites and preventing the band-to-band transitions of π electrons[52]. In this chapter the main reactions used during the thesis work will be described.

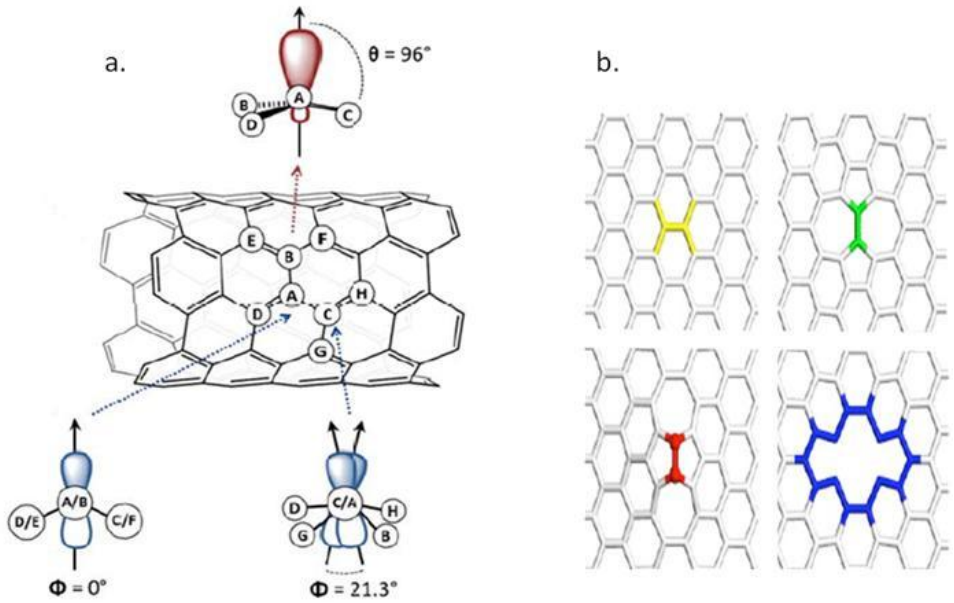

Figure 6. Representation of pyramidalization angle (θ – 90°) and π orbital misalignment (ϕ) for CNTs (a). Example of vacancy and pentagons/heptagons defects in the hexagonal CNTs network (b).

Oxidation of CNTs has been typically used in order to purify them by removing the traces of metallic catalysts employed in the fabrication processes. The most common way to oxidize CNTs involves an acidic treatment under heating or sonication. This process produces short opened tubes with oxygenated moieties. These carboxylic groups constitute possible anchor points where molecules can be conjugated by means of ester or amide bonds. The degree of the oxidation depends on the strength of the conditions and the acidic mixture[53-56].

Cycloadditon procedure comprises a large amount of reactions that have been usually employed in order to functionalize pristine CNTs. Most of these reactions are limited by the stability of the final product. During this work the 1,3-dipolar cycloaddition of azomethines ylides reaction has been largely employed to functionalize the starting material[57]. This reaction, the so-called Prato's reaction, turns out to be one of the most versatile and in general it is widely employed to functionalize the whole series of carbon nanostructures (fullerene[58], CNTs[57] and graphene[59]). The condensation of α-aminoacids with aldehydes generates a very reactive ylide specie, that reacts with the CNTs surface (Scheme 1). By this way it is possible to conjugate different appendages obtaining a better solubility and a selective tune of their properties. On the other hand, this reaction allows us to recover the pristine material after an heating treatment at 350 °C in a nitrogen atmosphere.

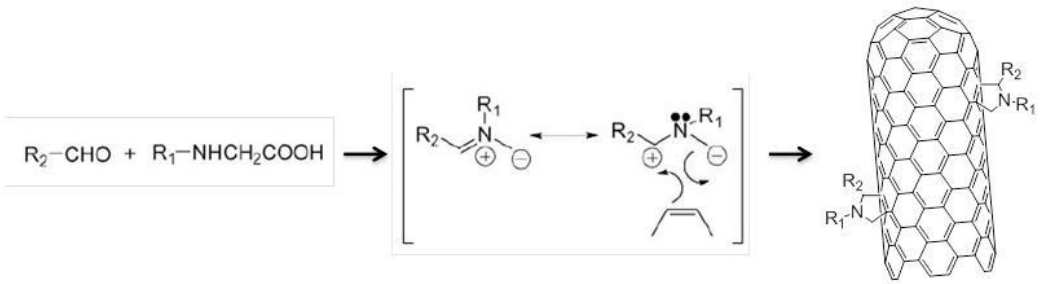

Scheme 1. General mechanism of 1,3-dipolar cycloaddition of azomethine ylides to CNTs

The last reaction employed during this thesis work is the diazonium salt based arylation reaction. Aryl diazonium salts are known to react with olefins and also with aromatic compounds (Scheme 2). For this reason the reactions has

been largely studied for the modification of CNTs sidewall. The arenadiazonium species can be also formed in situ by mixing in water an aniline and isoamylnitrite, the oxidative agent, generating the active diazo entity. After the elimination of N_2, the resultant aryl radical reacts with the aromatic sidewall of CNTs[60-63].

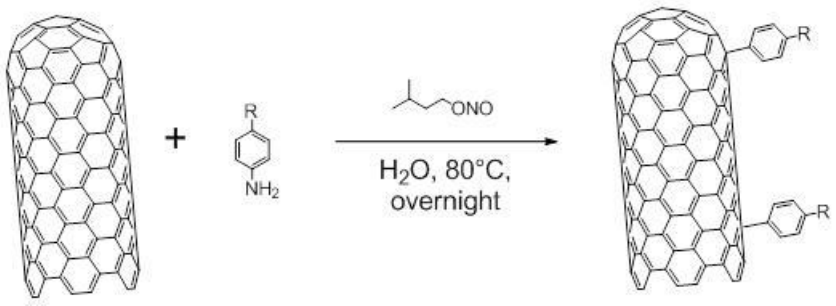

Scheme 2. Functionalization of CNTs by radical addition.

References

1. J. Shi *et al*., Nanotechnology in drug delivery and tissue engineering: from discovery to applications. *Nano Lett*, **2010**, 10, 3223-30.
2. U.S. Shin *et al*., Carbon nanotubes in nNanocomposites and hybrids with hydroxyapatite for bone replacements. *J. Tiss. Eng.* **2012**, 2, 1, 674287.
3. A. Fabbro *et al*., Carbon nanotubes: artificial nanomaterials to engineer single neurons and neuronal networks. *ACS Chem. Neurosci*. **2012**, 3, 611-8.
4. A. Oberlin *et al*., Filamentous growth of carbon through benzene decomposition. *J. Cryst. Growth*, **1976**, 32, 335-349.
5. S. Iijima, Helical microtubules of graphitic carbon. *Nature*, **1991**, 354, 56-58.
6. S. Iijima, Single-shell carbon nanotubes of 1-nm diameter. *Nature*, **1993**, 363, 603-605.
7. J. Li *et al*., Growing Y-junction carbon nanotubes. *Nature*, **1999**, 402, 253-354.
8. N. Hamada et al., New one-dimensional conductors: graphitic microtubules. Phys. Rew. Lett. **1992**, 68, 631-634.
9. S. Iijima, Carbon nanotubes: past, present, and future. *Physica B*, **2002**, 323, 1-5.
10. E. Katz *et al*., Biomolecule functionalized carbon nanotubes: applications in nanobioelectronics. *ChemPhysChem*, **2004**, 5, 1084-1104.

11. A. Javey *et al*., Ballistic carbon nanotube transistors. *Nature*, **2003**, 424, 654-657.
12. Z. K. Tang *et al*., Superconductivity in 4 angstrom single-walled carbon nanotubes. *Science*, **2001**, 292, 2462-2465.
13. P.L. McEwen *et al*., Single walled carbon nanotube electronics. *IEE trans. Nanotech*. **2002**, 1, 78-85.
14. M.M.J. Tracy *et al*., Exceptionally high Young's modulus observed for individual carbon nanotubes. *Nature*, **1996**, 381, 678-680.
15. E.W. Wong *et al*., Nanobeam mechanics: elasticity, strength and toughness of nanorods and nanotubes. *Science*, **1997**, 277, 1971-1975.
16. J.P. Salvetat *et al*., Elastic and shear moduli of single-ealled carbon nano tube ropes. *Phys. Rew. Lett.* **1999**, 82, 944-947.
17. S. Iijima *et al*., Structural flexibility of carbon nanotubes. *J. Chem. Phys.***1996**, 104, 2089-2090.
18. R.C. Haddon, The manifestation of strain in a class of continuous aromatic molecules. *Science*, **1993**, 261, 1545-1550.
19. H. Hiura *et al*., Role of sp^3 defect structure in graphite and carbon nanotubes. *Science*, **1994**, 367, 148-151.
20. M. Jose-Yacaman *et al*., Catalytic growth of carbon microtubuleswith fullerene structure. *Appl. Phys. Lett*. **1993**, 62, 202-204.
21. M. Paradise and T. Goswami, Carbon nanotubes – production and industrial applications. *Materials & design*, **2007**, 28, 1477-1489.
22. H. Li *et al*., *In vivo* evaluation of water-soluble carbon nanotubes. *Tox. Env. Chem*. **2011**, 93:3, 603-615.

23. C. Buzea *et al*., Nanomaterials and nanoparticles: sources and toxicity. *Biointerphases*, **2007**, 2, MR17.
24. C. M. Voge and J. P. Stegemann, Carbon nanotubes in neural interfacing applications. *J. Neural Eng*., **2011**, 8 011001.
25. G.M. Mutlu *et al*., Biocompatible nanoscale dispersion of single-walled carbon nanotubes minimizes *in vivo* pulmonary toxicity. *Nano Lett*. **2010**, 10, 1664-1670.
26. J.P. Ryman-Rasmussen *et al*., Inhaled carbon nanotubes reach the subpleural tissue in mice. *Nature Nanotech*. **2009**, 4, 747-751.
27. L. Mah-Hock *et al*., Inhalation Toxicity of Multiwall Carbon Nanotubes in Rats Exposed for 3 Months. *Toxicol. Sci*. **2009**, 112, 468-481.
28. S. Yazdan Madani *et al*., A concise review of carbon nanotube's toxicology. *Nano Rev*. **2013**, 4.
29. R. Li *et al*., Surface charge and cellular processing of covalently functionalized multiwall carbon nanotubes determine pulmonary toxicity. *ACS Nano*, **2013**, 7:3, 2352-2368.
30. X. Chen *et al*., Interfacing carbon nanotubes with living cells. *J. Am. Chem. Soc*. **2006**, 128, 6292-6293.
31. C. Salvador-Morales *et al*., Effects of covalent functionalisation on the biocompatibility characterisctics of multi-walled carbon nanotubes. *J. Nanosci. Nanotechnol*. **2007**, 8, 1-10.
32. Y. Lee & K.E. Geckler, Carbon nanotubes in the biological interphase: the relevance of noncovalence. *Adv. Mater*. **2010**, 22, 4076-4083.
33. F. Zao *et al*., Cellular uptake, intracellular trafficking, and cytoxicity of nanomaterials. *Small*, **2011**, 1322-1337.

34. B.D. Holt *et al*., Carbon nanotubes reorganize actin structures in cells and in ex vivo. *ACS Nano*, **2011**, 5, 4624-4633.
35. H. Dumortier *et al*., Functionalized carbon nanotubes are non-cytotoxic and preserve the functionality of primary immune cells. *Nano Lett*. **2006**, 6, 1522-1528.
36. C. Ge *et al*., Binding of blood proteins to carbon nanotubes reduces cytotoxicity. *PNAS*, **2011**,108:41, 16968–16973.
37. H.J. Lee et al., Amine-modified single-walled carbon nanotubes protect neurons from injury in a rat stroke model. *Nature Nanotech*. **2011**, 6, 121-125.
38. C. Gaillard *et al*., Carbon nanotubes carrying cell-adhesion peptides do not interfere with neuronal functionality. *Adv. Mat*. **2009**, 21, 2903-2908.
39. M.L. Shipper *et al*., A pilot toxicology study of single-walled carbon nanotubes in a small sample of mice. *Natute Nanotech*. **2008**, 3, 216-221.
40. A. Pietroiusti *et al*., Low doses of pristine and oxidized single-walled carbon nanotubes affect mammalian embryonic development. *ACS Nano*, **2011**, 5, 4624-4633.
41. V.E. Kagan *et al*., Carbon nanotubes degraded by neutrophil myeloperoxidase induce less pulmonary inflammation. *Nature Nanotech*. **2010**, 5, 354-359.
42. B.L. Allen *et al*., Biodegradation of single-walled carbon nanotubes through enzymatic catalysis. *Nano Lett*. **2008**, 8, 3899-3903.

43. A. Bianco & M. Prato. Can carbon nanotubes be considered useful tools for biological applications? *Adv. Mater*. **2003**, 15, 1765-1768.
44. A. Bianco *et al*., Making carbon nanotubes biocompatible and biodegradable. *ChemComm*, **2011**.
45. S.H. Park *et al*., Enhanced electrical properties in carbon nanotube/poly (3-hexylthiophene) nanocomposites formed through non-covalent functionalization. *Nano Res*. **2011**, 4, 1129-1135.
46. D. Tuncel. Non-covalent interactions between carbon nanotubes and conjugated polymers. *Nanoscale*, **2011**, 3, 3545-3554.
47. M. Zeng *et al*., DNA-assisted dispersion and separation of carbon nanotubes. *Nat. Mater*. **2003**, 2, 338-342.
48. R. Quiao & P.C. Ke, Lipid-carbon nanotube self-assembly in aqueous solution. *J. Am. Chem. Soc.* **2006**, 128, 13656-13657.
49. B.W. Smith & D.E. Luzzi, Formation mechanism of fullerene peapods and coaxial tubes: a path to large scalesynthesis. *Chem. Phys. Lett*. **2000**, 321, 169-174.
50. A. Hirsch, Principles of fullerene reactivity. **1999**, 199, 1-65.
51. X. Lu & Z. Chen. Curved Pi-Conjugation and the Related Chemistry of Small Fullerenes (smaller than C60) and Single-Wall Carbon Nanotubes. *Chem. Rev*. **2005**, 105, 3643-3696.
52. J. Zhao *et al*., Optical properties and photonic devices of doped carbon nanotubes. *Anal. Chem. Acta*, **2006**, 568, 161-170.
53. C.A. Furtado *et al*., Debundling and dissolution of single-walled carbon nanotubes in amide solvents. *J. Am. Chem. Soc*. **2004**, 126, 6095-6105.

54. C. Yang *et al*., Selective removal of metallic single-walled carbon nanotubes with small diameters by using nitric and sulfuric acids. *J. Phys. Chem. B*, **2005**, 109, 19242-19248.
55. Y. Wang *et al*., Rapidly functionalized, water-dispersed carbon nanotubes at high concentrations. *J. Am. Chem. Soc*. **2006**, 128, 95-99.
56. P. Singh *et al*., Organic functionalisation and characterisation of single-walled carbon nanotubes. *Chem. Soc. Rev*. **2009**, 38, 2214-2230.
57. V. Georgakilas *et al*., Organic functionalization of carbon nanotubes. *J. Am. Chem. Soc. Comm*. **2002**, 124, 760-761.
58. M. Prato & M. Maggini, Fulleropyrrolidines: a family of full-fledged fullerene derivatives. *Acc. Chem. Res*. **1998**, 31, 519-526.
59. M. Quintana *et al*., Organic functionalization of carbon nanostructures via 1,3-dipolar cycloadditions. *Phys. status solidi B*, **2010**, 247, 2645-2648.
60. J.L. Bahr & J.M. Tour, Covalent chemistry of single-wall carbon nanotubes*. J. Mater. Chem*. **2002**,12,1952-1958.
61. B.K. Price & J.M. Tour, Functionalization of single-walled carbon nanotubes in water. *J. Am. Chem. Soc*. **2006**, 128, 12899-12904.
62. M.S. Strano *et al*., Electronic structure control of single-walled nano tube functionalization. *Science*, **2003**, 301, 1519-1522.
63. J.L. Hudson *et al*., Triazenes as a stable diazonium source for use in functionalizing carbon nanotubes in aqueous suspensions. *Chem. Mater*. **2006**, 18, 2766-2770.

2. Carbon nanotubes in tissue engineering

Most tissues in the body can undergo to a self-repair to varying extents after injuries. Beyond the self-reparative threshold it is possible to obtain benefits from the therapeutic intervention in order to help and facilitate the healing processes. This type of approach often involves the transplantation of healthy tissues from a donor or from the patient himself. Unfortunately, this procedure is not always applicable and tissue engineering has been recognized as a potential therapeutic solution. Tissue engineering generally involves the use of biomaterials, cells and bioactive factors in various combinations to facilitate the regeneration of lost or injured tissues[1]. For example it is possible to exploit biomaterial scaffolds implanted at the site of injury to transfer primary progenitor cells previously harvested from a patient (Figure 1)[2,3].

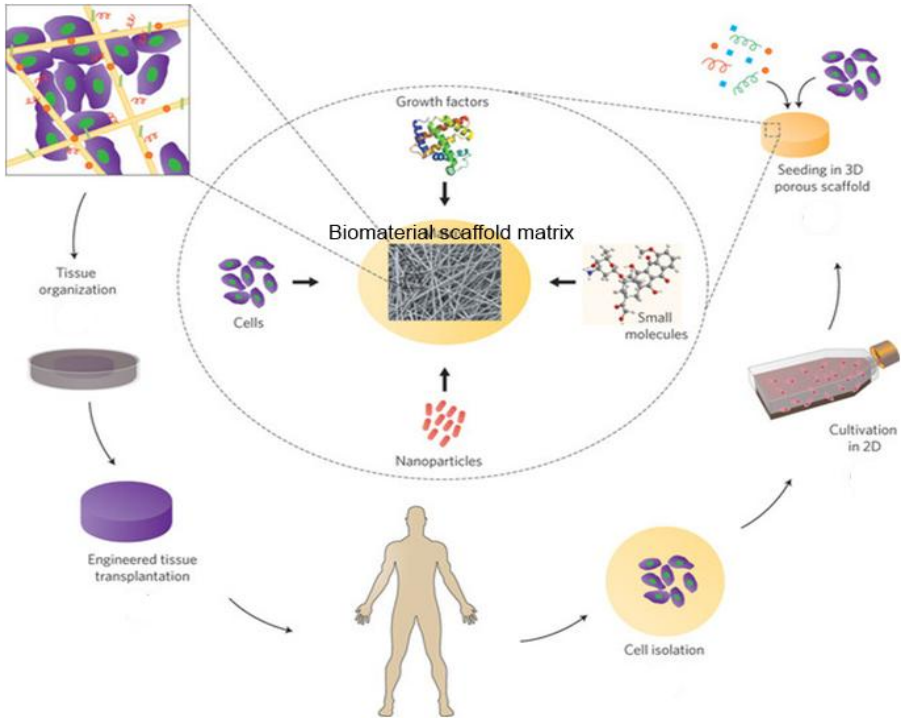

Figure 1. Tissue engineering strategies.

This technique is also employed for the release of bioactive factors able to attract cells and promote the repair of damage[4-6].Regardless of the specific tissue-engineering strategy employed, biomaterial scaffolds generally represent the foundation to guide and support the tissue regeneration mimicking as much as possible the natural environment. In general biomaterial scaffolds need a porous structure in order to allow optimal cell seeding, tissue construct viability, and vascularization of the regenerated tissue[7-10].

One of the branches of biomedical sciences where CNTs are finding application is precisely represented by tissue engineering. For their peculiar features of high mechanical strength, elasticity, good thermal and electrical conductivity CNTs are largely studied as key components for innovative materials in this field through the development of nanostructurated systems[11-13]. They have shown in many cases to be biocompatible and to support the growth and the proliferation of many classes of cells[14,15]. In this thesis work we have mainly dealt with the development of MWNTs-based biopolymeric systems for the neuronal and bone regeneration. Among the biomaterials, natural polymers (polysaccharides) have been taken into account due to their characteristics of biocompatibility. Polysaccharides like alginate, chitosan and hyaluronic acid[16-19] are largely employed for the development of nanostructurated systems. They turn out to be very versatile, enabling to be decorated with signal molecules (oligosaccharides, peptides) and to interact with inorganic components and to promote the cell attachment. These biopolymers have been widely employed to develop three-dimensional systems able to mimic the physical-chemical properties of the extracellular matrix (ECM) through the formation of hydrogels[20]. Hydrogels are 3D cross-linked networks composed of hydrophilic polymers with high water content. Chemical and/or physical cross-linking of hydrophilic polymers are typical approaches to form hydrogels. Their physical and chemical properties depends on the cross-linking type and cross-linking density, in addition to the molecular weight and chemical composition of the polymers[21,22]. CNTs-based biopolymeric devices have shown more stability and an increased mechanical resistance[23-25].

2.1 Carbon nanotubes for neuronal regeneration

SCI is a devastating clinical condition that significantly impacts the ability of affected individuals to produce functional movements and often results in paraplegia or quadriplegia. Unfortunately the complexity of the nervous system and the neuronal cells functionality makes the reparation of damaged nerves and the reinstatement of the electrical activity very difficult. Traditional approaches employed in the classical surgery reveal various problems as immune response, incomplete functional recovery, instability of the employed materials with the consequent rejection[26]. For the reasons during the last decades great efforts have been made to develop a biocompatible and long-term stable material able to promote the neural regeneration. A lot of polymers have been investigated as components of potential nerve guidance channels or as scaffolds, able to increase the reparative capacity of the peripheral nervous system[27]. We can do a breakdown: non-degradable and degradable materials. As for non-degradable materials, the permanent implantation of a nerve guidance channel could create a high risk of inflammatory events and a possible nerve compression over time[28]. Moreover, synthetic materials often turn out to be non-cell adhesive. Degradable materials (the majority comes from natural sources) present a smaller risk of nerve compression and they often result to be more inherently adhesive to neurons and glial cells[29]. On the other hand, the natural provenance entails problems in uniformity and reproducibility. We can extend all these issues to materials involved in the development of scaffolds. Both natural and synthetic materials have been studied to design a nerve

guidance channel. The key design elements in the construction of nerve guidance channels (Figure 2) are focused on the biocompatibility aspect (cell adhesion, internal matrix able to promote the colonization) and the structural aspect of the scaffold architecture[27]. The scaffold needs a longitudinal organization able to support and guide the axonal elongation. On the other hand the porosity of the system should improve the revascolarization of the regenerated tissue[30].

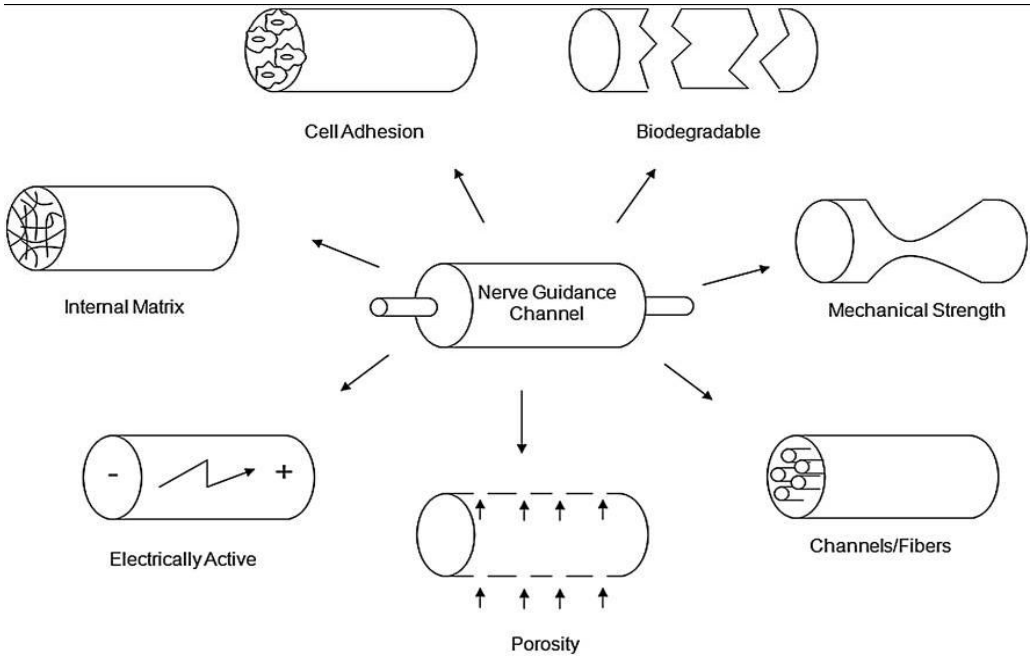

Figure 2. Key design elements in the construction of nerve guidance channels.

Regarding the biopolmeric systems, the lack of electrical conductivity turns out to be a disadvantage to restore the electrical communication between

neurons. For this reason, researchers thought to exploit both the electrical properties of CNTs and the tubular structure for the development of devices able to interface with damaged neuronal tissues. Mattson and collaborators in 2000 found that functionalized CNTs support the long term neural cells survival[31]. They demonstrated that rat hippocampal neurons deposited on a MWNTs layer on a glass coverslip support not only the cellular survival but also the elongation in all directions of the neurites and the growth of cones. In 2005 the biocompatibility of SWNTs supports was also demonstrated by Hu and collaborators. The charge surface of the CNTs sidewall turns out to be a crucial aspect for the cells survival and growth especially in case of positive charges[32]. Only in 2007 it was demonstrated by Galva-Garcia and collaborators that the orientation of CNTs can be controlled and is able to affect the direction of neurites outgrowth [33] and accordingly it should be possible that they drive the direction of the electric signal propagation. In 2005 for the first time Lovat and collaborators reported the relationship between CNTs and neurons in term of electrical activity of neuronal networks through the patch-clamp technique of recording. Hippocampal neurons have been directly seeded on a glass coverslip covered by a MWNTs homogenous layer[34]. The presence of CNTs in comparison to the simply glass substrate made the frequency of spontaneous events boosted and increased (figure 3).

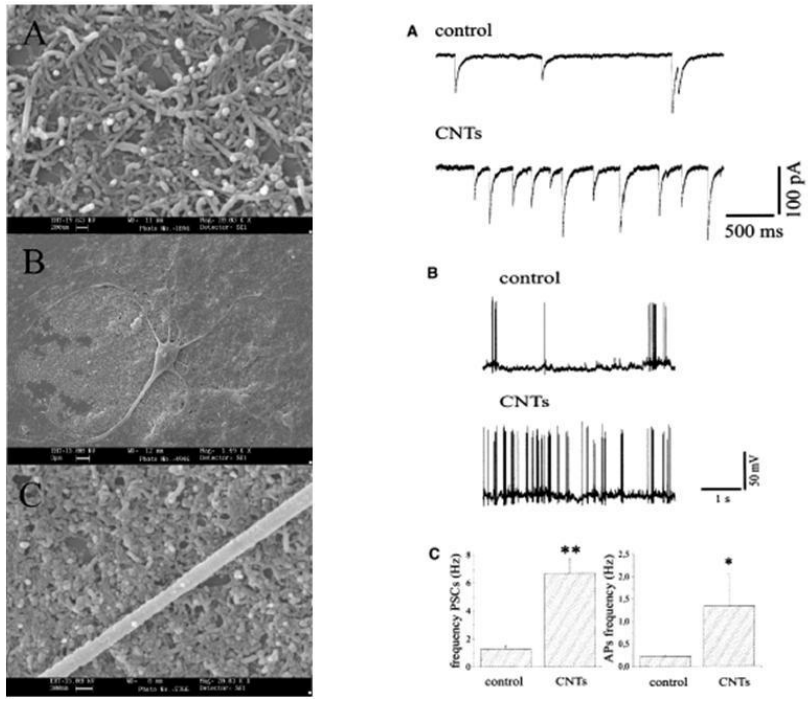

Figure 3. Purified multiwalled carbon nanotubes (MWNTs) layered on glass substrate (A). Neonatal hippocampal neuron growing on dispersed MWNT after 8 days in culture (B). The relationship between dendrite and MWNTs layer (C).In the right column of images: CNT substrate increases hippocampal neurons spontaneous synaptic activity and firing. (A) Spontaneous synaptic currents (PSCs) are shown in both control (top tracings) and in cultures grown on CNT substrate (bottom tracings). Note the increase in PSCs frequency under the latter condition. Recordings were taken after 8 days in culture. (B) Current clamp recordings from cultured hippocampal neurons in control (top tracings) and CNT growth conditions (bottom tracings). Spontaneous firing activity is greatly boosted in the presence of CNT substrates. (C) Histogram plots of PSCs- (left) and APs- (right) frequency in control and CNT cells; note the significant increase in the occurrence of both events when measured in CNT cultures. $^{**}P < 0.0001$ and $^{*}P < 0.05$.

In a recent study, Cellot and co-workers demonstrated that CNTs might improve the responsiveness of neurons by creating tight contacts with the cell membranes able to favour electrical shortcuts between different compartments of the neuron[35]. Moreover the synaptic plasticity is also

affected: cells grown on CNTs demonstrate an increased short-term synaptic condition instead of a normal depression after a presynaptic spike train. All these impressive effects are entirely attributable to the peculiar characteristic of conductivity and physical chemical properties of CNTs[36,37]. The interaction with CNTs based systems have been also tested with more complex neuronal tissues: embryonic spinal cord and dorsal root ganglia (DRG) explants have been placed in contact with a film of purified MWNTs[38]. DRG cultured on CNTs have shown a higher number of neuronal processes grown in contact with the substrate. Moreover the amplitude of the response to DRG stimulation turns out to be strongly increased in both its excitatory and inhibitory components (Figure 4,5).

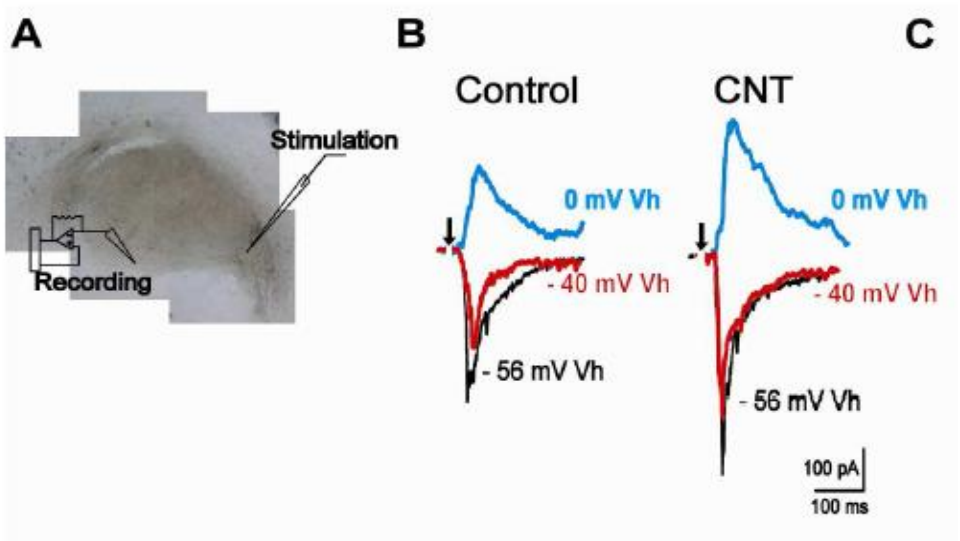

Figure 4. Evoked afferent responses of ventral spinal neurons to the electrical stimulation of the dorsal root ganglia (DRG) when interfaced to MWNTs. (A) Schematic representation of the experimental setting.

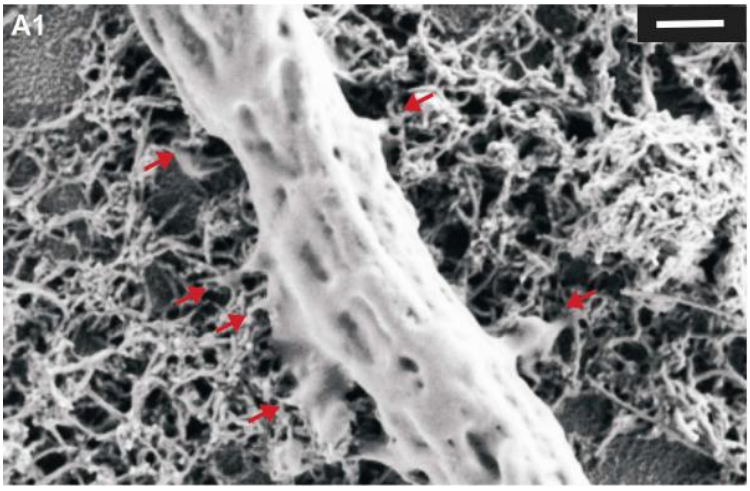

Figure 5. SEM image of a spinal explant peripheral neuronal fiber on a MWNT substrate; note the tight and intimate contacts (red arrows) between the neurite membrane and the MWNTs. Scale bar: 500 nm.

CNTs can be considered a promising material for the development of a neural prosthesis. Their electrical conductivity and the biocompatibility with neuronal cells make them good candidates for the field of neuronal tissue enginnering in order to create a biomimetic scaffold to promote axon regeneration and improve neural activities.

2.2 Carbon nanotubes for bone tissue regeneration

Bones have a capacity to regenerate themselves after suffering partial damage. However when a serious break or tumour lesion occurs and the loss of tissue is substantial, the regeneration of the tissues could be lengthy and not always possible. For these reasons the current tendency in tissue engineering is developing three-dimensional scaffolds or hydrogels temporarily placed in the site of the injury able to induce the bone regeneration. The term “temporarily” means that the device has to disappear as the bone recovers its space and so the employment of degradable materials is preferred. A balance between the device degradation and the new tissue regeneration is a crucial point[39,40]. The architecture, composition and mechanical properties are the basis to develop a device. Moreover an ideal scaffold for bone tissue regeneration should be able to promote osteoblasts proliferation and migration, and should have mechanical properties similar to those of bone. As previously said, a porous structure with interconnected pores and controlled size is required in order to allow an excellent osteointegration[41,42] and revascularization. The use of CNSs in combination with biopolymers could implement scaffold properties by modulating mechanical strength and osteoinductivity[43]. CNTs could find applications in bone tissue engineering to reinforce the devices. Moreover it has been demonstrated that carbon nanotubes are fully biocompatible with osteocytes and bone cells: the human osteoblast attachment, proliferation and differentiation is promoted. In 2006 Zanello and collaborators demonstrated that neutrally charged functionalized CNTs favorite the

osteblast proliferation and the bone-forming functions[44]. The production of plate-shaped crystals of mineralized bone matrix has been also noticed. On the other hand, in the same study, the cell morphology during the differentiation process is affected by the employment of SWNTs or MWNTs. Moreover in 2009 it has been demonstrated by Narita and coworkers that MWNTs are able to inhibit osteclastic bone resorption both *in vitro* and *in vivo*[45]. As previously outlined, CNTs have shown an incisive role in the formation and nucleation of hydroxyapatite, the mineral components of the bone tissue (Figure 6)[46,47].

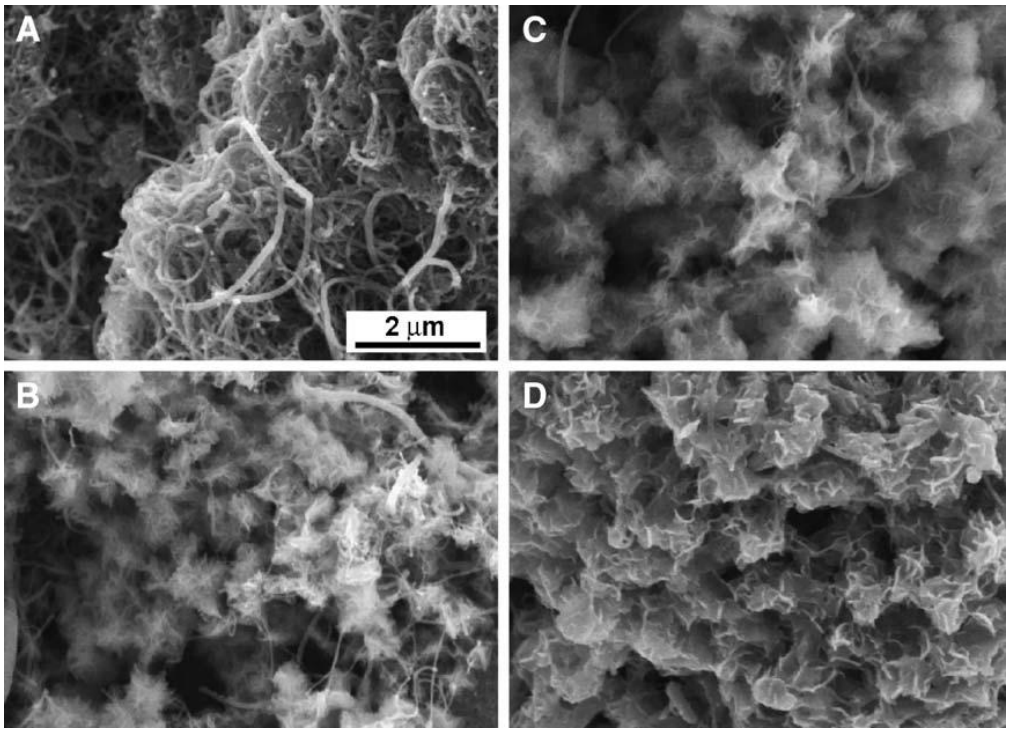

Figure 6. SEM images of the apatite nucleation on MWNTs substrate in PBS after immersion for 6 h (A), 1 day (B), 2 days (C), and 2 weeks (D).

This means that the presence of CNTs into the three-dimentional structure could accelerate the regeneration process of the damaged site. Hap has been also integrated into the CNTs-based scaffolds simply by mixing the mineral compound during the production process. For these reasons during the last decades more and more studies have been done focusing on the development of nanocomposite devices (Figure 7).

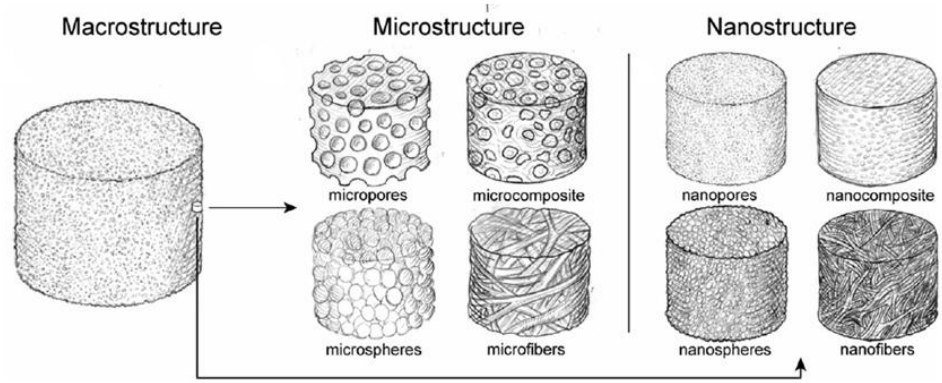

Figure 7. Schematic representation of scaffold structure from macrostructure to nanostructure.

Nanostructurated devices have been also produced incorporating molecules such as bone morphogenic proteins or growth factors in the biopolymeric matrix. In 2008 Abarrategi and coworkers developed a 3D MWNTs-based chitosan scaffold incorporating the recombinant human bone morphogenetic protein-2 (rhBMP-2)[48]. The scaffold has been tested both *in vitro* and *in vivo* obtaining the formation of regenerated tissue. Disassembly of the scaffold has been observed and they observed that fragments not incorporated into the surrounding tissue migrated into the blood circulation system, the way for

their elimination through the renal excretion. Possible limitations of the polymers currently used for bone regeneration include lack of bioactivity and poor mechanical properties. An ideal scaffold for bone tissue regeneration should be able to promote osteoblasts proliferation and migration, and should have mechanical properties similar to that of bone. Moreover it should have a porous structure with interconnected pores and controlled size in order to allow an excellent osteointegration. The use of CNSs in combination with biopolymers could implement scaffold properties by modulating mechanical strength and osteoinductivity[49]. In conclusion, CNTs demonstrate to be a very interesting choice as structural and functional constituent of 3D scaffolds for bone tissue engineering. Probably the best ideal scaffold consists in a complex mixture of nanocarbon materials, biopolymers and biominerals enriched with bone growth factors.

2.3 Aim of the work

As mentioned in this introductive chapter, carbon nanotubes are emerging in many areas of nanotechnology applications due to their peculiar features. The tissue engineering field is probably one of the most interesting and attracting field among the different applications of CNTs in the biomedical area. CNTs can be considered an ideal candidate to support the support growth and proliferation of cells like neurons and osteoblasts. My PhD was involved in two branches of the tissue engineering. In the first part of the work, involved into the field of neuronal regeneration, we focused our efforts in the development of a f-CNTs-based biopolymeric device able to support and boost the growth and the communication of complex nervous tissues. On the other hand, the second part of my PhD was focused on the study of the interaction between CNTs functionalized through different reaction and the alginate polymeric network of hydrogels and scaffolds largely employed in the bone tissue engineering field. The aim of this study could be summarized as the development of a tridimensional device based on the union of the structural properties of natural polymers and the electric features of CNTs and the comprehension of the interaction between these two species.

References

1. T. Rozario & D.W. DeSimone. The extracellular matrix in development and morphogenesis: a dynamic view. *Dev. Biol*. **2010**, 341, 126-140.
2. A. Atala *et al*., Tissue-engineered autologous bladders for patient needing cytoplasticity. *Lancet* **2006**,367, 1241-124.
3. E.S Place *et al.,* Complexity in biomaterials for tissue engineering. *Nat. Mater*. **2009**, 8, 457-470.
4. M.P. Lutolf & J.A. Hubbell. Synthetic biomaterials as instructive extracellular microenvironments for morphogenesis in tissue engineering. *Nature Biotech*. **2005**, 23, 47-55.
5. K.Y. Tsang *et al*., The developmental roles of the extracellular matrix: beyond structure to regulation. *Cell Tissue Res*. **2010**, 339, 93-110.
6. D.E. Cohen & D. Melton, Turning straw into gold: directing cell fate for regenerative medicine. *Nat. Rev. Genet*. **2011**, 12, 243-252.
7. J.L. Carvalho *et al*., Innovative strategies for tissue engineering. "Advances in Biomaterials Science and Biomedical Applications", R. Pignatello Publ., **2013**.
8. V. Mironov *et al*., Organ printing: tissue spheroids as building blocks. *Biomat*. **2009**, 30, 2164-2174.
9. A.G. Mikos *et al*., Prevascularization of porous biodegradable polymers. *Biotech. Bioeng*. **1993**, 42, 716-723.
10. T. Dvir *et al*., Nanotechnological strategies for engineering complex tissues. *Nat. Nanotech*. **2011**, 6, 13-22.

11. G.A.A. Saracino *et al*., Nanomaterials design and tests for neural tissue engineering. *Chem. Soc. Rev*. **2013**, 42, 225-262.
12. H. Haniu et al., Basic potential of carbon nanotubes in tissue engineering applications. *J. Nanomaterials*, **2012**, 343747, 10 pages.
13. S. Bosi *et al*., Carbon nanotubes in tissue engineering. *Topics in Current Chemistry* **2013**.
14. U.S. Shin *et al*., Carbon nanotubes in nanocomposites and hybrids with hydroxyapatite for bone replacements. *J. Tiss. Eng.* **2011**, 2, 1, 674287
15. A. Fabbro *et al*., Carbon nanotubes: artificial nanomaterials to engineer single neurons and neuronal networks. *ACS Chem. Neurosci*. **2012**, 3, 611-8
16. a) Z. Cao *et al., Biomacromolecules,* **2009**, 10, 2954-2959. b) T. Freier *et al., Biomaterials*, **2005**, 26, 4624-4632. c) T. Freier *et al., Biomaterials*, **2005**, 26, 5872-5878.
17. a) H. Nomura *et al., Neurosurgery*, **2008**, 63, 127-141. b) H. Nomura *et al., Tissue Eng.,* **2008**, 14, 649-665.
18. K. Kataoka *et al., Tissue Eng.,***2004**, 10, 493-504.
19. F. Z. Cui *et al., J. Mater. Sci. Mater. Med.,* **2006**, 17, 1393-1401.
20. M.W. Tibbitt & K.S. Anseth, Hydrogels as extracellular matrix mimics for 3D cell culture. *Biotechnol. Bioeng*. **2009**, 103, 655-663.
21. S. Varghese & J.H. Elisseeff. Hydrogels for musculoskeletal tissue engineering. *Adv. Polym. Sci.* **2006**, 203, 95–144.
22. K.Y. Lee & S.H. Yuk. Polymeric protein delivery systems. *Progr. Polym. Sci*. **2007**, 32, 669–97.

23. E.D. Yildirim *et al*., Fabrication, characterization, and biocompatibility of single-walled carbon nanotube-Rreinforced alginate composite scaffolds manufactured using freeform fabrication technique. *J. Biomed. Mater. Res., Part B*, **2008**, 406-414.
24. S.F. Wang *et al*., Preparation and mechanical properties of chitosan/carbon nanotubes composites. *Biomacromolecules*, **2005**, 6, 3067-3072.
25. J. Suhr *et al*., Fatigue resistance of aligned carbon nanotubes arrays under cyclic compression. *Nature Nanotech*. **2007**, 2, 417-421.
26. G. Perale *et al*., Hydrogels in Spinal Cord Injury Repair Strategies. *ACS Chem. Neurosci.* **2011**, 2, 336-345.
27. K.S. Straley *et al*., Biomaterial design strategies for the treatment of spinal cord injuries. *Journal of Neurotrauma*, **2010**, 27, 1–19.
28. A. Belkas *et al.,* Long-term in vivo biomechanical properties and biocompatibility of poly(2-hydroxyethyl methacrylate-co-methyl methacrylate) nerve conduits. *Biomaterials,* **2005**, 26, 1741-1749.
29. Z.Z. Khaing & C.E. Schmidt, Advances in natural biomaterials for nerve tissue repair. *Neurosci. Lett*. **2012**, 519, 103-14
30. E.J. Bradbury & S.B. McMahon, Spinal cord repair strategies: why do they work? *Nature*, **2006**, 7, 644-653.
31. M.P. Mattson *et al*., Molecular functionalization of carbon nanotubes and use as substrate for neuronal growth. *J. Mol. Neurosci*. **2000**, 14, 175-182.

32. H. Hu *et al*., Polyethyleneimine functionalized single-walled carbon nanotubes as a substrate for neuronal growth. *J. Phys. Chem. B*, **2005**, 109, 4285-4289.
33. P. Galva-Garcia *et al*., Robust cell migration and neuronal growth on pristine carbon nanotubes sheets and yarns. *J. Biomat. Sci*. **2007**, 18, 1245-1261.
34. V. Lovat *et al*., Carbon nanotubes substrates boost neuronal electrical signaling. *Nano Lett*. **2005**, 5, 1107-1110.
35. G. Cellot *et al*., Crbon nanotubes might improve neuronal performances by favouring electrical shortcuts. *Nat. Nanotechnol*. **2009**, 4, 126-133.
36. E.B. Malarkey *et al*., Conductive single-walled carbon nanotubes nsubstrates modulate meuronal growth. *Nano Lett*. **2009**, 9, 264-268.
37. X. Zhang *et al*., Guided neurite growth on patterned carbon nanotubes. *Sens Actuators*, **2005**, 106, 843-850.
38. A. Fabbro *et al*., Spinal cord explants use carbon nanotubes interfaces to enhance neurite outgrowth and to fortify synaptic inputs. *ACS Nano*, **2012**, 6, 2041-2055.
39. C.N. Rios *et al*., *In vivo* bone formation in silk fibroin and chitosan blend scaffolds via ectopically grafted periosteum as a cell source; a pilot study. *Tissue Eng. Part A*, **2009**, 15, 2717-2724.
40. T.A. Taton, Nanotechnology: boning up on biology. *Nature*, **2001**, 412, 491-492.

41. N.J. Castro *et al*., Recent progress in interfacial tissue engineering approaches for osteochondral defects. *Ann. of Biomed. Eng*. **2012**, 40, 1628-40.
42. E.L. Fong *et al*., Building bridges: leveraging interdisciplinary collaborations in the development of biomaterials to meet clinical needs. *Adv. Mater*. **2012**, 24, 4995-5013.
43. K. Sahithi *et al*., Polymeric composites containing carbon nanotubes for bone tissue engineering. *Int. J. Biol. Macromol*. **2010**, 46, 281-3
44. L.P. Zanello *et al*., Bone cell proliferation on carbon nanotubes. *Nano Lett*. **2006**, 6, 562-567.
45. N. Narita *et al*., Multiwalled carbon nanotubesspecifically inhibit osteoclast differentiation and function. *Nano Lett.* **2009**, 9, 41406-1413.
46. T. Akasaka *et al*., Apatite formation on carbon nanotubes. *Mater. Sci. Eng., C*, **2006**, 26, 675– 678.
47. Y. Xiao *et al*., The functionalization of multi-walled carbon nanotubes by in situ deposition of hydroxyapatite. *Biomaterials*, **2010**, 31 5182-5190.
48. A. Abarrategi *et al*., Multiwall carbon nanotube scaffolds for tissue engineering purposes. *Biomaterials*, **2008**, 29, 94-102.
49. P.R. Supronowicz *et al*., Novel current-conducting composite substrates for exposing osteblasts to alternatin current stimulation. *J. Biomed. Mater. Res. A*. **2001**, 59, 1026-1037.

3. Materials

MWCNTs have been purchased from Nanostructured & Amorphous Materials Inc. Huston, TX. Stock #1237JS, 95% purity, 20-30 nm diameter, 0.5-2 µm length. Stock #1229YJ, 95% purity, 20-30 nm diameter, 10-30 µm length.

Sodium alginate samples isolated from Laminaria hyperborea has been provided by KERRY (France). The weight average has been found to be 186600 ± 1100, as determined by viscosimetry[1] The composition of this alginate sample has been determined by means of 1H-NMR[2,3] and resulted to be FG = 0.71, FM = 0.29, FGG = 0.55, FGM+MG = 0.31, FMM = 0.13, FGGG = 0.50, FGGM+MGG = 0.10, FMGM = 0.11, NG>1 = 12.2. Materials employed for the development of neuronal tissue regeneration devices have been purchased from Sigma-Aldrich (sodium alginate, chitosan and hyaluronic acid sodium salt).

SIGMA TOX-7LDH assay, trypsin/EDTA solutions, phosphate-buffered saline (PBS), CaCO3 and GDL have been purchased from Sigma-Aldrich; fetal bovine serum (FBS), penicillin streptomycin 100X, l-glutamine 100X were purchased from EuroClone. Dulbecco's modified Eagle's medium (DMEM) has been purchased either from Sigma and EuroClone. The Live/Dead assay (Invitrogen™ LIVE/DEAD Viability/Cytotoxicity Kit) has been purchased by InvitrogenTM.

Chemicals and solvents for synthesis have been purchased from Sigma-Aldrich and they have been used without further purification.

Standard dissociated hippocampal cultures and spinal cord have been prepared according to Malgaroli[4]. Hippocampi have been dissected from 0- to 3-dayold animals killed by decapitation in accordance with the regulations of the Italian Animal Welfare Act and approved but the local Authority Veterinary Service.

3.1 CNTs functionalizations

F1-CNTs

Pristine MWNT (100 mg) have been dispersed in distilled water (100 mL) by sonication. Then 4-[(N-Boc) aminomethyl] aniline (2 g, 8.9 mmol) and isoamyl nitrite (2 ml, 14.8 mmol) have been added to the suspension and the reaction has been refluxed at 80 °C overnight. The suspension has been filtered and washed with dimethylformannide and methanol. The obtained black solid has been dried under vacuum overnight. The cleavage of the protective Boc group has been carried out in 4 M HCl using 1,4-Dioxane as solvent. The reaction has been carried out under magnetic stirring at room temperature overnight. The day after the deprotected CNTs have been filtered and washed again with DMF and methanol and finally dried under vacuum before the characterizations.

F2-CNTs

Pristine MWNTs (100 mg) have been suspended in 100 mL of *ortho* diclorobenzene and sonicated for 30 minutes. Sarcosine (600 mg, 6.73 mmol) and Heptanal (588 mg, 5.14 mmol) have been added every 2 hours for 5 times and the reaction mixture has been heated at 180 °C. CNTs have been washed several times by filtration (pore size = 0.45 μm) with DMF and MeOH. Finally the f-CNTs have been dried under vacuum before the characterizations.

F3-CNTs

Pristine MWNTs have been dispersed in a solution of H_2SO_4/HNO_3 in 3:1 ratio. It has been reacted for 30 minutes under magnetic stirring at 130 °C. After 30 minutes the solution has been filtered and washed with distilled water until the neutral pH has been reached. Finally the f-CNTs have been dried under vacuum before the characterizations.

F4-CNTs

Pristine MWNTs have been dispersed in a solution of 4N of HNO_3 in water. It has been reacted over night under magnetic stirring at 120 °C. The solution has been filtered and washed with distilled water until the neutral pH has been reached. Finally the f-CNTs have been dried under vacuum before the characterizations.

F5-CNTs

Pristine MWNTs (100 mg) were suspended in 100 mL of ortho diclorobenzene and sonicated in a water bath for 30 min. N-Pht-amino-diethoxy-ethylamino-acetic acid (1.4 g, 4.57 mmol) and paraformaldehyde (750 mg, 57.85 mmol) have been added portion-wise for 5 times every 2 hours under magnetic stirring at 180 °C. CNTs have been washed several times by filtration (pore size = 0.45 µm) with DMF and MeOH. Finally the f-CNTs have been dried under vacuum before the characterizations. Then, the phthalimido group has been cleaved by dispersing CNTs in EtOH in presence of hydrazine hydrate. After sonication, the dispersion has been stirred overnight at room temperature. The functionalized CNTs have been washed by filtration (pore size = 0.45 µm) with ethanol, aq. HCl 1N, distilled water and MeOH. Finally the f-CNTs have been dried under vacuum before the characterizations.

F6-CNTs

Pristine MWNT (100 mg) have been dispersed in distilled water (100 mL) by sonication. Then diethyl 4-aminobenzylphosphonate (2.2 g, 8.9 mmol) and isoamyl nitrite (2 ml, 14.8 mmol) have been added to the suspension and the reaction has been refluxed at 80 °C overnight. The suspension has been filtered and washed with dimethylformannide and methanol. The obtained black solid has been dried under vacuum overnight.

Syntheses of the aminoacid

N-Boc-amino-diethoxy-ethyl amine (1)

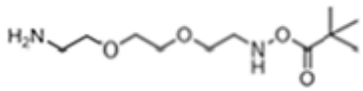

To a solution of amino-diethoxy-ethyl amine (20 g, 134.9 mmol) in CH2Cl2 (100 mL), a solution of Boc_2O (11.79 g, 54 mmol) in CH_2Cl_2 (100 mL) has been added drop-wise over 3 hours under magnetic stirring at 0 °C. The reaction has been stirred at room temperature for other 24 hours. The solvent has been evaporated under vacuum and the resulting white semi-solid has been dissolved in H_2O (70 mL) and filtered over celite to remove the white precipitate corresponding to the doubly substituted by-product. The aqueous filtrate was extracted with CH_2Cl_2 (50 mL x 3). The organic phase was backwashed with H_2O (50 mL) to remove the excess of diamine and then dried with Na_2SO_4. Evaporation of the solvent under vacuum yielded compound 1 (7.9 g, 58%) as a colourless viscous oil. Characterizations in accordance with literature[5].

N-Pht-N-Boc-amino-diethoxy-ethyl amine (2)

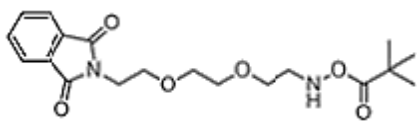

N-Boc-amino-diethoxy-ethyl amine 1 (4 g, 16.1 mmol) and phthalic anhydride (2.39 g, 16.1 mmol) have been dissolved in toluene (80 mL) and the mixture stirred at 120°C in a Dean-Stark apparatus for 20 hours. The solvent has been evaporated under vacuum and chromatographic column purification (toluene/AcOEt 7:3) afforded the pure product (4.33 g, 71%) as a colourless oil. Characterizations in accordance with literature[5].

N-Pht-amino-diethoxy-ethyl amine (3)

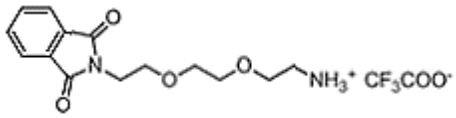

The N-phthalimido-N-Boc-amino-diethoxy-ethyl amine 2 (4 g, 10.6 mmol) has been dissolved in CH_2Cl_2 (15 mL) and trifluoroacetic acid (15 mL) has been slowly added to the solution under magnetic stirring at 0 °C. The reaction mixture has been then allowed to reach the room temperature and it has been stirred for other 2 hours. The solvent has been removed under vacuum and the resulting product, as trifluoroacetic acid salt, has been triturated in diethyl ether to give a white solid in quantitative yield. Characterizations in accordance with literature[5].

N-Pht-amino-diethoxy-ethylamino-acetic acid benzyl ester (4)

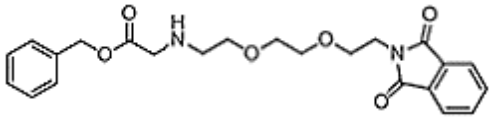

Triethylamine (3.64 mL, 26.1 mmol) hes been added to a solution of 3 (3.41 g, 8.7 mmol) in tetrahydrofuran (40 mL) at 0 °C. Then, a solution of benzyl bromoacetate (1.99 g, 8.7 mmol) in THF (60 mL) has been added drop-wise over 3 hours at 0 °C and the reaction mixture has been maintained under magnetic stirred at room temperature for 6 hours. The solvent has been evaporated under vacuum and the residue was dissolved in CH_2Cl_2 (50 mL) and washed with H_2O (50 ml x 3). The combined organic phases have been dried over Na_2SO_4 and the solvent has been removed under vacuum. Purification by column chromatography (AcOEt/MeOH 95:5) afforded the desired product 4 (1.48 g, 40%) as a colourless oil. Characterizations in accordance with literature[5].

N-Pht-amino-diethoxy-ethylamino-acetic acid (5)

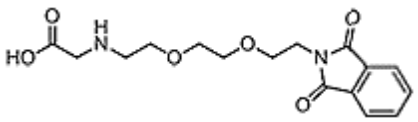

To a deoxygenated MeOH solution (40 mL) of 4 (1.48 g, 3.5 mmol), 10% Pd/C (40 mg) has been added and the reaction flask has been purged with H_2 three times and then stirred at room temperature for 24 h. The catalyst has been

removed by filtration over celite and the solvent has been evaporated. The resulting product has been triturated in diethyl ether to give a white solid in quantitative. Characterizations in accordance with literature[5].

4. Methods

Thermogravimetric analysis (TGA)

TGA is one of the most important analytical techniques used to determine the amount of functionalization present on the CNTs surface. It is based on the thermal stability of materials. This techniques allows us to check the change of weight of the sample increasing the temperature. All the functionalized CNTs employed in this work have been characterized by means of TGA in order to evaluate in terms of µmol/g the functional groups. TGA can be performed in different environments (Figure 1): inert atmosphere (nitrogen in our case) or oxidative (air). In case of oxidative conditions, the combustion takes place in the range of 400-600 °C. The presence of impurities affects the temperature of combustion: higher is the temperature detected at the moment of combustion, higher is the purity of the sample[6]. On the other hand, CNTs structure turns out to be stable up to ~ 800 °C while the organic material present in the sample (functionalization moieties) burn at lower temperatures.

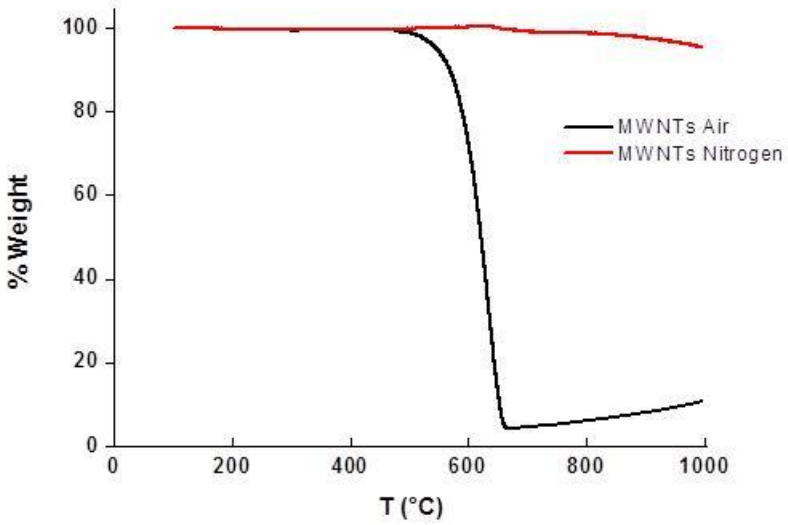

Figure 1. TGA of MWNTs in air and in nitrogen

It is possible to estimate the degree of functionalization of CNTs after a chemical modification through the amount of weight loss. We usually adopt a linear temperature ramp (10°C/min) from 100 °C to 800 °C of detection after a previous equilibration step in which the sample is stabilized at 100°C for 20 minutes. The amount of functionalization has been calculated through the following equations:

$$Carbon\ atoms/_{Funct\ Gr} = \frac{Weight\ \% \times Molecular\ weight\ of\ funct\ gr}{Molecular\ weight\ of\ C \times Loss\ of\ weight\ \%}$$

$$\frac{mmol}{g} = \frac{Loss\ of\ weight\ \% \times 10}{Molecurar\ Weight\ of\ functional\ group}$$

Thermogravimetric analysis have been performed employing a TGA Q500 TA Instruments following the procedure: isotherm step at 100 °C for 20 minutes, ramp from 100 to 830 °C at 10 °C/min under N_2 with a flow rate of 90 mL/min.

Transmission electron microscopy (TEM)

Transmission Electron Microscope (TEM) is based on the detection of high electron energy transmitted through a very thin sample (<100 nm thick). In the bright-field imaging mode, the contrast is obtained from the different absorption of the portions of the sample. TEM is widely used in our field in order to investigate the dispersion and the purity of functionalized nanotubes, while giving essential morphological information (Figure 2). Indeed it is possible to obtain precious information about the diameter and length. Metal nanoparticles can be easily detected and consequently the purity of the carbon nanotubes can be instantly evaluated. TEM analysis have been performed employing a Philips EM 208 microscope with an accelerating voltage of 100kV.

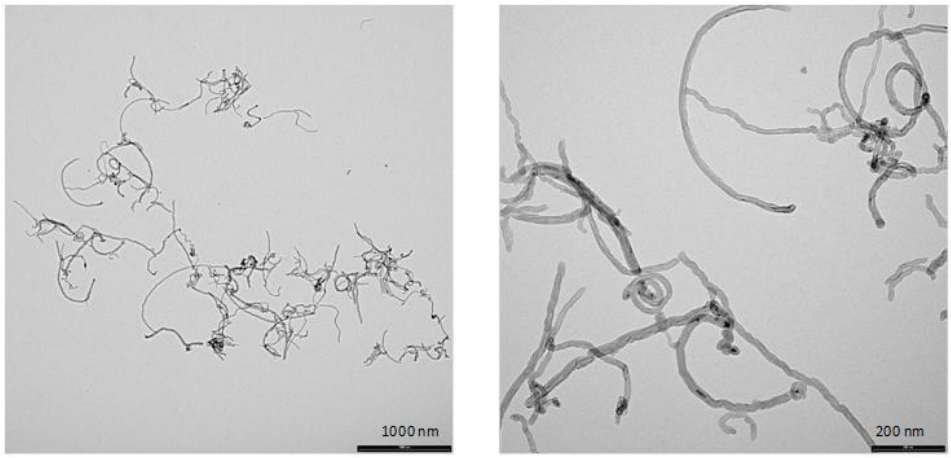

Figure 2. Example of TEM images of MWNTs

Scanning electron microscopy (SEM)

Scanning electron microscopy is a fundamental technique to image the surface topography of micro and nano structured samples without any requirements for sample preparation. A focused beam is scanned over the surface and the emitted electrons derived by the interactions with the sample are detected. This technique has been very useful to analyze the surface of 2D and 3D nanocomposite materials developed during the thesis work. Also with SEM it is possible to perform EDX analysis: chemical elements present on the surface of the sample can be determined with this analysis method. The electron beam stimulate the atoms in the sample with uniform energy and they instantaneously send out X-rays of specific energies for each element. Scanning electron microscopy analysis have been performed with a Philips 500 SEM, voltage of 10 kV.

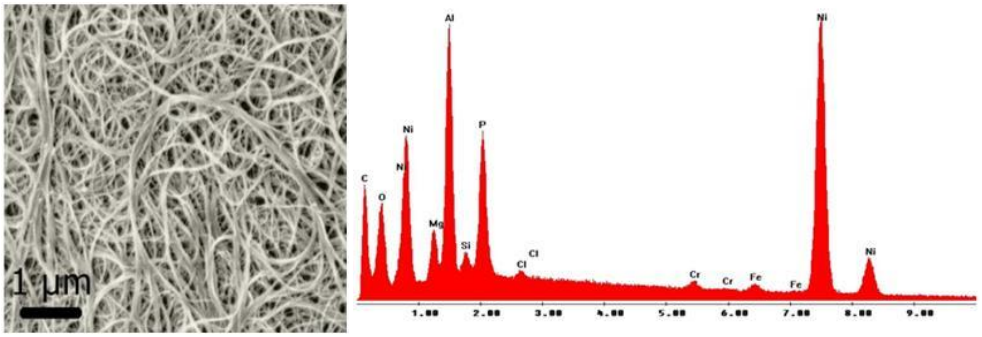

Figure 3. Example of SEM analysis of CNTs carpet (left) and EDX graph (right)

Kaiser test

This test, introduced in 1970[7], is a quantitative measurement of free amino groups in solid state peptide synthesis. Kaiser Test is a simple ninhydrin test, which follows the reaction shown in Figure 4:

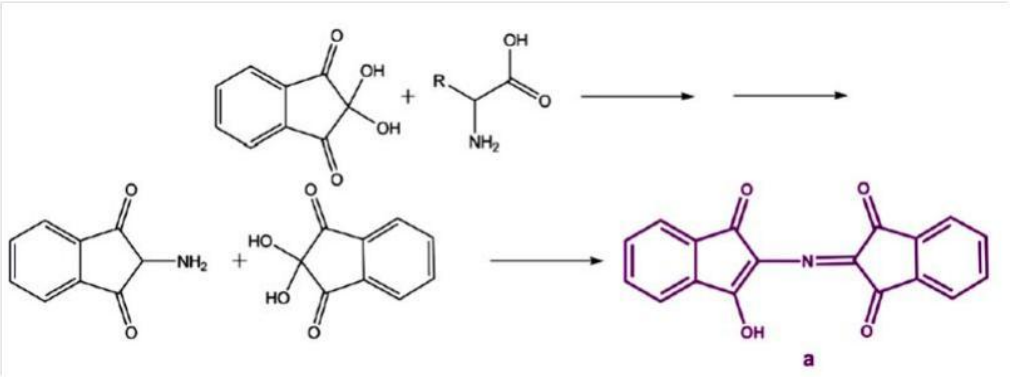

Figure 4. Schematic representation of the reaction of free amino groups during the Kaiser Test.

This reaction, which takes place at 100°C, produces a ninhydrin complex (complex a in Figure 4) which absorbs light at 570 nm. According to the Lambert-Beer law, absorbance can be correlated with the concentration of amino groups following the equation:

$$\frac{mmol}{g} = \frac{(Abs\ sample - Abs\ blank) \times dilution\ (mL) \times 10^3}{Extinction\ coefficient \times Sample\ weight\ (mg)}$$

Where the *Abs sample* is the absorbance of resulting complex, *Abs blank* is referred to the absorbance of the blank (the mixture of ethanolic solution of phenol, KCN in pyridine and ethanolic solution of ninhydrine) at 570 nm; *dilution* is related to the reaction process (the final volume of or sample to be analyzed at the spectrophotometer is diluted of 3 mL); *Extinction coefficient* is 15000 m^{-1} cm^{-1}; *Sample weight* is referred to the weight of CNTs used in the analysis. The sensitivity reported for this test is up to 5 µmol/g. Usually this colorimetric assay is employed in the field of the peptide synthesis in solid phase. In our case, the Kaiser test turns out to be very useful to quantify the amount of free amino groups on the CNTs surface after the functionalization through the 1,3-dipolar cycloaddition of azomethine ylides and the diazonium salt-based arylation reactions. Moreover the procedure need a small quantity of CNTs for the analysis (~0,5 mg), a positive aspect since not always large quantities of functionalized material can be recovered after the reactions.

Rheological measurements

The investigation and the comprehension of the internal architecture of our hydrogels and especially the interaction between CNTs and biopolymeric chains and the influence of CNTs on the classical properties of polymers represents an important aspect of this study. Since in the field of the chemical and pharmaceutical sciences these aspects are not frequently studied, it could be appropriate to describe in detail the techniques employed for the characterization of our materials[8].

Materials are generally characterized by an internal microstructure where the elemental units determine the macroscopic behavior based on their distribution and their interaction. Rheological science has the goal of studying the relationship between the microstructure of the material and its macroscopic behavior. Rheology is the science entailed in the study of the mechanical answer of the materials under the effect of one or more applied stresses. More precisely, it describes the relationship between stress and strain. The stress represents the ratio of the applied force on a surface and the surface itself. Usually the value of the stress is represented by the symbol σ and by the symbol τ for the shearing ones. The concept of deformation can be explained as the variation of the dimension related to the applied stress. In case of compression/extension, the deformation is indicated through the value ε, whereas γ indicates the shearing one. In the figure it is possible to observe the different types of stress that could be applied to the material (Figure 5).

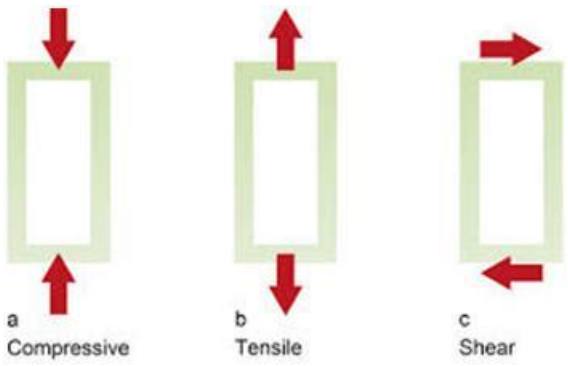

Figure 5. Different types of stress that could be applied to the material. a) Compressive, b) tensile and c) shear.

Linear elastic solids under the influence of a stress they show an elastic deformation proportional to the entity of the applied force and after the application they recover completely the initial shape. In parallel newtonian fluids show a shear rate proportional to the applied stress and the viscosity represents the proportionality constant. On the other hand, fluids with a non-Newtonian behavior are characterized by a variable value of viscosity depending on the entity of the stress. The analysis of rheological properties can follow two approaches: the measurement of the deformation under the application of a known stress or the measurement of the required stress necessary to reach a specific degree of strain. The principal behavior of the materials related to the rheological science are the elasticity, the viscosity and the viscoelasticity. A material has an elastic behavior when it recovers the original shape after the removal of the applied stress. The elasticity of the material is described through the Hook's law:

$$\sigma = \frac{E(L-L_0)}{L_0} = E\varepsilon$$

Where σ is the normal strain, ε represents the deformation in terms of ΔL and E is the Young's modulus.

For shearing deformations:

$$\tau = G\gamma$$

where τ is the strain, G is the shear modulus and γ is the shear strain. It is very important to highlight the correlation between the shear and the Young's moduli valid for incompressible materials **E = 3G**.

The concept of viscosity represents for a fluid its capacity to flow or rather its resistance to flow. In this case the stress is not proportional to the strain γ but to the shear rate through a constant η which is the viscosity of the material and it is measured in (Pa*s). As enunciated in Newton's law:

$$\tau = \eta\dot{\gamma}$$

Viscoelastic materials are placed between the two categories of solids and fluids. This is the example of polymeric materials, the subject of this work, characterized by viscous and elastic properties. The rheological investigations of viscoelastic materials are carried out into the linear viscoelastic range where the deformation is lower than 0,02%. The intensity of the applied stresses needs to be under the threshold of breakdown of the micro and nano structures of the system. Therefore, the linear viscoelasticity is limited to the range of small deformations and for these reasons the mechanical answers are dictated only by the inner micro-nano architecture of the material. Rheological characterization of biopolymeric hydrogels has been performed by means of a controlled stress rheometer Haake Rheo-Stress RS150. A system of shagreneed plate and plate system (HPP20 profiliert, diameter 20 mm) have been used for the analysis of hydrogels. The rheological experiments performed on the hydrogels allow us to describe their

viscoelastic behavior in terms of both elastic and viscous properties represented respectively by the storage (G') and the loss (G'') moduli. All of the experiments have been carried out at room temperature and to avoid water evaporation from our systems, the measurements have been led in a water saturated environment employing a glass bell (solvent trap) containing a wet cloth. In order to characterize a gel, it is necessary to perform a series of tests. First of all short stress sweep tests have been performed in order to achieve the correct gap between the two plates. The thickness of the hydrogels is not always the same: the gap has been selected to maximize the value of the storage modulus G'. On the other hand these measurements allow us to obtain the correct gap where the material behavior is placed in the linear range of deformation. SSs tests have been performed employing a stress range of 1-5 Pa with a constant solicitation frequency of 1 Hz. After this preliminary phase, the mechanical spectra of hydrogels have been detrmined according to a frequency sweep: the storage (G') and loss (G'') moduli variation has been calculated maintaining the shear stress constant (5 Pa) and decreasing the pulsation ω from 10 to 0.01 Hz. Finally a long stress sweep test has been performed to study the properties of the material in order to evaluate its behavior both in viscoelastic range and outside of the same (Figure 6).

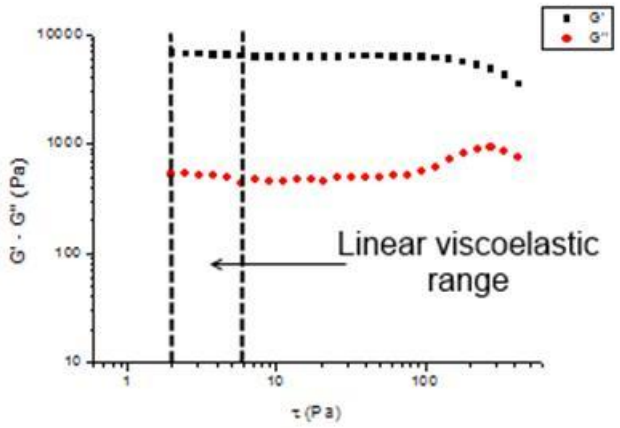

Figure 6. Typical long stress sweep graph for a material characterized by a viscoelastic behavior.

In this case it is possible to measure the variation of G' and G'' gradually increasing the shear stress from 1 to 1000 Pa and maintaining the solicitation frequency constant (1 Hz). Through the FS, experimental G' and G'' have been obtained and processed through the generalized Maxwell model to determine the shear modulus of the hydrogels. Maxwell model ideally considers the systems as composed by a perfectly viscous component "dashpot", with viscosity η, and a perfectly elastic component "spring", with stiffness *g*. These two parameters are connected in series and the relationship η/*g* (Pa*s/Pa) represents the relaxation time λ of the system that indicates the required time to relax the stress after the application of a constant deformation. The storage and the loss moduli can be described as a function of the pulsation ω according to the following equations:

$$G'(\omega) = \frac{\eta\lambda\omega^2}{1+(\lambda\omega)^2}$$

$$G''(\omega) = \frac{\eta\omega}{1+(\lambda\omega)^2}$$

On the other hand the Maxwell model is not sufficient to describe the material. In order to describe completely the viscoelastic behavior of the material, the Maxwell model has been applied considering a sequence of *n* Maxwell elements in parallel. Each element is composed by the elastic and the viscous contributions and is described through the values (g_i, η_i) or (g_i, λ_i).

$$\lambda_i = {}^{\eta_i}/_{g_i}$$

Considering all the elements, the storage and loss moduli can be modeled as a function of the pulsation ω according to the following equations:

$$G'(\omega) = \sum_{i=1}^{n} \frac{\eta_i\lambda_i\omega^2}{1+(\lambda_i\omega)^2}$$

$$G''(\omega) = \sum_{i=1}^{n} \frac{\eta_i\omega}{1+(\lambda_i\omega)^2}$$

where n is the number of Maxwell elements considered, η_i and λ_i represent the viscosity and the relaxation time of the i^{th} Maxwell element. Through the fitting of the experimental values of G' and G'' it is possible to determine the Maxwell elements that correctly describe the system under investigation. The shear modulus is obtained from the summation of the spring constants of all the Maxwell elements through the following equation:

$$G = G_e + \sum_{i=1}^{n} g_i$$

Where G_e represents the spring constant of the last Maxwell element which is supposed to be purely elastic and g_i represents the spring constant of the i^{th} Maxwell element. In terms of the rubber elasticity theory or Flory's theory, from the value G it is possible to obtain the number of elastically active chains ρ for an ideal network that has the same viscoelastic properties of our investigated hydrogel through the following relation:

$G = \rho RT$

where R is the universal gas constant and T the absolute temperature. The theory enables us to identify the cross-linking points of the gels. From the value ρ it is also possible to know the average network mesh size ζ. This parameters shows the correlation between the macro- and microscopic properties of the systems. At the beginning of the paragraph we spoke about the goal of the rheological science. From the macroscopic behavior (the shear

modulus G) it is possible to obtain the description of the microscopic structure of the material in terms of number of elastically active chains and average network mesh size.

Concerning the evaluation of the viscosity of the solutions, rheological experiments have been performed employing the cone and plate system (Figure 7). This peculiar geometry of the system enables us to apply a constant shear rate through all the radius.

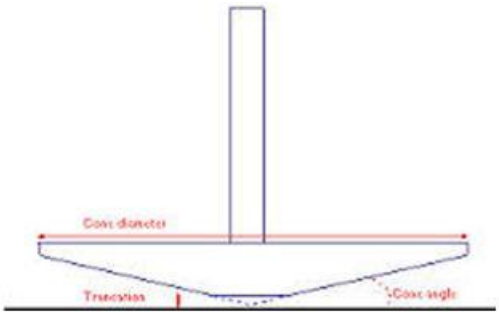

Figure 7. Cone and plate system to measure the viscosity of solutions.

The viscosity of the polymeric solution is identified as the ratio between the shear stress and the shear rate on the basis of the Newton's law:

$$\eta = {}^{\tau}/_{\dot{\gamma}}$$

The viscosity of the material depends on the pressure and temperature as "external" factors, and also on the motion conditions in terms of shear rate. In order to determine this properties of our solutions, steady value (SV) tests

have been performed. For low values of stress, the material turns out to have a constant viscosity identified by the Newtonian plateau in the flow curve. Increasing the intensity of the stress applied, it is possible to observe a drastic fall of the viscosity explained through the split of the structure. The SV tests have been performed increasing the stress from 0.1 to 100 Pa in conditions of controlled temperature.

Compression tests

In order to study and characterize the biopolymeric systems containing carbon nanotubes, many techniques have been employed. Through the rheological tests it has been possible to see how the presence of CNTs could affect the macroscopic properties of the material (solution or hydrogel) applying a stress. Briefly we will introduce also the description of the compression test of the hydrogels, tests done to obtain other information about the macroscopic behavior of the materials. Mechanical properties of the hydrogels (elasticity and strength) have been investigated by the determination of the Ultimate Compression Strength σ_{UCS} and the compression modulus E. To do that uniaxial compression tests have been performed on the cylindrically shaped hydrogels with an Universal Testing Machine (Mecmesin MultiTest 2.5-I) coupled with a 100N Load Cell. In order to obtain a regular shape, hydrogels have been produced exploiting a 24 multi-well (h 18 mm, Ø 16 mm). The compression stress-strain curves of the polysaccharide based composites have been recorded and the compression

modulus of the sample has been obtained from the linear region of the stress-strain relationship (Figure 8).

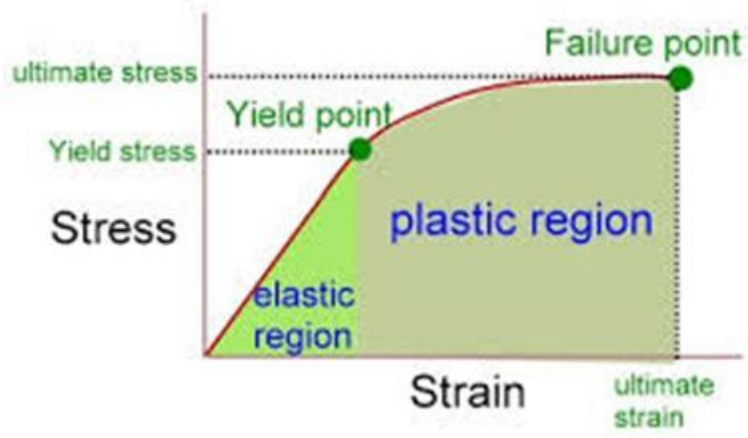

Figure 8. Graph stress/strain obtained from compression test.

The compression modulus is determined as the slope of the stress (Pa)/strain (mm/mm) curve in the range of 2-5% of deformation. In this range the material shows an elastic behavior and the strain turns out to be proportional to the applied stress. Through the compression tests it is possible to also determine the strength of the gels in terms of the stress at brake. Integrating the stress/strain curve we calculate the stored energy until the failure point.

Low field NMR

In order to obtain more information about the microscopic structure of the material, low field NMR experiments have been performed both on solutions and hydrogels. Precisely through this technique it has been possible to evaluate how the CNTs could affect the structure of the biopolymeric systems in terms of interaction with water molecules. Transverse relaxation time (T_2) determinations allow to determine the presence of relaxation rates of the water entrapped within the hydrogel network. A magnetic field B_0 is applied to the sample and a second rotating magnetic field B_1 is also generated (perpendicular to B_0) to get a phase coherence spin-spin. M_{xy} components of the magnetization vector are generated. After the removal of B_1, a relaxation process put off the phase coherence and all the magnetic moments realign with B_0 leading to a position of equilibrium ($M_{xy} = 0$) after a certain time. The relaxation of the system is accompanied by an exponential decay of M_{xy} with a time constant T_2 (transverse or spin-spin relaxation time). Usually this technique is coupled with the rheological characterization to estimate the mesh size distribution of the inner matrix of the gels. During this thesis study, we exploited the low field technique to evaluate how the presence of carbon nanotubes affects the water entrapment and distribution both in the solutions and hydrogels. In a polymeric system electromagnetic interactions between water molecules and polymeric chains are present. For water molecules, the polymeric chains turn out to be a binding network that is translated into a decreasing of the T_2 compared to the free water one. The relaxation time will be much quicker as more nuclei are constrained by the

environment. Into the pores of the network there is the bulk water, that is not affected by the surrounding structures and it behaves as free molecules, and the water affected by the affinity of the polymeric chains. The linked water convey the presence of the polymeric molecules and consequently the shape and the size of the links. Due to the presence of different types of water the decay of the M_{xy} is described by the sum of many exponential functions in terms of many T_2 (T_{2x}). Low field NMR characterization on hydrogels and solutions has been performed by means of a Bruker Minispec mq20 (0.47 T). Transverse relaxation time (T_2) measurements have been carried out according to CPMG (Carr-Purcell-Meiboom-Gill) sequence with a 90-180°pulse separation of 1 ms at T=25°C. The T_{2x} discrete distribution has been obtained by fitting the experimental time (t) decay of the signal (I), related to the extinction of the xy component of the magnetization vector (M_{x-y}) by a sum of m exponential functions. The number of the T_{2X} obtained reveals the different types of water molecules entrapped into the matrix. In addition to the bulk water, it is possible to observe many relaxing times related to the interaction with different components of the material[9].

Biological tests.

Cytotoxicity and cells viability have been evaluated for an osteosarcoma cell line (MG63 ATCC® Number: CRL-1427™) and a fibroblast cell line (NIH/3T3 ATCC® CRL1658™) cells lines. Cytotoxicity has been evaluated by the lactate dehydrogenase cytotoxicity assay (SIGMA TOX-7LDH assay) and the Live/Dead

assay (Invitrogen™ LIVE/DEAD Viability/Cytotoxicity Kit). Viability has been evaluated through a modified LDH assay. Absorbance measurements have been performed on Tecan Nano Quant Infinite M200 Pro plate reader. MG63 and NIH/3T3 monolayers have been cultured in DMEM medium supplemented with 10% fetal bovine serum FBS (v/v), 100 U penicillin, 0,1 mg/ml streptomycin, L-glutamine 2 mM and maintained at 37 °C and 5% (v/v) CO_2. Once reached the 80-90% of confluence, Cells have been passaged twice a week using trypsin/EDTA 0.25%.

LDH assay: MG63 cells are seeded into a 24-well plates (50000 cells per well) and left to attach 24 hours before incubation with the material under investigation. Cells are incubated for 24 and 72 hours. After the incubation period, the cell medium (45µL) is mixed with 90µL of the reagent substrate mix in a 96-well plate and incubated for 30 minutes at room temperature in shelter from the light. The reaction is stopped by adding HCl 1M (1/10 volume). The absorbance is measured at 490nm and 690nm (phenol red). The amount of released LDH indicates the amount of both damaged and lysed cells. The percentage of death cells is calculated using the following equation:

$$\%Cytotoxicity = \frac{(Abs_{490} - Abs_{690} treated\ and\ untreated\ cells) - (Abs_{490} - Abs_{690} blank)}{(Abs_{490} - Abs_{690} untreated\ cells) - (A_{bs490} - Abs_{690} blank)} * 100$$

Live/Dead tests: the assay stain solution is a mixture of two highly fluorescent dyes that differentially label live and dead cells. The Live cell dye labels intact, viable cells green. It is membrane permeant and non-fluorescent until ubiquitous intracellular esterases remove ester groups and render the

molecule fluorescent. The Excitation (max) and Emission (max) are 494 nm and 515 nm, respectively. The Dead cell dye labels cells with compromised plasma membranes red. It is membrane impermeant and binds to DNA with high affinity. Once bound to DNA, the fluorescence increases >30-fold. The Excitation (max) and Emission (max) are 528 nm and 617 nm, respectively. The incubation time we employed depends on the tested material (6, 24 or 48 hours). After the incubation, the culture medium has been removed and the cells have been washed twice with PBS 1% (w/v). After the washing process, the cell have been incubated in presence of 90µL of assay stain solution for 45 minutes. The live and dead cells have been counted from 3 random snapshot per well. The cytotoxicity has been evaluated through the count of green and red labeled cells observed in the snapshots.

Modified LDH assay: cells have been seeded into 24-well plates (30000 MG63 cells per well and 40000 NIH/3T3 cells per well) and left 24 hours before incubation in presence of the material to promote the adhesion. The modified LDH assay has been employed to evaluate the degree of cell proliferation in presence of suspended CNTs. Cells have been incubated for 24 and 72 hours in presence of functionalized CNTs at different concentrations (10, 50 and 100 µg/mL). The LDH assay, previously described, has been modified to avoid the interference on the UV-Vis absorbance due to the presence of suspended CNTs. According to the LDH assay, the amount of released LDH is calculated on the culture medium after the induced-cell death. In the modified LDH assay proposed by Ali-Baucetta *et al.* the LDH content is assessed in intact cells that

survived the treatment[10]. Briefly, the medium culture is removed after the incubation period and cells are lysed in presence of 10 µL of lysis buffer (SIGMA TOX-7 kit) mixed with 100 µL of serum free medium for 45 min at 37°C. The cell lysate is diluted with 800 µl of serum free medium and centrifuged at 16100×g for 5 minutes in order to pellet down the suspended CNTs. 45 µL of the supernatant is mixed with 90 µL of LDH reagent substrate mix in a 96-well plate and incubated for 20 minutes at room temperature in shelter from the light.. The absorbance is measured at 490 nm and 690 nm (phenol red). The amount of detected LDH represents the number of cells that survived the treatment. The percentage of cell survival is calculated using the following equation:

$$\%Cell\ Survival = \frac{(Abs_{490} - Abs_{690} treated\ and\ untreated\ cells) - (A_{bs490} - Abs_{690} blank)}{(Abs_{490} - Abs_{690} untreated\ cells) - (Abs_{490} - Abs_{690} blank)} * 100$$

Cell counting

Cells proliferation has been also evaluated through the cell counting technique in presence of different concentrations of suspended functionalized CNTs (10, 50 and 100µg/mL). Cells have been seeded into 24-well plates, 30000 MG63 cells per well, and left to reach the adhesion for 24 hours before incubating. Cells have been incubated for 24 and 72 hours in presence of CNTs. Media has been removed and the wells have been washed twice with PBS 1%. Cells have been detached using trypsin-EDTA 0.25% and nuclei have

been counted with the particles counter COULTER Z Series (Instrumentation Laboratory, Beckman Coulter) with a size range of 4.55-15.55 µm.

References

1. I.M.N. Vold *et al*., A study of the chain stiffness and extension of alginate, in vitro epimerized alginate, and periodate-oxidized alginateusing size exclusion chromatography combined with light scattering and viscosity detectors. *Biomacromolecules*, **2006**, 7, 2136-2146.
2. H. Grasdalen *et al*., A p.m.r. study of the composition and sequence of uronate residues in alginates. *Carbohydr. Res*. 1979, 68, 23–31.
3. H. Grasdalen, High-field, 1H-n.m.r. spectroscopy of alginate: sequential structure and linkage conformations. *Carbohydr. Res*. 1983, 118, 255–260.
4. A. Malgaroli & R. Tsien. Glutamate-induced long-term potentiation of the frequency of miniature synaptic currents in cultured hippocampal neurons. *Nature*, **1992**, 357, 134-139.
5. G. Pastorin *et al*., Double functionalization of carbon nanotubes for multimodal drug delivery. *Chem. Comm*. **2006**, 1, 1182-1184.
6. S. Arepalli *et al*., Protocol for the characterization of single-wall carbonnanotube material quality. *Carbon*, **2004**, 42, 1783-1791.
7. E. Kaiser *et al.,* Color test for detection of free amino groups in the solid-phase synthesis of peptides. *Anal. Biochem.* **1970**, 34, 595-598.
8. R. Lapasin & S. Pricl. Rheology of industrial polysaccharides, theory and applications. *Chapman & Hall, London, GB*, **1995**.

9. G. Turco *et al*., Mechanical spectroscopy and relaxometry on alginate hydrogels: a comparative analysis for structural characterization and mesh size determination. *Biomacromolecules*, **2011**, 12, 1272–1282.
10. H. Ali-Boucetta *et al*., Cellular uptake and cytotoxic impact of chemically functionalized and polymer-coated carbon nanotubes. *Small,* **2011**, 7 (22), 3230-8

5. Carbon nanotubes-based substrates for neuronal cells and tissue cultures

As mentioned in the introduction nanodevices and nanomaterials can stimulate, respond to and interact with specific cells and tissues in order to induce desired physiological responses. Carbon nanotubes (CNTs) appear well suited for the design of novel neural and bone biomaterials[1].

During my PhD, we focused our efforts in this field of research. In particular the work did during

this period can be divided into two parts: the development of a conductive scaffold based on CNTs and biopolymers for the neuronal tissue regeneration and the characterization of CNTs based-alginate hydrogels and scaffolds for the bone tissue regeneration, both the mechanical and biological aspects.

Alginate (Alg) is an acidic block copolymer ables to crosslink through divalent cations forming 3D scaffolds that have demonstrated a good profile in the regeneration of myelinated and non-myelinated axons across spinal cord gaps[2-4].

Chitosan (CS), a natural polysaccharide, has been widely employed in the field of tissue regeneration due to its biocompatibility and cell adhesive behavior. Recently it has been also studied for the neuronal growth in three dimensions: the cationic nature is believed to contribute to increase the cell adhesion[5,6].

Hyaluronic acid (HA) is a non-sulfated glycosaminoglycane present in many tissues of the body such as connective, epithelial and neural tissue. As the materials described above, HA is also to be biocompatible and it crosslink very

easily using chemical agents. It has been demonstrated that modified hyaluronic acid based scaffolds enhance the neuronal cell proliferation and outgrowth[7,8].

5.1 CNTs and neuronal tissue regeneration

First of all I would like to describe the research activity developed by my colleagues in collaboration with Professor Ballerini's group within the framework of the "CarbonanoBridge" project. The electrophysiological and immunostaining studies reported in this chapter have been performed in collaboration with Alessandra Fabbro and Ambra Villari, neurophysiologists from the Life Science Department, B.R.A.I.N., University of Trieste. First of all the interaction and the effect of CNTs and others carbonaceous nanomaterial with hippocampal neuronal cells have been studied. The procedure to prepare CNTs-coated substrates mainly follows the work of Lovat and collaborators[9]. Basically the interaction between CNTs and hippocampal neuronal cells is based on the seeding of cells on a homogeneous carpet of pristine CNTs. On the other hand, organic functionalization was necessary to increase the solubility of CNTs in organic solvents and to improve the homogeneity on the glass substrate. The 1, 3-dipolar cycloaddition demonstrates more advantages with respect to other reactions, such as arylation reaction, probably because the introduction of less functional groups on the sidewalls allows a better dispersion of CNTs but permits to preserve the electronic structure of the aromatic network. Conductivity measurements of different networks of CNTs (pristine and functionalized) have been performed. The conductivity has been measured through a Jandel multimeter linked with a four-point probe. In particular, the different types of CNTs have been filtered on PTFE (polytetrafluoroethylene) filters paper by vacuum filtration and the conductivity of the network has been measured on the films obtained on the surface of the filters. This work has been done by Antonio Turco, PhD student

of professor Prato's group. Concerning the pristine material, the conductivity was 384.62 S/m. MWNTs functionalized through the 1,3-dypolar cycloaddition (heptanal/sarcosine) presented a conductivity of 500 S/m. The conductivity of the positively charged MWNTs functionalized trough the Tour reaction network decreased drastically up to 0.13 S/m. In order to perform biological tests, the spray coating technique to a glass coverslip support for functionalized f_2-MWNTs has been employed.

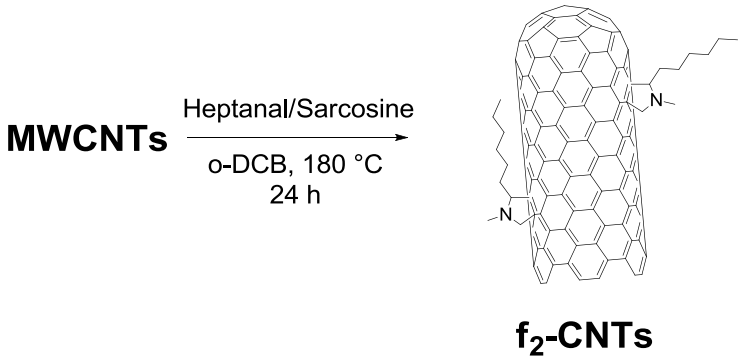

Scheme 1. Schematic representation of 1,3-dipolar cycloaddition of azomethine ylides reaction to CNTs.

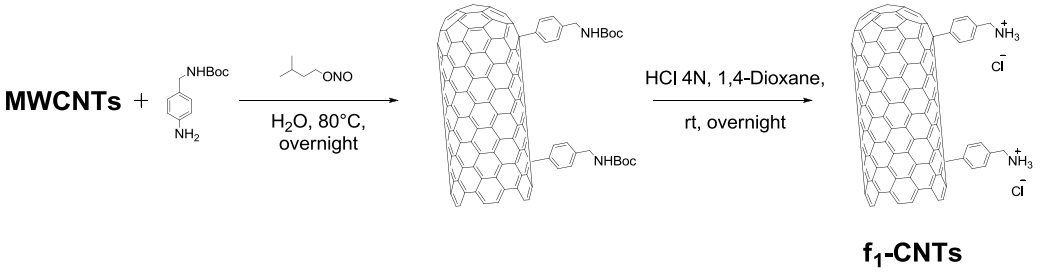

Scheme 2. Schematic representation of diazonium salt based arylation reaction to CNTs

In particular f_1-CNTs have been suspended in ethyl acetate and the solution has been sprayed on a glass coverslip placed in contact with a hot plate at 100°C. After the spray process, a density of f_1-CNTs film over the glass of about $7*10^{-5}$ mg/mm^2 has been achieved. The layered coverslips have been processed in an oven at 350°C under nitrogen atmosphere for 20 min in order to de-functionalize the CNTs avoiding damages to the electronic structure of the sidewalls. The presence

of a continuous conductive network on the surface of the glass support has been obtained. The sheet resistance of the CNTs layer has been measured through a Jandel four tips probe linked to Jandel RM3000 multimeter. The calculated value of conductivity is 6.25 S/cm. Neuronal cultures have been prepared from dissociated hippocampal neurons obtained from brains of neonatal rats. Cells have been grown on the substrates for 8 days at 37 °C in a humified incubator with 5% CO_2. SEM images show a high affinity between the spinal neurons and the carbonaceous substrate in terms of numerous and tight contacts (figure 1).

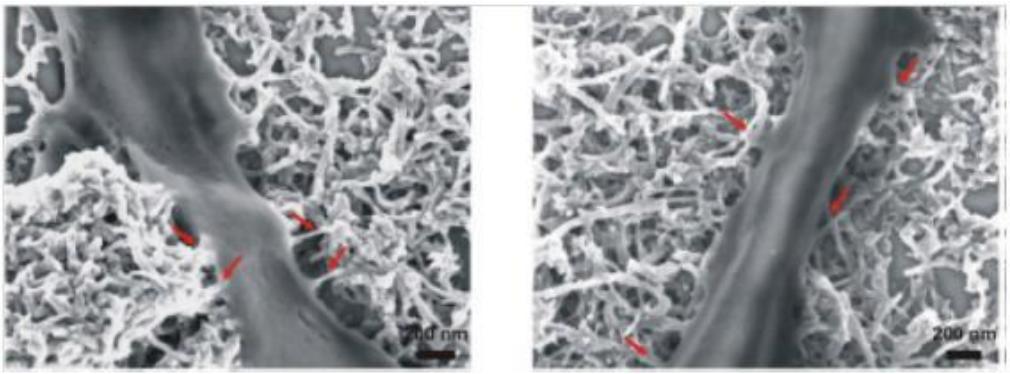

Figure 1. SEM images of neurites from spinal neurons grown on a MWCNT layer, showing the numerous and very tight contacts between MWCNTs and neuronal membranes (red arrows).

Electrophysiological recordings of the cellular activity has been performed employing the patch-clamp technique. A glass micropipette with an open tip with a diameter of about one micrometer is employed as electrode. The pipette is filled with a solution that mimic the ionic composition
of the extracellular medium. A chloride silver wire is placed in contact with the inner solution and conducts electric current to the amplifier. The micropipette is pressed against the cell membrane and a suction is applied to promote the formation of high resistance seal between the glass and the cell membrane (Figure 2). The presence of the seal allows us to electronically isolate the currents measured across the patched membrane with little competing noise.

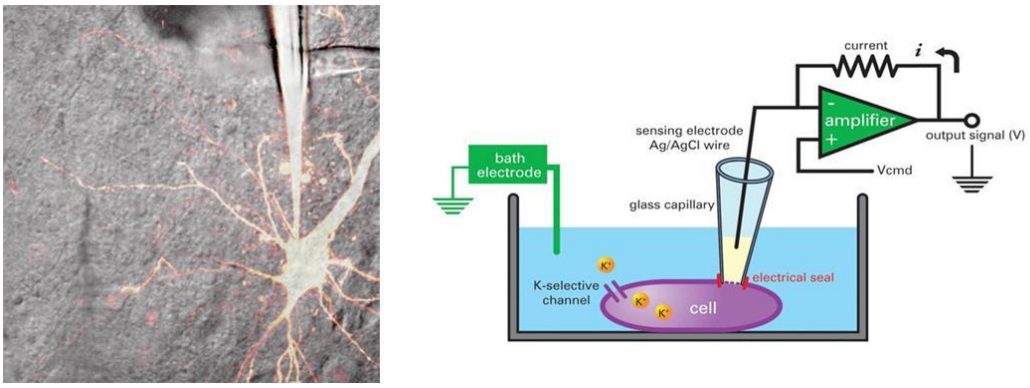

Figure 2. Patch pipette on a cultured neuron (left) and a schematic representation of the patch clamp mechanism.

In order to evaluate the presence of synaptic connections among the seeded neurons and the entity of the synaptic transmissions, it is possible to perform pairs of neuron recordings. The first presynaptic cell is stimulated in a current clamp configuration to generate an action potential. At the same time the activity of the second postsynaptic cell is recorded in a voltage clamp configuration. If the cells are not synaptically coupled, no electrical activity will be recorded on the

postsynaptic cell. If the two neurons form a synapse every presynaptic action potential will generate a correspondent postsynaptic current (PSC) at the postsynaptic site[10,11].

In conclusion of these experiments it has been possible to show a facilitation of functional maturation of spinal neurons seeded on a CNTs-covered substrate coupled with a selective modulation of gene expression. This peculiar behavior is probably due to a boost effect of CNTs in terms of increased adhesion of neurons to the substrate. The tight contact between the cellular membrane and the CNTs carpet might activate a cascade of

intracellular signaling events absent in fibers grown on control substrate[12,13]. As described in the previous chapters, in the last years, a huge numbers of papers have been published about the use of CNTs to support and favour neuronal growth. In the most of this published papers all known effects are limited to carbon nanotube/neuronal hybrids formed on a monolayer of dissociated brain cells[14,15]. On the other hand, studies involving more complex tissue model are still missing. For this purpose, slices of spinal cord explants have been used to monitor for several weeks the multi-layered nerve tissues in contact with MWNTs-based scaffolds[16].

5.2 Layer-by-layer technique

At the beginning of the work we tried to develop a bi-dimensional system based on the layer-by-layer technique to evaluate the compatibility with spinal cord slices[17,18]. This technique allows the stepwise growing up of multilayers based on the electrostatic self-assembly of positively and negatively charged compounds (Figure 3). In literature it is possible to find many applications and different types of material are employed for the growing up such as polyelectrolytes, proteins, nucleic acids, polymers, *etc*. We exploited this technique to produce thin films of functionalized CNTs and biopolymers. First of all, glass coverslip has been processed into a "Piranha" solution (H_2SO_4/30% H_2O_2 3:1) for 16 hours in order to clean the glasses and to produce negative charges on the surface[19,20].

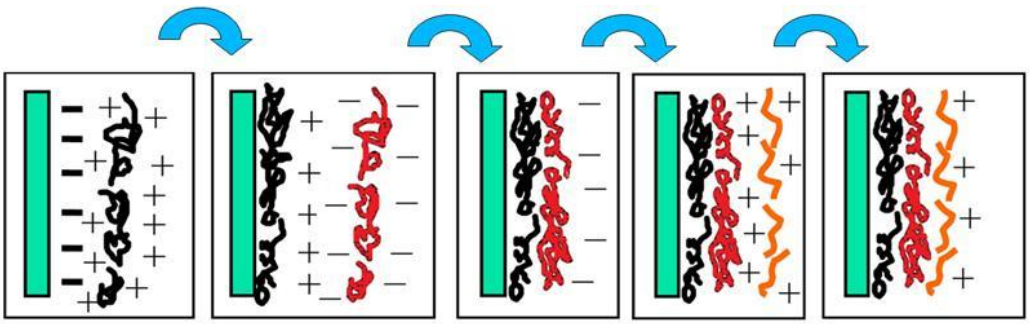

Figure 3. Schematic representation of the layer-by-layer technique on a glass substrate previously treated in piranha solution and dipped into positively and negatively charged polyelectrolitic solutions.

The glasses have been dipped into a polyelectrolyte solution of poly(dimethyldiallylammonium chloride) as first positively charged layer. After that, the glasses have been dipped for 30 minutes into the polymeric solution:

sodium alginate aqueous solution 1% (w/v) or hyaluronic acid sodium salt aqueous solution 1% (w/v). Glasses have been dipped into an aqueous solution of positively charged f_5-CNTs (Scheme 3) previously sonicated in order to obtain a good dispersion.

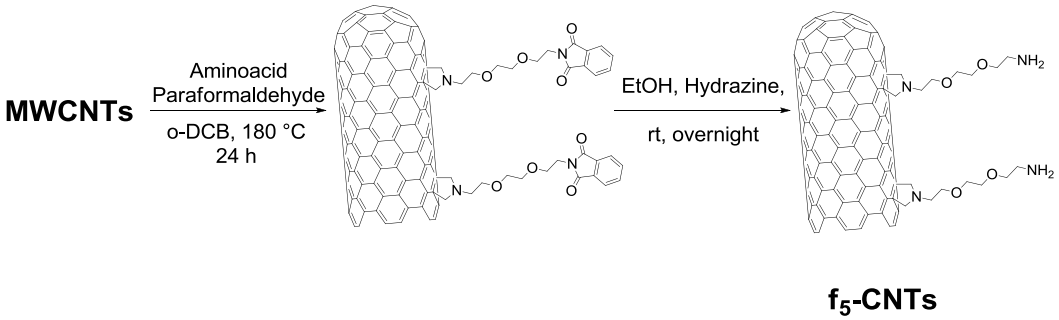

Scheme 3. Schematic representation of 1,3-dipolar cycloaddition of azomethine ylides reaction to CNTs.

After each dipping process (30 minutes), the glasses have been rinsed for 5 minutes in water and placed for other 5 minutes on a hot plate at 100 °C. The dipping process has been repeated 5 or 10 times in order to obtain a multilayer thin film. After SEM analysis, it has been possible to observe the presence of agglomerates on the surface both for alginate and hyaluronic acid (Figure 4).

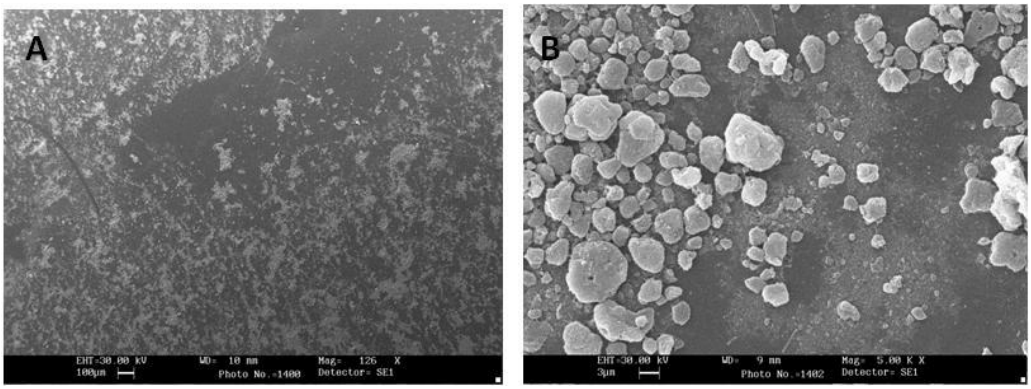

Figure 4. SEM images of alginate/f_5-CNTs layer-by-layer film. Scale bar is 100 µm A and 3 µm B.

In order to avoid the formation of aggregates, the polymer concentration has been decreased up to 0.05%. Unfortunately no good results have been obtained after the SEM analysis (data not shown). Anyway biological tests have been performed for LBL thin films: organotypic spinal cord slices have been deposited on the glass substrate in order to evaluate the biocompatibility with the material (Figure 5).

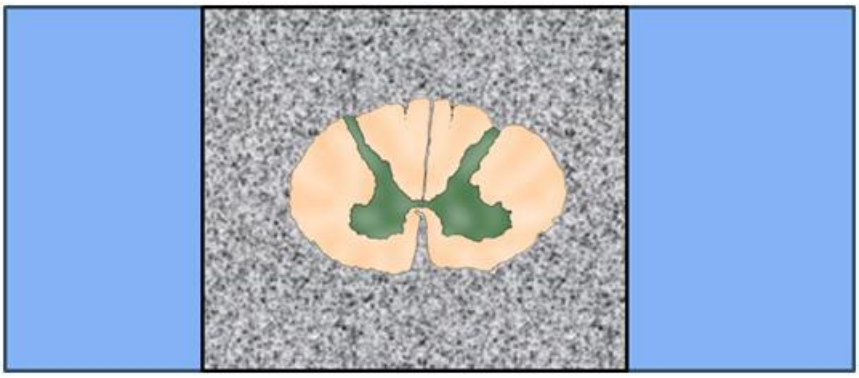

Figure 5. Schematic representation of organotypic spinal cord slices deposited on the glass substrate

Bright field images of spinal cord slices deposited on the LBL substrates show the lack of homogeneity of CNTs and after 1 or 2 weeks of incubation the neuronal tissue detached from the supports (Figure 6).

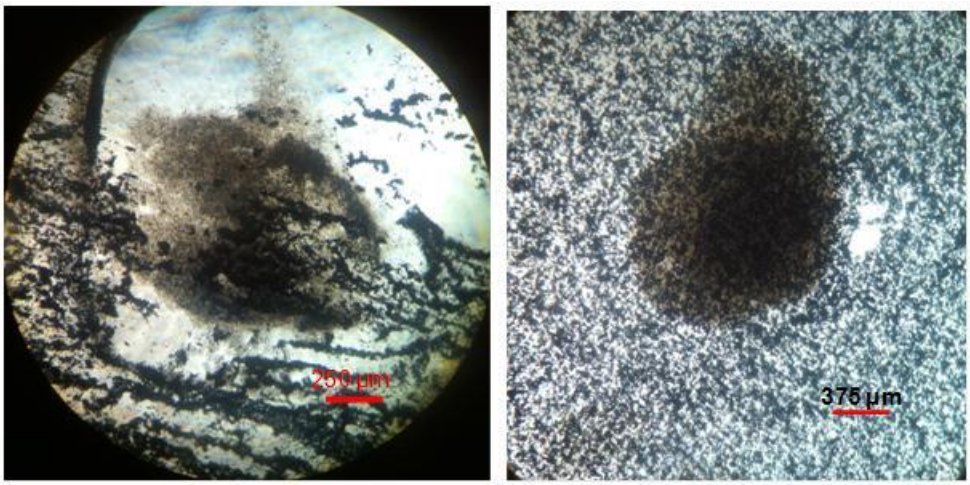

Figure 6. Bright field images of spinal cord slices deposited on the LBL substrates

On the other hand it has been possible to observe the complete detachment of the alginate/f_5-CNTs film from the glass coverslip. For this reason we decided to create a LBL film based on the interaction of two solutions of negatively and positively charged biopolymers, alginate 1% (w/v) and chitosan 0.5% (w/v). Functionalized CNTs (0.1% w/v as final concentration) have been suspended into the chitosan acidic solution (CH_3COOH 0.2 M) obtaining a very good dispersion[21]. It is demonstrated that solutions of polymers facilitate the suspension of CNTs. Unfortunately no good results have been obtained and for this reason we decides to change approach. Indeed also in this case the film detached from the glass coverslip and the film was too dark to allow the

use of the bright field microscope. By the LBL technique it has not be possible to verify and evaluate the viability and electrical activity of the spinal cord slices.

5.3 3D f-CNTs/alginate scaffolds

We decided to develop a three dimensional system able to electrically reconnect the communication among the nervous tissues[22-25]. First of all it has been employed the alginate polymer and MWNT modified through the 1,3-dipolar cycloaddition of azomethine ylides (f_5-CNTs). Alginate has been dissolved in milli-Q water and after its complete dissolution f_5-CNTs have been added under magnetic stirring in order to obtain a good dispersion of the tubes. After that, the solutions has been cured into 24-wells plates and the mixture has been freeze-dried to eliminate the presence of the water molecules obtaining a tridimensional structure like 'sponge' with cylindrically shape. In fact, the formation of ice crystals during the freezing process makes the scaffold porous. Then the scaffold was dipped into a $CaCl_2$ solution to crosslink the polymeric chains and after some washing cycles it was freeze-dried again (Figure 7).

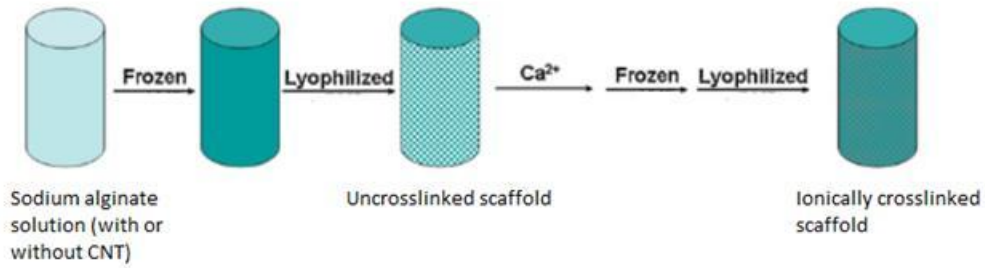

Figure 7. Schematic representation Ca^{2+} cross linked alginate porous scaffold preparation.

We decided to produce scaffolds with different ratios between polymer and CNT. Each scaffold hs been analyzed by thermogravimetric analysis (TGA) to

verify the ratio between the two components and by scanning electron microscopy (SEM) to observe the morphological aspect. On the other hand, each kind of scaffold has been produced also without CNT for comparison. The figure 3A represents a SEM image of a freeze-dried alginate scaffold without the nanostructure material where it is possible to appreciate the high porosity of the structure (Figure 8). It has been demonstrated that an higher concentration of the polymer produces a lower degree of porosity. On the other hand, a too low starting concentration makes the final crosslinked scaffold unstable during the rehydration process before the spinal cord slices culture tests (the explanation of the procedure is described later). The optimum starting concentration of alginate was found to be an alginate 2% w/v aqueous solution.

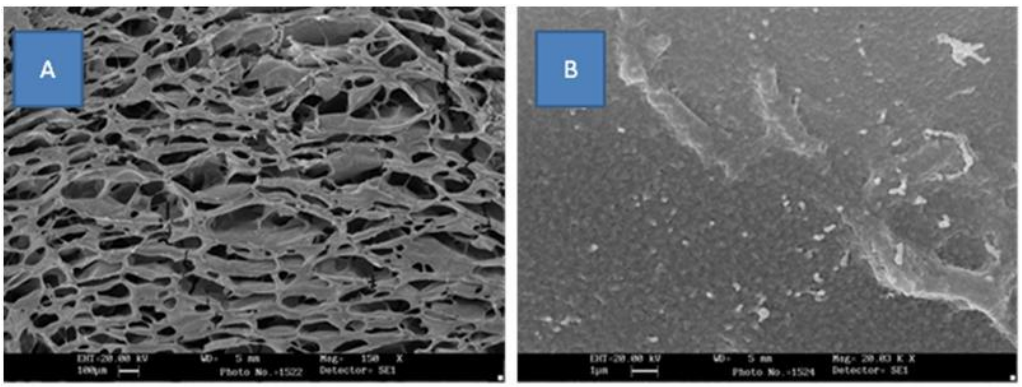

Figure 8. SEM micrographs of A) a freeze-dried alginate scaffold (scale bar 100 µm) B) the surface of alginate 2%/CNT 0.1% w/v scaffold (scale bar 1 µm).

After these considerations, two alginate 2% f-CNTs based scaffolds have been produced increasing the amount of nanotubes from 0.1% to 1% w/v. The

alginate 2% f-CNTs 0.1% w/v sample presented a low amount of CNT on the surface as it is possible to see from the SEM image (Fig. 3B). Only a limited number of CNT tips comes out from the polymeric matrix. Increasing tenfold the amount of CNT, the presence of the nanomaterial on the surface turns out to be greater but unfortunately there is a high presence of agglomerates as demonstrated by SEM images (Fig. 9).

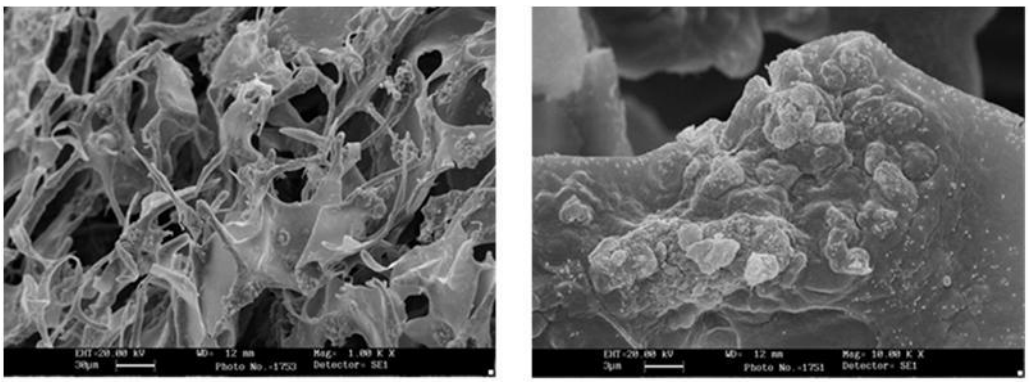

Figure 9. SEM micrographs of alginate 2% f-CNTs 0.1% scaffold (scale bars 30 µm and 3 µm respectively).

Thermogravimetric analysis has revealed a thermal stability of alginate and alginate/CNT scaffolds up to about 200 °C (Data not shown). In the range of 200-300 °C the weight decreases quickly due to the initial degradation of the polymeric chains. After 300 °C the samples lose weight gradually. This kind of analysis has been very useful to guarantee the stability of the scaffold after the sterilization procedure for the spinal cord slices culture tests.

We decided to perform a TEM analysis on a thin section of the scaffold in order to see the distribution of the tubes in the inner matrix (Figure 10). This

experiment confirmed the presence of CNT within the polymeric matrix in the form of agglomerates. From the TEM image it is possible to observe that only few carbon nanotubes, that form the aggregate, are coming out from the left side of the polymer section.

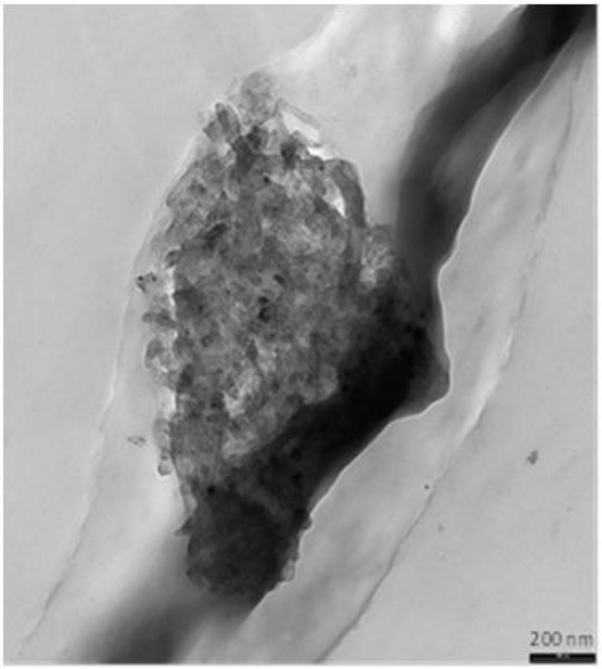

Figure 10. TEM image of a thin section of alginate/CNT scaffold.

To avoid the formation of aggregates, the procedure of production has been modified. The powder of alginate has been dissolved in water with a double concentration while the CNT have been solubilized in the same quantity of water by sonication. The CNT solution has been added dropwise to the polymer under magnetic stirring finally reaching the desired ratio. Apart the first step, the procedure is unchanged. The SEM analysis (Figure 11) has

confirmed that through the new procedure the formation of aggregates is decreased, which implies a greater dispersion of CNT into the polymeric matrix despite the sample has the lowest amount (0.1% f-CNTs).

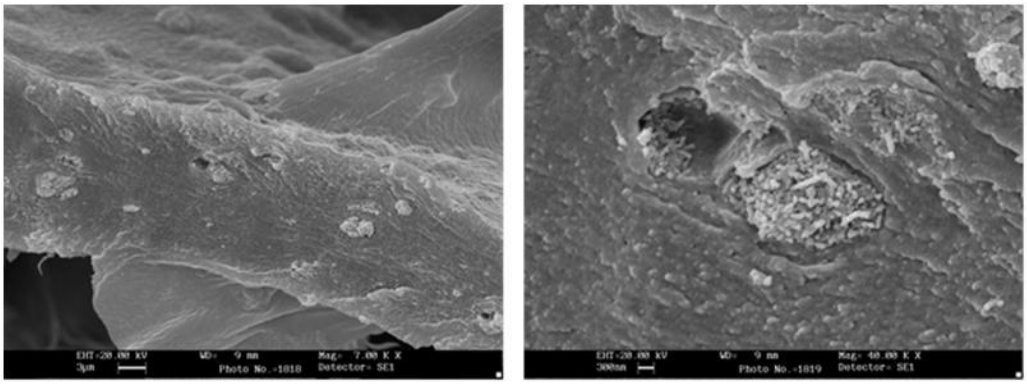

Figure 11. SEM micrographs of alginate 2% f-CNTs 1% scaffold (scale bars 3 µm and 300 nm respectively).

In order to study the interaction between the spinal cord tissue and the devices, the MWNTs-polymer scaffolds have been tested by prof. Ballerini's group through a spinal cord slices test. Sterilized and rehydrated hydrogel has been put in culture between two slices of spinal cord obtained from mouse embryos and fixed on a glass coverslip (Figure 12).

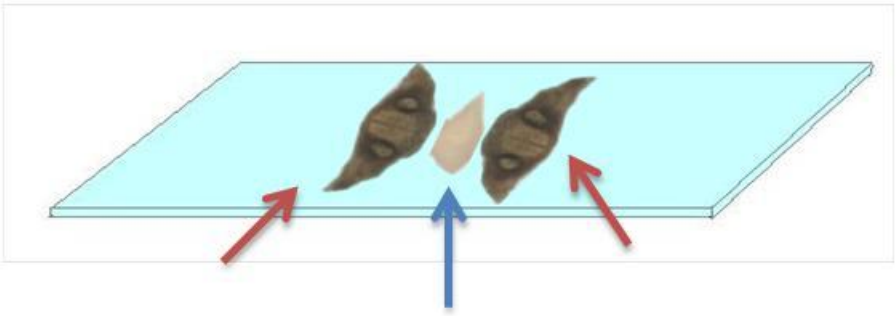

Figure 12. Schematic representation of electrophisiological experiment. Sterilized and rehydrated fragment of hydrogel (blu arrow) put in culture between two slices of spinal cord (red arrows).

After 1 week in culture, the hydrogel scaffold Alg 2% f-CNTs 0.1% w/v appeared stable and well integrated with the slices. After two weeks in culture, the appearence of the hydrogel was overall unchanged and the slices were healthy compared to the control. Electrophysiological recordings have been carried out and showed a physiological network activity of the slices. Bright field images have been taken during the electrophysiological investigation sessions (Figure 13) where it is possible to observe an evident physical interaction between the slices and the hydrogel through some elongations coming from the neural tissue.

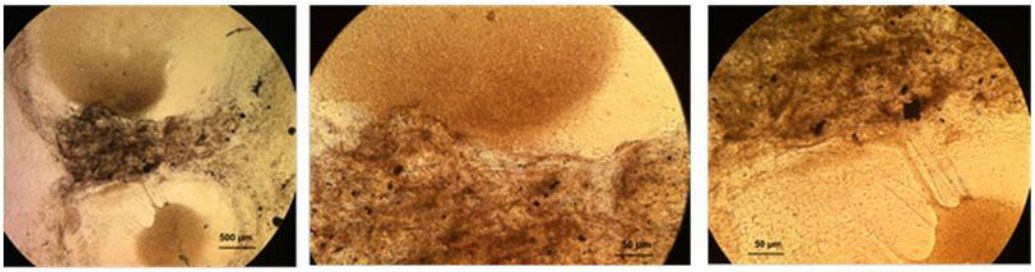

Figure 13. Bright field images of the two spinal cord slices and the hydrogel "bridge" in the middle (first image) and two enlargements focusing the interaction between the slice and the hydrogel.

5.4 2D f-CNTs/chitosan membranes

Regarding the 2D film we decided to create a different system of glass coverslip. In order to obtain a better view of the spinal cord slices we decided to apply the "bridge" technique seen previously for the alginate scaffold also to the films. By this way we decided to develop a conductive f-CNTs-based biopolymeric membrane previously cut in form of strip and fixed on a glass coverslip (Figure 14).

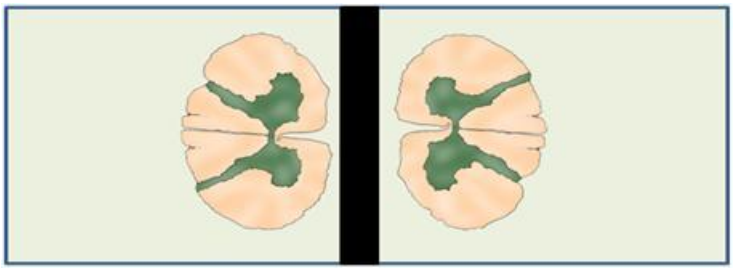

Figure 14. Schematic representation of electrophisiological experiment: a strip of a conductive f-CNTs-based biopolymeric membrane between two spinal cord slices.

To this purpose it has been necessary to develop a monolayared film based on the mixture of CNTs and biopolymers. Our attention has been focused on the chitosan polymer due to its behavior to get solubilized[26-28]. First of all a solution of chitosan and positively charged CNTs has been produced in acetic acid 0.2 M. F_1-CNTs (Tour reaction) have been employed in order to obtain a good dispersion into the acidic system. The first membrane (CS 2% w/v f_1-CNTs 1% w/v) has been obtained by pouring the solution onto a watch glass after a previous sonication of CNTs to avoid the formation of aggregates. The

solution has been left under the fume hood to allow the evaporation of the solvent. Five days later a dark layer upon the glass substrate has been obtained and it has been possible to easily detach the film. The free-standing membrane presents two sides: the opaque side (the one facing the air during the evaporation process) and the shiny side (the one facing the glass substrate). The membrane has been characterized through SEM analysis (Figure 15 and 16). It is possible to observe the presence of CNTs in both sides but the dimensions of the tubes suggest us that the polymeric chains are completely wrapping the tubular structure.

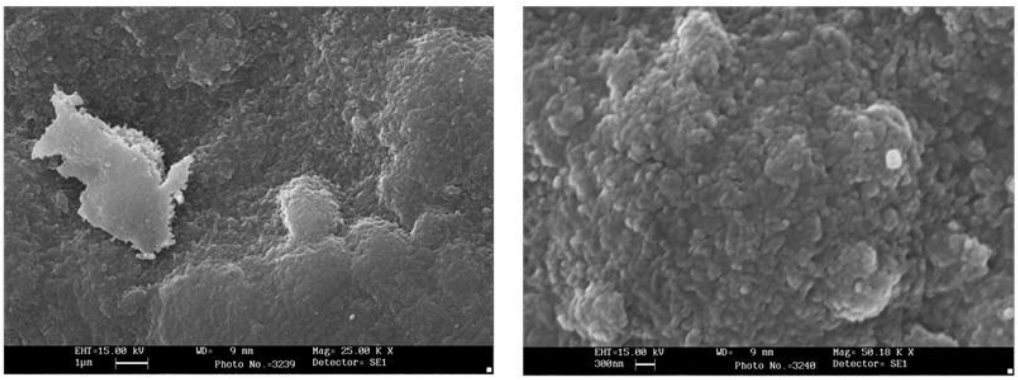

Figure 16. SEM images of the opaque side of the membrane. Scale bar 1 µm on the left and 300 nm on the right.

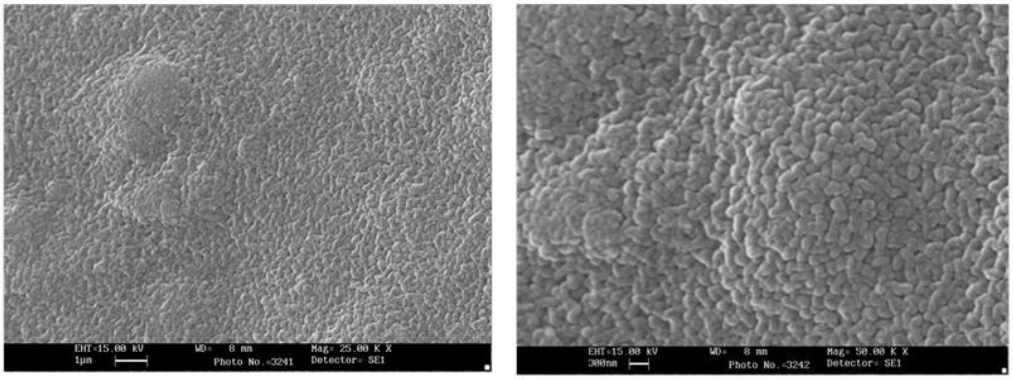

Figure 17. SEM images of the shiny side of the membrane. Scale bar 1 µm on the left and 300 nm on the right.

Conductivity measurements have been performer on the membrane but unfortunately no electrical activity has been recorded. On the other hand the membrane showed a perfect resistance during the dipping test in aqueous solution. No morphological changes have been observed.

Another membrane has been produced decreasing the amount of chitosan to the ratio 1:1 polymer/CNTs according to the methodology seen before. SEM analysis of the shiny and opaque sides has been performed (Figure 18 and 19).

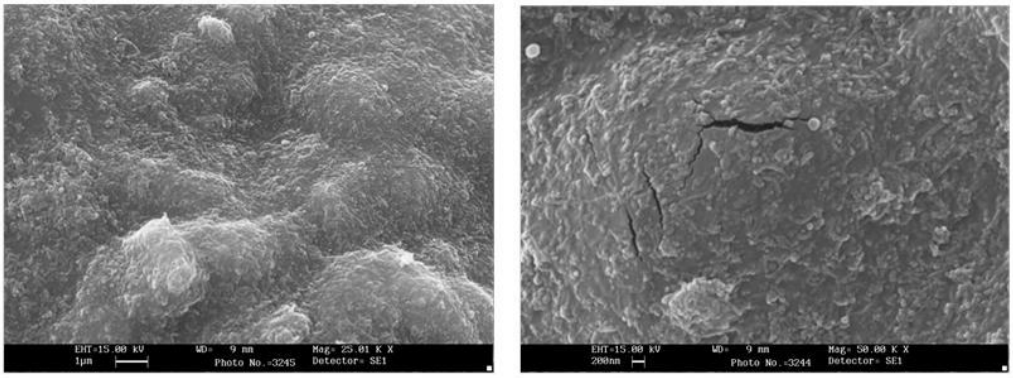

Figure 18. SEM images of the opaque side of the membrane. Scale bar 1 µm on the left and 200 nm on the right.

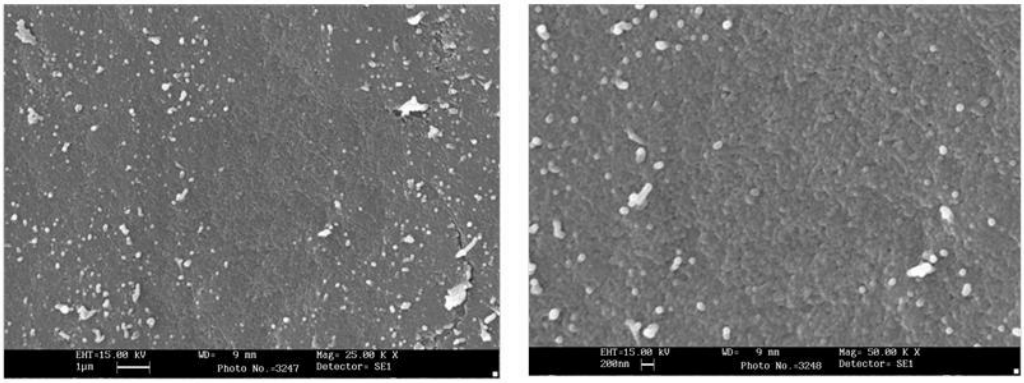

Figure 19. SEM images of the shiny side of the membrane. Scale bar 1 µm on the left and 200 nm on the right.

Conductivity measurements have been performer in order to verify if the decreased amount of polymer could had allowed the electrical conductivity into the nanostructured material (Table 1). It has been demonstrated that decreasing the amount of chitosan the stability of the membrane dipped in

aqueous solutions remains stable and the material turns out to be electrically conductive.

	opaque side	shiny side
Ω	1300	1400
ρ(Ω*cm)	49,89	53,73
ς (S/m)	2,004	1,86

Table 1. Conductivity values of both opaque and shiny sides of the membrane.

However it has not be possible to calculate the absolute value of sheet resistance of the membrane since the two sides are characterized by different values of conductivity. Irrespective of the differences in conductivity, the thickness has been measured and the membrane is homogeneous (29,5 µm ± 8,1).

In order to have a blank substrate for comparison, a chitosan membrane has been produced from a starting solution of polymer 1% w/v in acetic acid 0.2 M. SEM analysis has been performed and in this case no morphologic differences between the two sides have been detected (Figure 20). Moreover no electrical conductivity has been recorded.

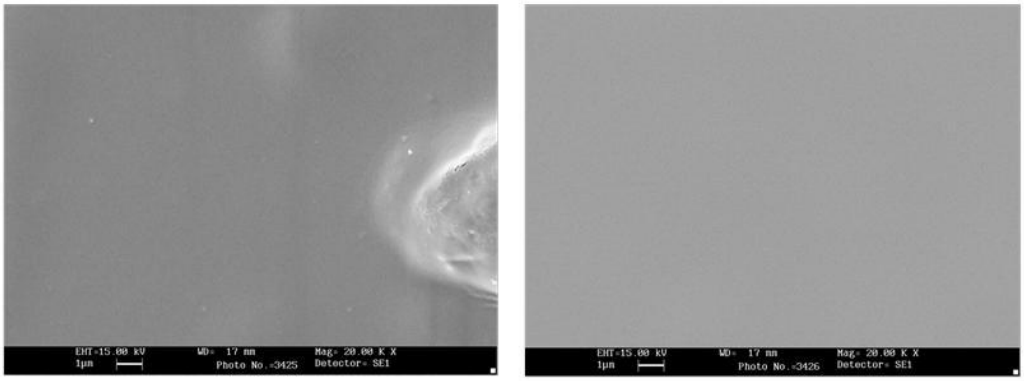

Figure 20. SEM images of chitosan membrane, opaque side on the left and shiny side on the right. Scale bar 1 µm.

Employing the Chitosan 1% f_1-CNTs 1% it has been possible to prepare the glass coverslip substrate with the conductive strip exploiting the polydimethylsiloxane as adhesive agent to fix the extremities of the membrane to the glass. Polydimethylsiloxane (PDMS) belongs to a group of polymeric organosilicon compounds that are commonly referred to as silicones. The chemical formula for PDMS is $CH_3[Si(CH_3)2O]_nSi(CH_3)_3$. PDMS is optically clear, inert, non-toxic and non-flammable. The biocompatibility of the material with neuronal cells has been already demonstrated by many papers that describe the use of PDMS as a material ables to promote the neuronal cells growth and differentiation[29,30]. SYLGARD® 184 Silicone Elastomer from Dow Corning (PDMS) was prepared in a glass dish using 10 parts of monomer and one part of curing agent by weight. After the deposition of the PDMS drops and the membrane strip, the substrate has been cured at room temperature for 3 days.

The same typology of chitosan/f_1-CNTs membrane has been produced employing Millipore filters degradable in acetone. The solution has been poured into the filtration apparatus and after 7 days the filter has been recovered. In parallel the membrane has been also produced employing pristine CNTs in order to evaluate the effect of the positively charged moiety on the carbonaceous sidewall (Figure 21).

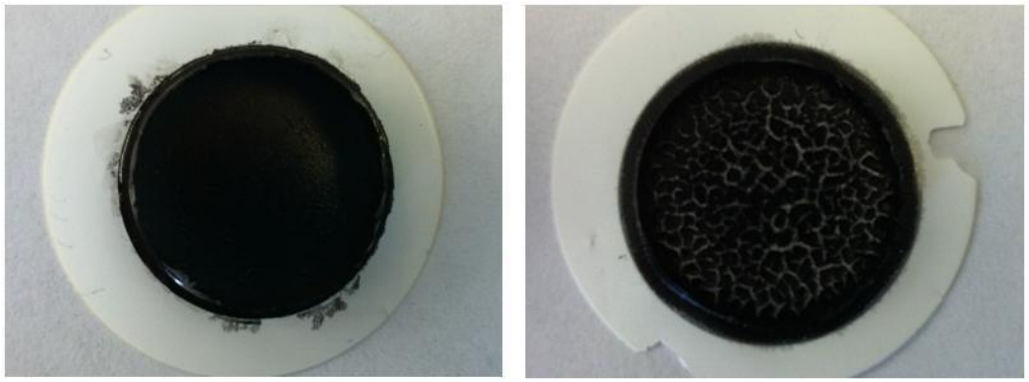

Figure 21. Chitosan/f_1-CNTs membrane produced on degradable filters with positively charged f-CNTs (left) and pristine CNTs (right).

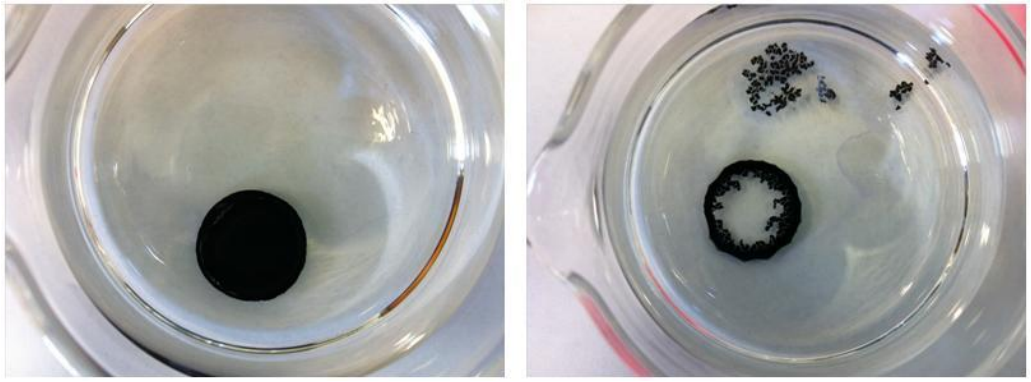

Figure 22. Chitosan/CNTs membrane with positively charged f_1-CNTs (left) and pristine CNTs (right) dipped in acetone during the degradation process of the filter.

After the degradation of the filter, the CS 1% f_1-CNTs 1% was perfectly intact and handle, while the CS 1% pristine CNTs 1% collapsed (Figure 22). Also in this case a chitosan 1% membrane has been produced and it remained intact after the removal of the filter. For the membranes SEM analysis has been performed. The chitosan 1% membrane the membrane exhibits a smooth surface with respect to the side exposed to the air during the evaporation of the solvent, while the side in contact with the filter presents aggregates (Figure 23). On the other hand, CS 1% f_1-CNTs 1% showed at SEM analysis a continuous layer of nanotubes for both sides (Figure 24 and 25).

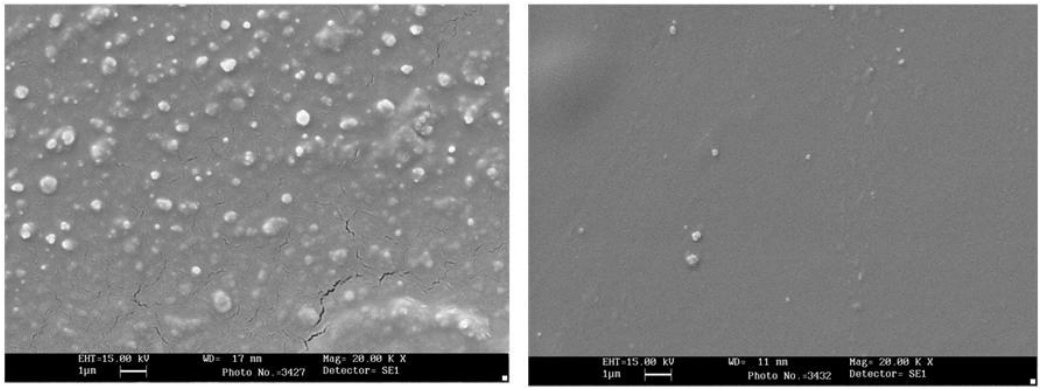

Figure 23. SEM images of chitosan membrane, filter side on the left and air side on the right. Scale bar 1 µm.

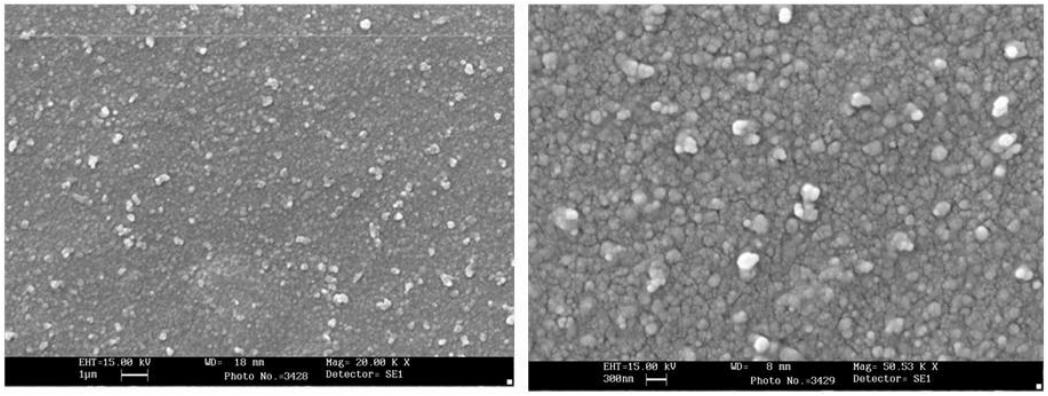

Figure 24. SEM images of chitosan/f_1-CNTs membrane filter side. Scale bar 1 µm (left) and 300 nm (right).

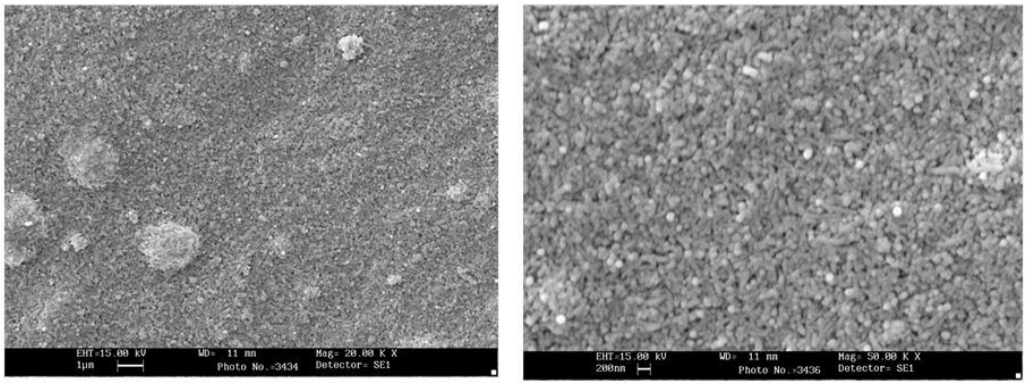

Figure 25. SEM images of chitosan/f_1-CNTs membrane air side. Scale bar 1 µm (left) and 200 nm (right).

Also in this case, from SEM images it is possible to observe a difference between the CNTs aspect comparing the two sides. The CNTs in contact with the filter present a larger diameter than the layer of the air side. That could be due to a segregation process between the polymeric chains and the functionalized nanostructures seen also for the previous membrane prepared

on the watch glass. However The membrane showed a conductivity values for both sides comparable to the previous one. On the other hand, the membrane obtained by pouring the solution onto the watch glass was much more handle during the rinsing process in milli-Q water before the attachment on the glass coverslip. Through this simple technique it has been possible to fix a thin strip of a conductive membrane on a glass coverslip creating by this way a system to be tested with spinal cord slices.

5.5 3D f-CNTs/chitosan scaffolds

The transition from 2D to 3D structures based on chitosan and functionalized CNTs followed different approaches[31-34]. In this part of the work, both f_1-CNTs (diazonium salt-based arylation reaction) and f_5-CNTs (1,3-dipolar cycloaddition of azomethine ylides reaction) have been employed. The production of chitosan/CNT scaffolds has followed a similar procedure of freeze-drying described previously. F_5-CNTs have been dispersed in acetic acid and then added to the chitosan acidic solution under magnetic stirring in order to avoid the formation of agglomerates into the polymer network. After a previous first freeze-drying step, the tridimensional structure have been covalently or ionically crosslinked. The crosslinked scaffolds have been washed in a milli-Q water bath to remove the excess of chemical agents and freeze-dried again. The solubility of chitosan in acidic solutions makes the scaffolds stable in the buffers employed in the culture tests independently of its starting concentration. Nevertheless, it has been selected the 2% w/v chitosan concentration for the preparation of next devices. The SEM analysis of the first trial of scaffolds (CS 2% CNTs 0,1%) has shown a placement of the carbon nanotubes very similar to the alginate/CNT scaffolds seen before (Figure 26).

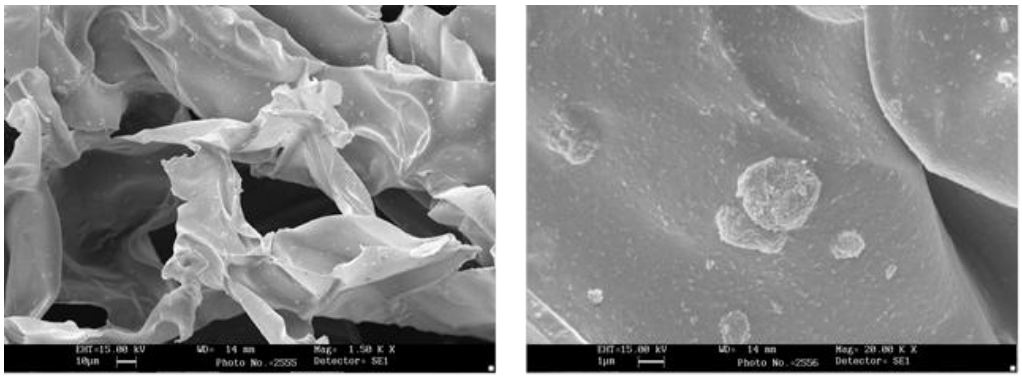

Figure 26. SEM micrographs of chitosan 2% f_5-CNT 0,1% scaffold (scale bars 10 µm and 1 µm respectively).

We decided to make the same structure employing carbon nanotubes modified through the diazonium salt-based arylation reaction and the result has been a better dispersion into the polymeric network. We decided to make a new scaffold increasing tenfold their amount. Chitosan 2% f_1-CNT 1% scaffolds both chemically and ionically crosslinked have shown from SEM images a high presence of carbon nanotubes on the polymeric network surface (Figure 27). The surface of the polymeric network is characterized by a limited number of aggregates surrounded by a great amount of carbon nanotubes. It hasn't been possible to obtain a tridimensional structure completely covered by CNT, nevertheless the last trial of samples exhibits a much more homogeneous dispersion of the tubes into the polymeric architecture.

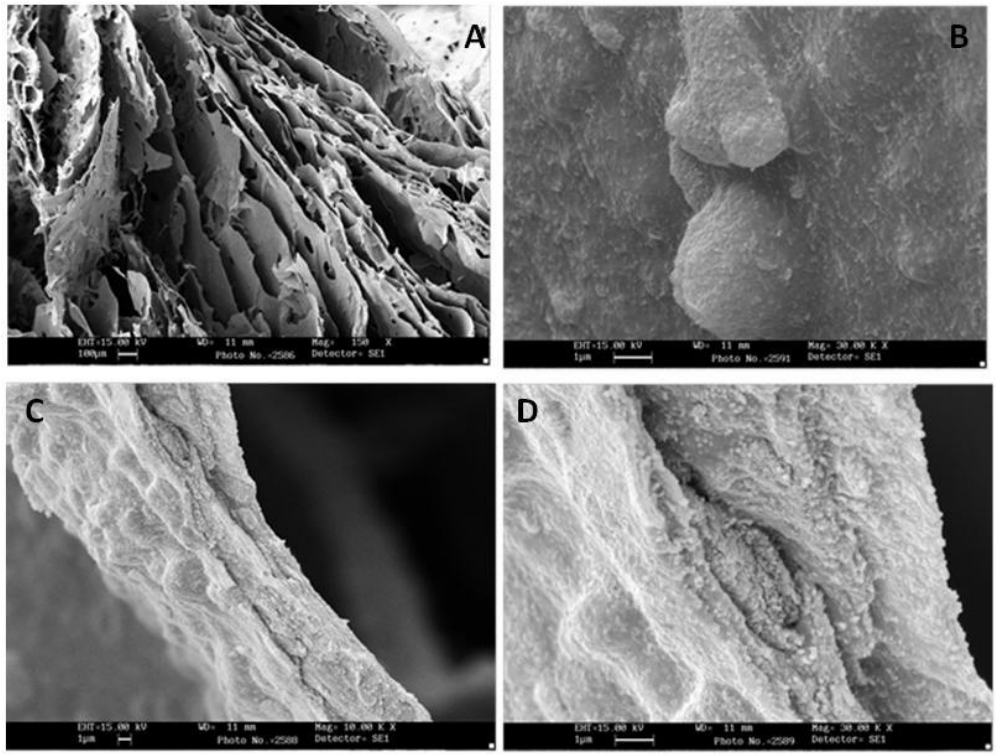

Figure 27. SEM micrographs of chitosan 2% f_1-CNTs 1% scaffold covalently crosslinked (scale bars 100 µm A and 1 µm B,C and D).

Nevertheless the high presence of CNTs into the 3D polymeric structure, the scaffold didn't show the electrical conductivity. Considering the stability of the material we decided to change approach in the production procedure. The ISISA process (ice segregation induced self assembly) has been employed to reach both a stable and conductive CNTs-based biopolymeric scaffold.

5.6 The ISISA technique

The ISISA technique consists in a bottom-up process based on the unidirectional immersion in liquid nitrogen of a colloidal aqueous suspension and subsequent freeze-drying. The process has already demonstrated its suitability for the preparation of inorganic, organic and hybrid macroporous monoliths and fibers by freezing of different gels and colloidal suspensions. The formation of crystalline ice during the dipping phase in liquid nitrogen causes the rearrangement of the solute initially dispersed in the aqueous medium. The solute in fact tends to be organized in planes parallel with the direction of immersion interspersed with ice crystals[35-37] (Figure 28).

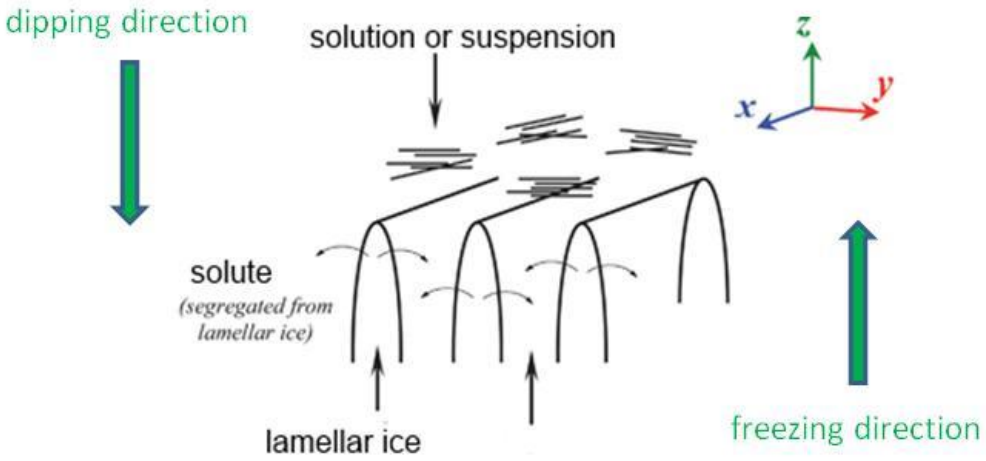

Figure 28. Schematic representation of the directional freezing process.

A cryogel is obtained after the freeze drying process. Cryogels are macroporous structures characterized by walls of matter enclosing empty

areas where ice crystals originally resided. Recently the ISISA technique has been widely employed and the capacity of ice-templating processes to control the morphology of the resulting macroporous structures has been demonstrated. by the use of unidirectional freezing at a controlled immersion rate[38]. The freezing step is very important to produce desirable porous structure. Different conditions of freezing including the freezing temperature, the solute concentration, the solvent, the direction of freezing and the immersion rate are very crucial on the resulting pore structure of the materials. First of all CNTs have been functionalized through the 1,3-dypolar cycloaddition (heptanal/sarcosine) to obtain f_2-CNTs. Contrary to scaffold seen before, it has been necessary to employ neutral charged CNTs in order to obtain the desired result. CNTs have been dispersed in CH_3COOH 0.2 M, sonicated and mixed with the chitosan solution under magnetic stirring obtaining the final concentration of CS 2% w/v f_2-CNTs 3% w/v. The solution has been dipped into the liquid nitrogen through the use of an insulin syringe in order to finally obtain a cylindrical shape scaffold. A specific dipping rate(2.6 mm/min) has been achieved through the use of a syringe pump. After the freezing process the sample has been freeze-dried. SEM analysis confirmed the lamellar inner structure and the presence of CNTs on the surface (figure 29).

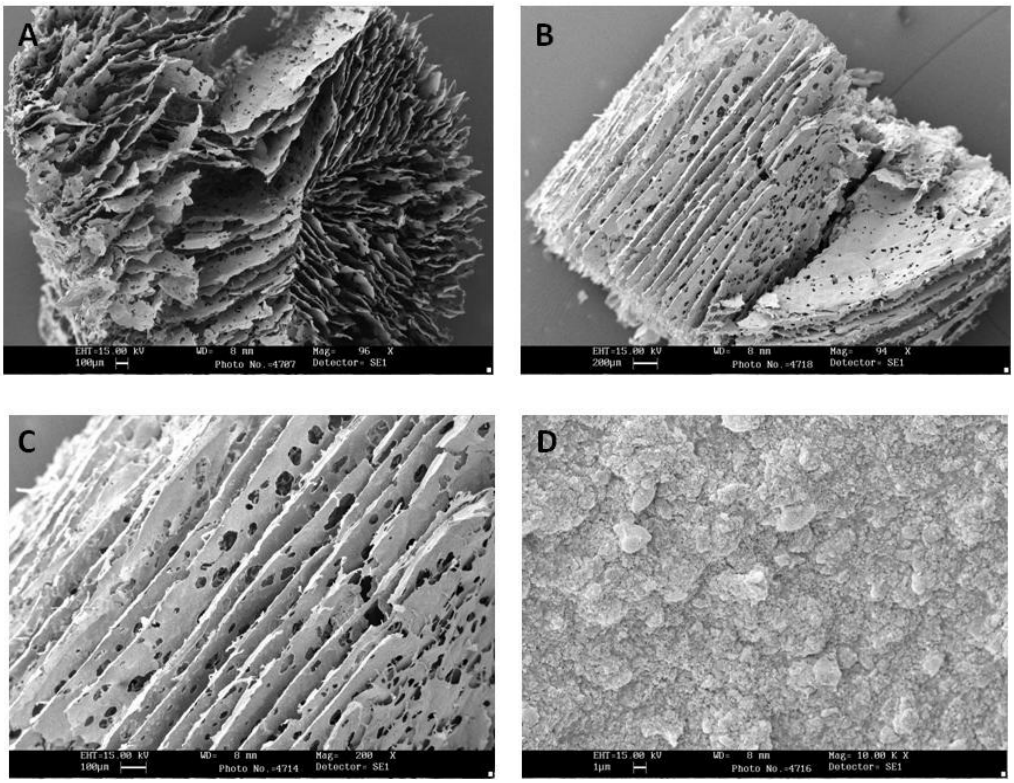

Figure 29. SEM micrographs of chitosan 2% f_2-CNTs 3% ISISA scaffold. Images A,B and C: lamellar inner structure. Image D: lamellar surface completely covered by CNTs. (scale bars 100 µm A and C, 200 µm B and 1 µm D).

For our purpose we decided to set a low dipping rate in order to obtain an increased spacing among the aligned "sheets" of chitosan and CNTs[39,40]. As already reported in literature, when the dipping rate decreases, the water molecules crystallized slowly and the solute has more time to pour out from the in-growing crystals. Unfortunately in this case the production of the blank sample of chitosan has not be possible due to the instability of the freeze-dried scaffold.

Conductivity measurements have been carried out. First of all the material has been tested through the tester in order to verify the current propagation. After that immediate check, conductivity characterization has been performed through the four-point probe (previously described).

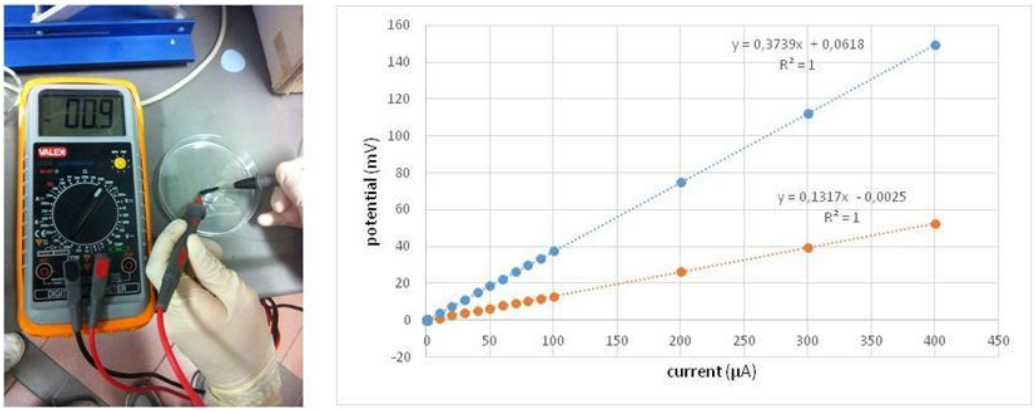

Figure 30. Conductivity measurement with the tester through the entire length of the scaffold (left). Current vs potential plot (right): dipping direction (orange dots) and horizontal plane (blu dots).

The conductivity measurements demonstrates how the alignment of the inner structure of the scaffold confers a preferential directionality to the conductivity. In both the directions, the material showed an ohmic behavior. The ratio of the voltage to the current gives the value called resistance (Ω). The resistance indicates the ability of the material to be crossed by a current. The slope of the curves in Figure 30 shows a lower resistance value for the vertical line following the dipping direction (0.13 MΩ) than the resistance registered along the horizontal line (0.38 MΩ). Also the stability of the

material has been evaluated. A fragment of the scaffold has been dipped in milli-Q water under magnetic stirring and in parallel another fragment in ethanol. The scaffold shows a complete instability in water since after few minutes whereas after 7 days in ethanol it is perfectly intact. After 7 days in ethanol the fragment of the scaffold has been recovered and dipped in milli-Q water. The scaffold remained stable also in water probably due to the denaturation process of biopolymeric chains in presence of alcohols (Figure 31). Despite the denaturation process, the scaffold remained electrically conductive.

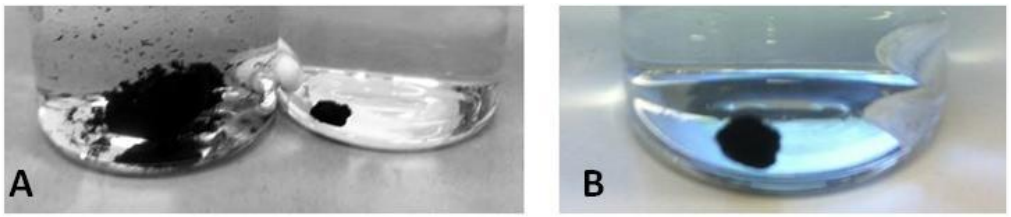

Figure 31. ISISA scaffold fragments dipped in water and ethanol (A, lef and right respectively). Fragment dipped in water after the first step in ethanol (B).

Through the ISISA technique it has been possible to produce a three dimentional CNTs-based biopolymeric scaffold that follows different requirements described in the introductive chapters. The biocompatibility of the materials, the guide channel inner structure, the stability in aqueous media and the directional conductivity. Thanks to this directionality we hope to be able to maintain the directionality of an electrical neuronal signal as usually happens in a neuronal network, where the back propagating

phenomena are prevented. For these reasons the CS/CNTs ISISA scaffold could be a good candidate to be tested on complex nervous tissues.

References

1. S. Bosi *et al*., Carbon nanotubes in tissue engineering. *Topics in Current Chemistry* **2013**.
2. J.L. Bron *et al*., Engineering alginate for intervertebral disc repair. *J. Mech. Behav. Biomed*. **2011**, 4, 1 1 9 6 – 1 2 0 5.
3. T. Hashimoto *et al*., Peripheral nerve regeneration using non-tubular alginate gel crosslinked with covalent bonds. *J. Mater. Sci.: Mater. Med*. **2005**, 16, 503– 509.
4. D. Szarek *et al.,* Influence of calcium alginate on peripheral nerve regeneration: *In vivo* study. *Biotechnol. Appl. Biochem*. **2013**, 60, 547–556.
5. J.M Zuidema *et al*., Fabrication and characterization of tunable polysaccharide hydrogel blends for neural repair. *Acta Biomater*. **2011**, 7, 1634–1643.
6. Y.C. Huang *et al*., Effects of laminin-coated carbon nanotube/chitosan fibers on guided neurite growth. *J. Biomed. Mater. Res. A,* **2011**, 99, 86-93.
7. B.C. Thompson *et al*., Carbon nanotube biogels. *Carbon*, **2009**, 4 7, 1282–1291.
8. X. Wang *et al*., Hyaluronic acid-based scaffold for central neural tissue engineering. *Interface Focus*, **2012**, 2, 278-291
9. V. Lovat *et al*., Carbon nanotubes substrates boost neuronal electrical signaling. *Nano Lett.* **2005**, 5, 1107-1110.

10. A. Mazzatenta *et al*., Interfacing neurons with carbon nanotubes: electrical signal transfer and synaptic stimulation in cultured brain circuits. *J. Neurosci*. **2007**, 27, 6931-6936.
11. N.W.S. Kam & N. Kotov, Electrical stimulation of neural stem cells mediated by humanized carbon nanotube composite made with extracellular matrix protein. *Nano Lett*. **2009**, 9, 273-278.
12. G. Cellot et al., Carbon nanotubes might improve neuronal performance by favouring electrical shortcuts. Nature Nanotechnol. 2009, 4, 126-133.
13. P. Galva-Garcia *et al*., Robust cell migration and neuronal growth on pristine carbon nanotubes sheets and yarns. *J. Biomat. Sci*. **2007**, 18, 1245-1261.
14. G. Cellot *et al*., Carbon nanotube scaffolds tune synaptic strength in cultured neural circuits: novel frontiers in nanomaterial-tissue interactions. *J. Neurosci*. **2011**, 31, 12945-12953.
15. E. Malarkey *et al*., Conductive single-walled carbon nanotube substrates modulate neuronal growth. *Nano Lett*. **2009**, 9, 264-268.
16. A. Fabbro *et al*., Adhesion to carbon nanotube conductive scaffolds forces action-potential appearance in immature rat spinal neurons. *Plos One*, **2013**, 8, 1-14.
17. E. Jan & N.A. Kotov, Successful differentiation of mouse neural stem cells on Layer-by-Layer assembled single-walled carbon nanotube composite. *Nano Lett*. **2007**, 7, 1123-1128.
18. T. Boudou *et al*., Multiple Functionalities of Polyelectrolyte Multilayer Films: New Biomedical Applications. *Adv. Mater*. **2010**, 22, 441-467.

19. S.W. Lee *et al*., Layer-by-layer assembly of all carbon nanotube ultrathin films for electrochemical applications. *J. Am. Chem. Soc*. **2009**, 131, 671–679.
20. F. Rivadulla *et al*., Layer-by-layer polymer coating of carbon nanotubes: tuning of electrical conductivity in random networks. *J. Am. Chem. Soc***. 2010**, *132*, 3751–3755.
21. T.I. Croll *et al*., A blank slate? Layer-by-layer deposition of hyaluronic acid and chitosan onto various surfaces. *Biomacromolecules*, **2006**, 7, 1610-1622.
22. G. Perale et al., Hydrogels in Spinal Cord Injury Repair Strategies. *ACS Chem. Neurosci*. **2011**, 2, 336-345.
23. M. Kawaguchi *et al*., Preparation of carbon nanotube-alginate nanocomposite gel for tissue engineering. *Dental Materials Journal*, **2006**, 25,719—725.
24. N.N. Madigan *et al*., Current tissue engineering and novel therapeutic approaches to axonal regeneration following spinal cord injury using polymer scaffolds. *Respiratory Physiology & Neurobiology*, **2009**, 169, 183–199.
25. L.N. Novikova *et al*., Alginate hydrogel and matrigel as potential cell carriers for neurotransplantation. *J. Biomed. Mater. Res. A*. **2006**, 77, 242-252.
26. S-F. Wang *et al*., Preparation and mechanical properties of chitosan/carbon nanotubes composites. *Biomacromolecules*, **2005**, 6, 3067-3072.

27. S. Amado *et al*., Use of hybrid chitosan membranes and N1E-115 cells for promoting nerve regeneration in an axonotmesis rat model. *Biomaterials*. **2008**, 29, 4409-4419.
28. Y. Yuan *et al*., The interaction of Schwann cells with chitosan membranes and fibers in vitro. *Biomaterials,* **2004**, 25, 4273–4278.
29. S.-J. Kim *et al*., Surface modification of polydimethylsiloxane (PDMS) induced proliferation and neural-like cells differentiation of umbilical cord blood-derived mesenchymal stem cells. *J. Mater. Sci.: Mater. Med*. **2008**, 19, 2953-2962.
30. P. Thiébaud *et al*., PDMS device for patterned application of microfluids to neuronal cells arranged by microcontact printing. *Biosens. Bioelectron*. **2002**, 17, 87-93.
31. L. Zeng *et al.,* Evaluation of the chitosan/glycerol-*β*- phosphate disodium salt hydrogel application in peripheral nerve regeneration. *Biomed. Mater*. **2010**, 5, 035003.
32. C.Y. Hsieh *et al*., Analysis of freeze-gelation and cross-linking processes for preparing porous chitosan scaffolds. *Carbohydr. Polym*. **2007**, 67, 124–132.
33. S. Chatterjee *et al*., Enhanced mechanical strength of chitosan hydrogel beads by impregnation with carbon nanotubes. *Carbon*, **2009**, 47, 2933-2939.
34. C. Lau & M.J. Cooney. Conductive Macroporous Composite Chitosan-Carbon Nanotube Scaffolds. Langmuir, 2008, 24, 7004-7010.
35. M.F. Butler *et al*., Growth of solutal ice dendrites studied by optical interferometry. *Cryst. Growth Des*. **2001**, 2, 59-66.

36. M.F. Butler *et al*., Freeze concentration of solutes at the ice/solution interface studied by optical interferometry. *Cryst. Growth Des*. **2002**, 2, 541-548.
37. H. Zhang & A.I. Cooper. Aligned porous structures by directional freezing. *Adv. Mater*. **2007**, 19, 1529-1533.
38. S. Deville *et al*., Ice-templated porous alumina structures. *Acta Biomater*. **2007**, 55, 1965-1974.
39. A. Abarrategi *et al*., Multiwall carbon nanotube scaffolds for tissue engineering purposes. *Biomaterials,* **2008**, 29, 94-102.
40. S.-M. Kwon *et al*., Multiwalled carbon nanotube cryogels with aligned and non-aligned porous structures. *Polymer*. **2009**, 50, 2786–2792.

6. Carbon nanotubes-based substrates for bone tissue engineering

An ideal scaffold for bone tissue regeneration should be able to promote osteoblasts proliferation and migration and should have mechanical properties similar to those of bone. Moreover it should have a porous structure with interconnected pores and controlled size in order to allow an excellent osteointegration[1,2]. During the last decades bioactive polymers have been developed for use as bone composite scaffolds[3-5]. They are particularly amenable for implantation and can be easily manufactured into desired shapes. They demonstrate excellent biocompatibility and suitable mechanical properties, and they can be loaded with growth factors involved in bone formation. In the bargain natural polymers show the advantage of being very similar to the natural macromolecular environment of cells. This aspect introduces the interesting capability of designing biomaterials with a true molecular biological functionality, rather than a mere morphological similarity. Among the natural polymers, polysaccharides turn out to be versatile, enabling to be decorated with signal molecules (oligosaccharides, peptides) and to interact with inorganic components[6-8]. Alginate is the name of a family of linear copolymers (produced by brown algae and bacteria), that has widely been used in biotechnological and industrial applications for its gel forming properties and behavior[9,10]. Alginic acid is a linear copolymer with homopolymeric blocks of (1-4)-linked β-D-mannuronate (M) and its C-5 epimer α-L-guluronate (G) residues, respectively, covalently linked together in

different sequences or blocks. The monomers can appear in homopolymeric blocks of consecutive G-residues (G-blocks), consecutive M-residues (M-blocks) or alternating M and G-residues (MG-blocks).The model proposed to describe the gelation process of alginate is indicated as “egg-box” and describes junctions as composed by two opposing G-blocks which form a cavity that can accommodate divalent cations such as Ca^{2+} and Ba^{2+} (Figure 1).

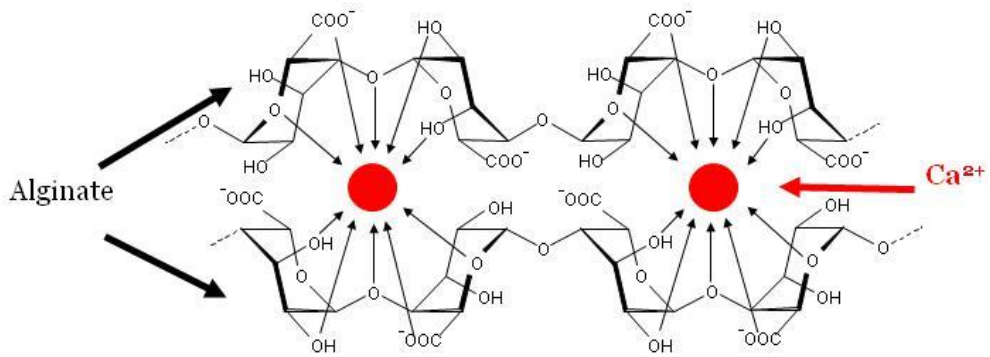

Figure 1. “Egg-box” model of gelation process of alginate.

Alginate-based scaffolds have shown marked resemblance with the porous structure of bone inducing positive effects on bone cell proliferation. Moreover, while calcium cross-linked gels make use of a simple chemistry and can be introduced into the body in a minimally invasive surgery, they are generally associated over longer time intervals with poor shape definition and volume instability in vivo. Possible limitations of the polymers currently used for bone regeneration include lack of bioactivity and poor mechanical properties. The use of CNSs in combination with biopolymers could implement scaffold properties by modulating mechanical strength and osteoinductivity[11-14].

6.1 Functionalized CNTs-based alginate hydrogels and scaffolds

In order to develop the project focusing our attention on the evaluation of the interactions between carbon nanomaterials and alginate, we decided to test multi-walled carbon nanotubes functionalized through different reactions (f-CNTs):

- diazonium salt-based arylation reaction (Scheme 1)
- 1,3-dipolar cycloaddition of azomethin ylides reaction (Scheme 2)
- Oxidative reaction (Scheme 3)

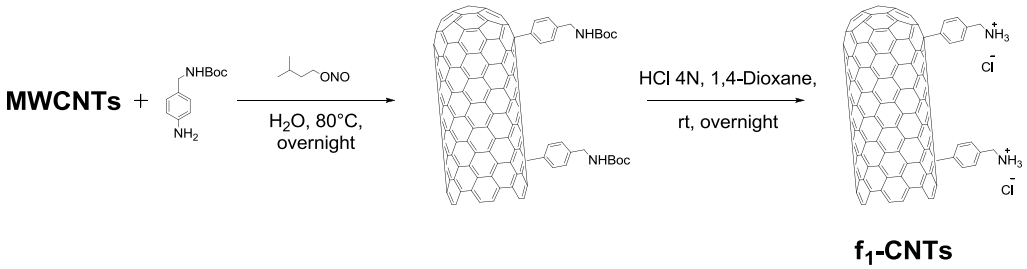

Scheme 1. Diazonium salt-based arylation reaction.

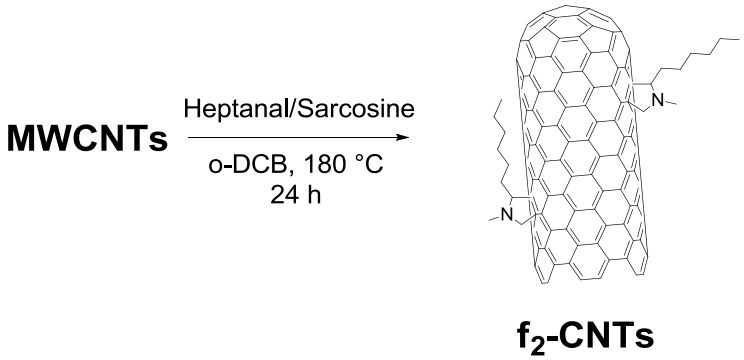

Scheme 2. 1,3-dipolar cycloaddition of azomethin ylides reaction.

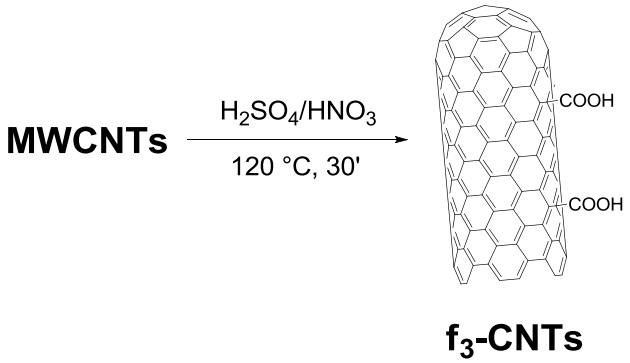

Scheme 3. Oxidative reaction.

On the other hand, we decide also to test CNTs of different length:

- "Long" CNTs 20-30 nm diameter, 10-30 µm length
- "Short" CNTs 20-30 nm diameter, 0,5-2 µm length

All of the modified MWCNTs have been characterized by thermo gravimetric analysis (TGA), transmission electron microscopy (TEM) and Kaiser test (to detect the positively charged moieties) in order to obtain a value of

functionalization. By this way we obtained neutral modified CNTs and positively/negatively charged. Functionalized CNTs turn out to be much more soluble than pristine material and consequently the toxicity decreases[15-19].

Homogeneous saturated calcium gels were prepared by blending the alginate solution (final concentration 2% w/v, with or without f-CNTs) with an inactivated form of Ca^{2+} ($CaCO_3$, 30mM) followed by the addition of the slowly hydrolyzing D glucono-δ-lactone (GDL, 60mM). A f-CNTs acqueous solution has been sonicated for 30 minutes and then added to a solution of sodium alginate and $CaCo_3$. The mixture has been stirred to achieve an homogenous solution and after that it has been degassed under vacuum to avoid the formation of bubbles during the gelation process before the addition of GDL. The Ca-polymer gelling solutions were cured in a Petri dish for 24 h to get cylindrically shaped hydrogels. We obtained nanostructured gel with a 0.1% or 1% w/v final concentration of functionalized CNTs (Figure 2 A,B).

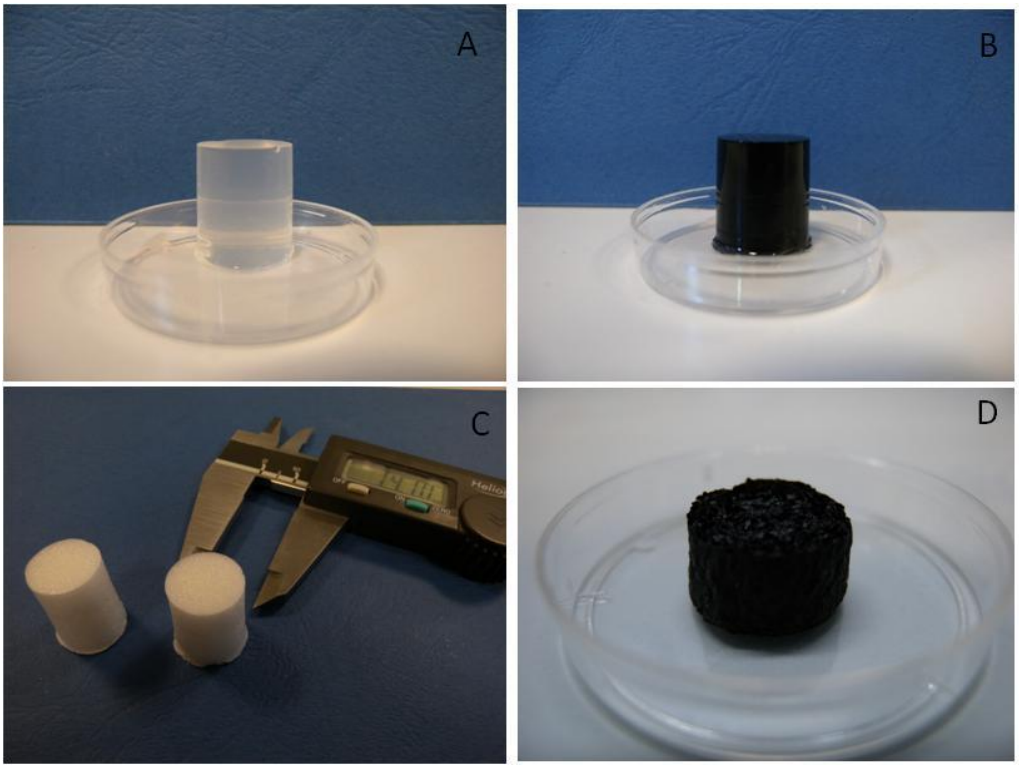

Figure 2. Pictures of alginate (A) and f-CNTs-based alginate (B) hydrogels, alginate (C) and f-CNTs-based alginate (D) scaffolds.

After the gelation period we obtained gels with a good dispersion of f-CNTs with the exception of heptanale/sarcosine CNTs. Indeed the absence of charge prevents the formation of a stable suspension resulting in the formation of aggregates in the gel matrix. In order to perform citotoxicity experiments, CNTs/alginate gels have been lyophilized (Figure 2 C,D). Hydrogels in the tissue-culture plate have been step-wise cooled by immersion in a liquid cryostat. After the freezing process the samples have been freeze-dried for 24 h obtaining porous scaffolds. Mechanical and

biological characterizations have been carried out in collaboration with Prof. S. Paoletti's group and Prof. M. Grassi's group.

6.2 Compression tests on f-CNTs/alginate hydrogels

In order to analyze the influence of f-CNTs in the gel matrix, mechanical properties of the hydrogels (elasticity and strength) have been investigated by the determination of the Ultimate Compression Strength σ_{UCS} (Fig.1) and the Compression Modulus E (Fig.2). We performed compression tests on the cylindrically shaped hydrogels (Figure 3). Compression tests have been performed on 6 repetitions at least per sample.

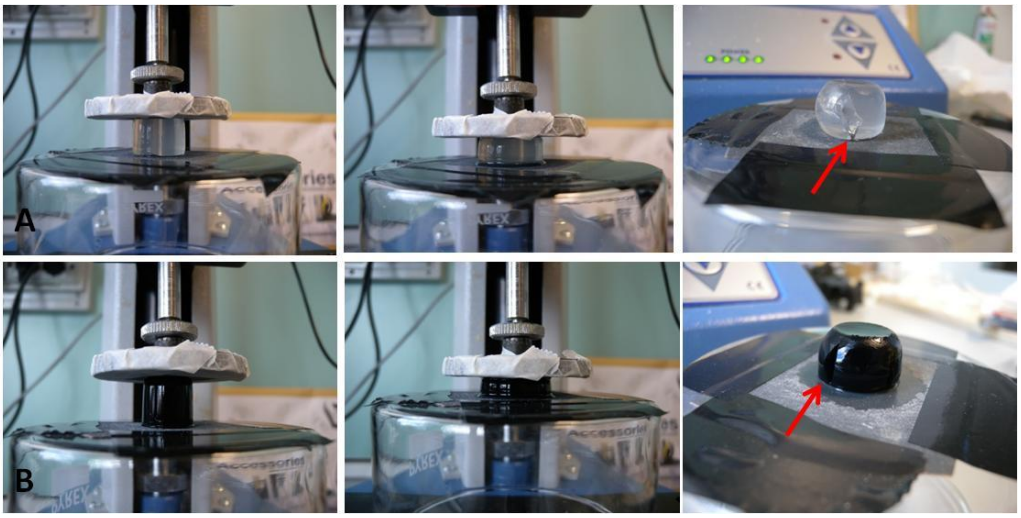

Figure 3. Series of pictures representing the sequence of compression for alginate hydrogel (line A) and f-CNTs-based hydrogel (line B) up to the collapse of the structures (red arrows).

In the following graphs we summarized all the results obtained from the mechanical tests. We proceeded by this way: first of all we decided to evaluated the interaction of 0.1% w/v long and short f-CNTs (Table 1). After

the preliminary results we decided to focus our study on short f-CNTs due to their larger employment in the field of nanocomposite biomaterials and to their lower toxicity[20-22]. On the other hand it is possible to observe from the table that the values of ultimate compression strength decrease for long f-CNTs whereas the compression modulus remains almost constant.

	Alginate	Long f-CNTs 0.1% w/v			Short f-CNTs 0.1% w/v		
		f_1-CNTs	f_2-CNTs	f_3-CNTs	f_1-CNTs	f_2-CNTs	f_3-CNTs
Compression Modulus (kPa)	34.99	31.2	28.67	24.92	28.69	24.19	29.27
Ultimate Compression Strength (kPa)	444.64	153.29	198.08	145.36	240.31	189.23	171.28

Table 1. Compression modulus and ultimate compression strength values of long and short f-CNTs.

For these reasons we produced new gels with positively and negatively charged f-CNTs, tenfold increasing their amount. We decided to abandon the study on neutral nanotubes due to their bad capability to form stable suspensions in water. At the same time cytotoxicity tests have been performed (as described hereunder) on f-CNTs/alginate scaffolds. During the rehydration step, it has been observed the release of fragments from the oxidized f-CNTs/alginate scaffold in terms of a changed color of the culture medium. We concluded that the strong oxidative reaction affects the structure of nanotubes producing small fragments easily released from the polymeric matrix. We decided to use a mild oxidative reaction (Scheme 4) in order to achieve carboxylic groups on the surface of the tubes avoiding any

damage to the structure[23,24]. Changing the conditions of the oxidative reaction, from TGA analysis we decreased the weight loss at 600 °C from 9% for f_3-CNTs to 1% for f_4-CNTs (Figure 4).

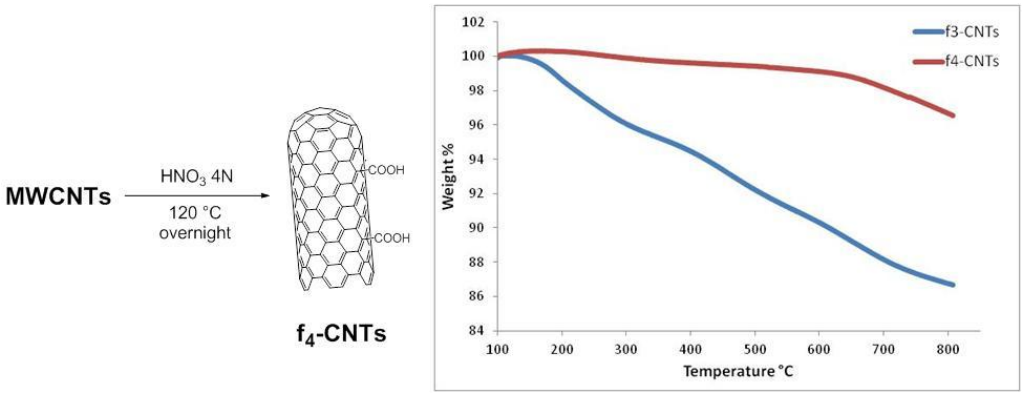

Scheme 4. Oxidative reaction on CNTs to achieve carboxylic groups on the surface avoiding damages to the carbon structure (left). Figure 4. TGA graph of f_3 and f_4-CNTs.

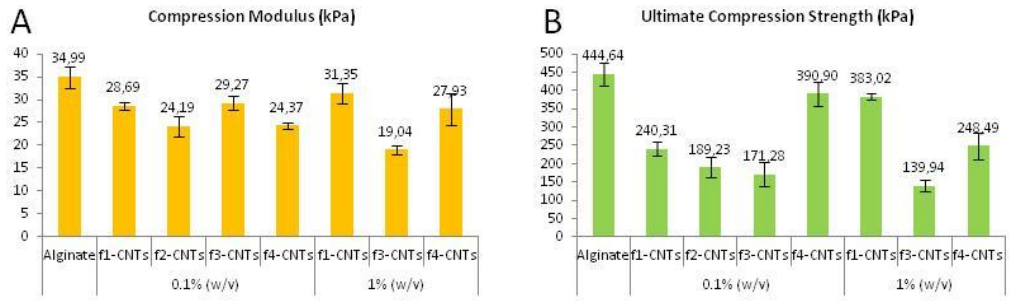

Figure 5. Compression modulus (A) and Ultimate compression strength (B) data of short f-CNTs-based hydrogels (0.1 and 1% w/v content of CNTs).

Compression tests show that mechanical properties are influenced by the concentration, the type of functionalization and the dimension of CNTs. In general a reduction of the mechanical properties is observed in presence of f-CNTs. Gels containing short positively charged f_1-CNTs (1% w/v) show a value of the compression modulus very closed to the blank alginate gel and the highest value of σ_{UCS} has been found among the hydrogels containing CNTs with other functionalization. It has been very interesting to observe the high value of σ_{UCS} of f_4-CNTs 0.1% gels very closed to the f_1-CNTs 1% one. On the other hand it is possible to observe the opposite behavior for short negatively charged f_3-CNTs: increasing the amount of nanotubes the compression modulus decreases. That is probably due to the competition between the carboxylic groups on the CNTs and the alginate for the Ca^{2+} ions resulting in a weak tridimensional structure. That behavior is not observed in the case of CNTs functionalized through the mild oxidative reaction. In fact compression tests performed on f_4-CNTs/alginate gels show better mechanical properties both in terms of compression modulus that compression strength at break

than the strongly oxidized f_3-CNTs/alginate gels. The mild oxidation in fact produces less carboxylic groups on the surface of nanotubes and the competition with alginate for the cations turns out to be lower. In any case the best result obtained in terms of both compression modulus and ultimate compression strength is attributed to the f_1-CNTs 1%-based alginate hydrogels.

6.3 Rheological measurements on f-CNTs/alginate hydrogels

Rheological characterization has been performed on alginate and f-CNTs hydrogels and on the alginate f-CNTs solutions. Negatively charged CNTs obtained by the mild oxidative reaction have been employed consequently the better results of compression tests. For each hydrogel the linear viscoelastic range has been determined through a stress sweep test and the mechanical spectrum through a frequency sweep test. From the mechanical spectrum it is possible to determine the shear modulus G that express the elastic and viscous components of the hydrogels. The shear modulus is theoretically related to the compression modulus by the correlation $E = 3G$.

In order to perform rheological measurements on hydrogels, it has been necessary to produce them with the proper shape. To obtain hydrogel discs, the solutions of alginate, CNTs, $CaCO_3$ and GDL have been poured into a petri dish. After 24 hours (gelation period) the probing of the hydrogels has been done in order to obtain the disc to be tested by the rheometer (Figure 6).

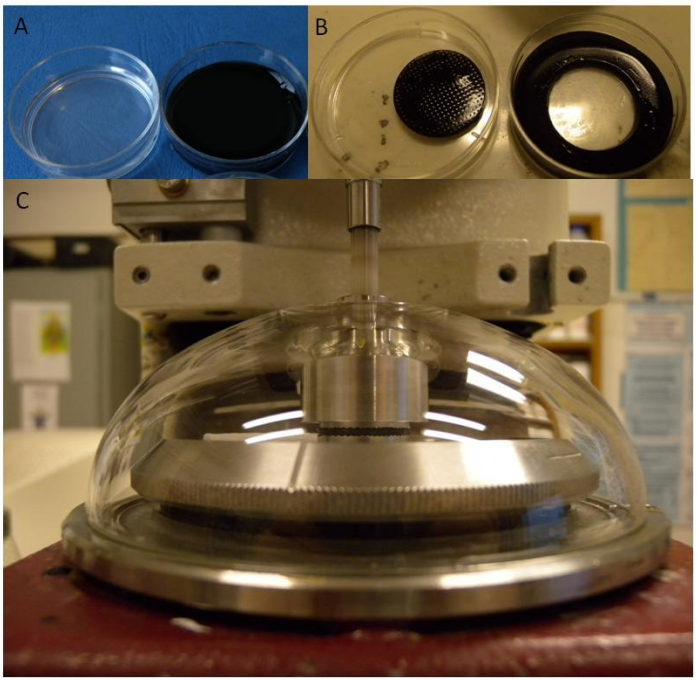

Figure 6. Preparation of the hydrogel discs for the rheological test (A,B) and the rheological test apparatus during the experiments.

The presence of f-CNTs in the alginate matrix increases the elastic properties in particular for 1% w/v f-CNTs both positively and negatively charged (Figure 7). Nevertheless the mechanical spectroscopy shows differences in the elastic behavior of the hydrogels not linked to the results obtained through the compression test. In some cases the correlation E = 3G is not maintained. This behavior could depend on the degree of strains applied on the material. During the rheometry measurements the material is less stressed than the compression tests. During the compression experiments it is possible to observe the release of water entrapped in the polymeric matrix. In order to

investigate the proton nucleus of the water within the polymeric structure in presence of f-CNTs, Low Field NMR relaxometry studies have been performed both on hydrogels and solutions.

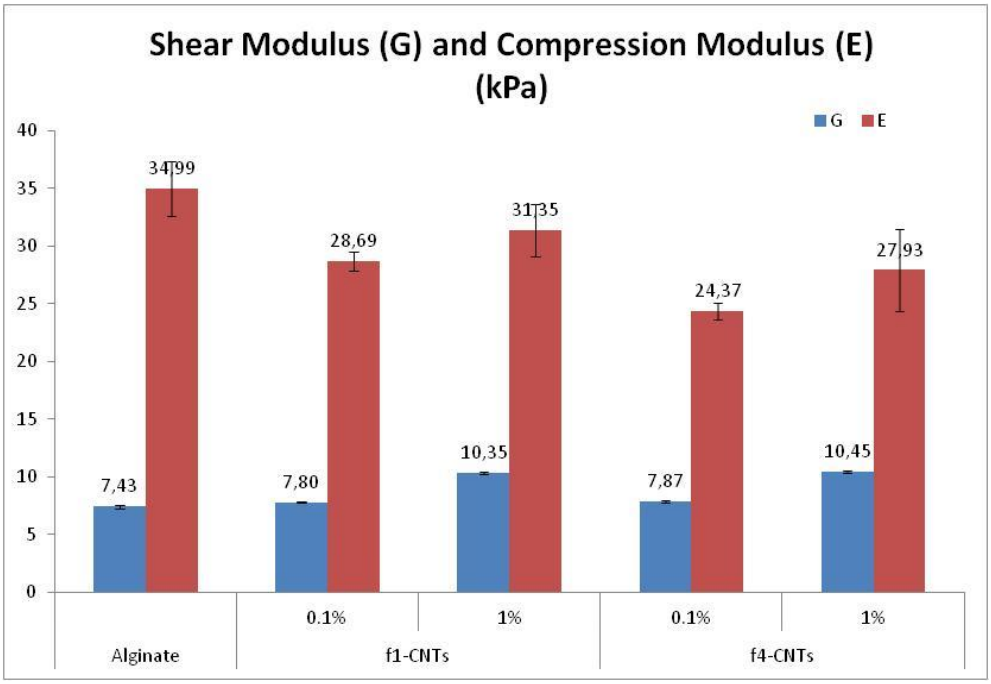

Figure 7. Comparison of Shear modulus and Compression modulus obtained from compression and rheological tests on f_1-CNTs/Alginate and f_4-CNTs/Alginate hydrogels.

After the preliminary analysis an additional type of functionalization has been introduced. We decided to employ CNTs functionalized through the 1,3-dipolar cycloaddition of azomethin ylides reaction (aminoacid/paraformaldehyde; Scheme 5).

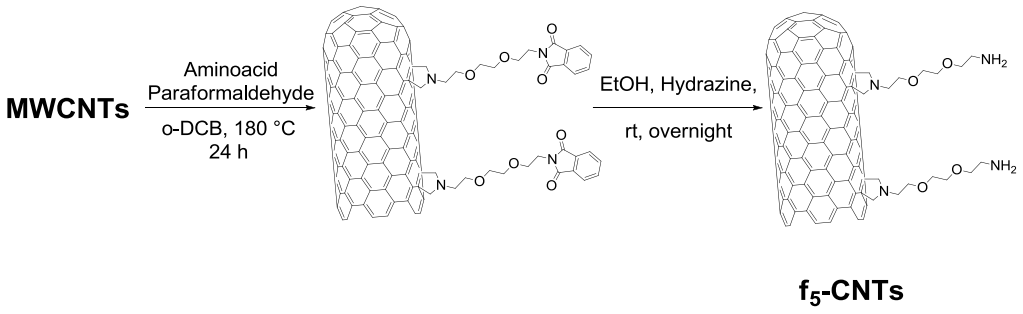

Scheme 5. 1,3-dipolar cycloaddition of azomethin ylides reaction (aminoacid/paraformaldehyde).

The second type of positively charged CNTs has been analyzed in order to evaluate the interaction of a different moiety of functionalization with polymeric chains both in terms of hydrogel and solution. One of the most important aspect of the CNTs functionalized through the 1,3-dypolar cycloaddition is the good dispersibility in water[25-27]. From rheological measurements it has been possible to appreciate the high value of shear modulus for hydrogels containing f_5-CNTs 0.1% comparable to 1% CNTs-based hydrogels.

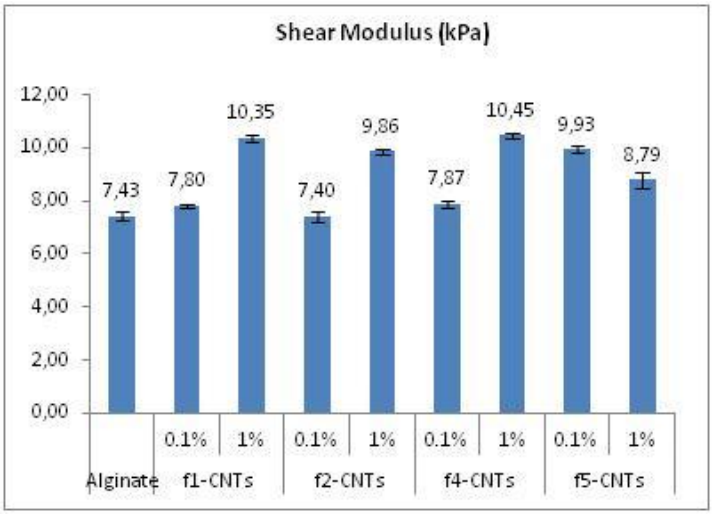

Figure 8. Summarizing graph of the shear modulus values obtained for the f-CNTs under investigation.

In the summarizing graph also the shear modulus of f_2-CNTs has been reported (Figure 8). During the first phase of our study about compression tests, neutrally charged CNTs have been discarded due to their low capability to remain suspended and form stable dispersions in water. Through the rheological studies and low field NMR relaxometry, it has been interesting to understand the behavior of f_2-CNTs during the aggregation process.

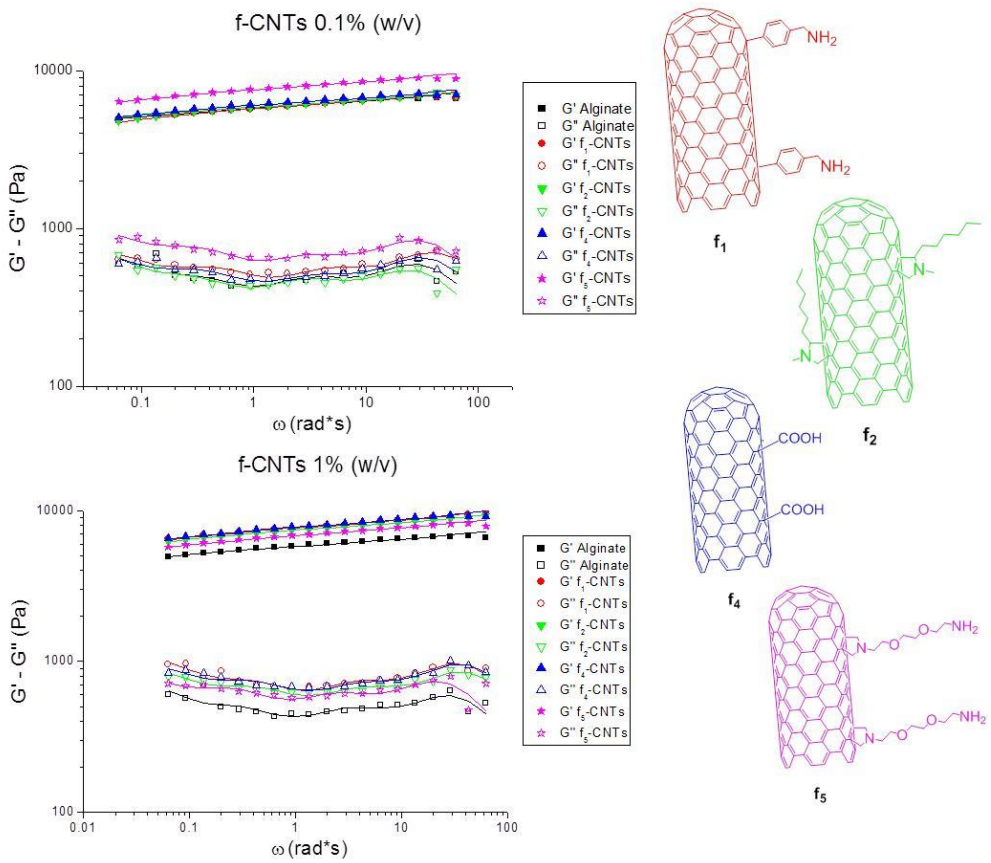

Figure 9. Frequency sweep graphs for hydrogels containing both 0.1% and 1% w/v f-CNTs.

From the frequency sweep graphs it is possible to appreciate the increased values of G' and G'' for hydrogel discs containing CNTs with different functionalizations (Figure 9). As we mentioned before, for all materials with the presence of CNTs 1% w/v the elastic properties are strengthened.

6.4 Rheological Measurements on f-CNTs/alginate solutions

During the development of this study it has been appropriate to assess the interaction between nanotubes and alginate chains in terms of viscosity. The viscosity of f-CNTs/alginate solutions has been obtained through the flow curves varying the shear stress. The solution have been prepared following the procedure for hydrogel. Alginate aqueous solution has been added to CNTs suspension in milli-Q water previously sonicated for 30 minutes to finally achieve the concentration of Alg 2% w/v f-CNTs 0.1 or 1% w/v. As we mentioned before, we were to analyze the behavior of neutrally charged f_2-CNTs. It has not been possible to evaluate the viscosity of the solution due to the presence of aggregates between the two plates of the rheometer and the viscosity has not been recorded. The analysis of the solution of alginate in presence of f-CNTs reveals that the 0.1% w/v concentration of f-CNTs does not significantly affect the rheological properties compared to the alginate solution alone (Figure 10). Whereas in the case of carbon nanotubes at concentration of 1% w/v we can observe differences in the viscosity at low shear rates.

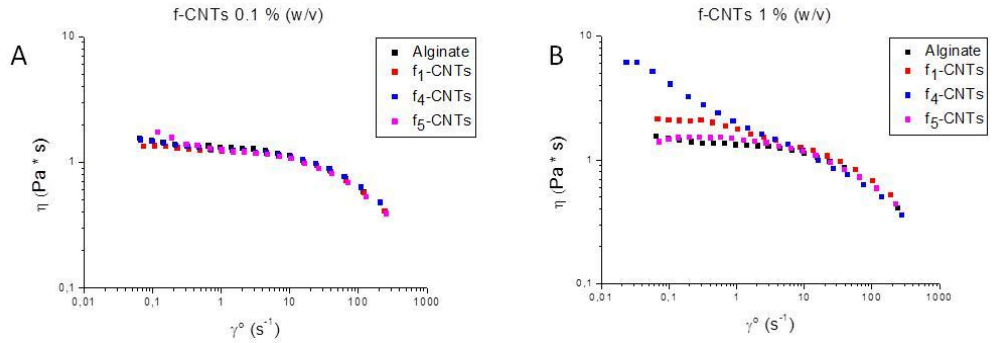

Figure 10. Flow curves varying the shear stress of 0.1% w/v f-CNTs/alginate solutions (A) and 1% w/v f-CNTs/alginate solutions (B).

The viscosity of the solutions increases in the case of positively charged f_1-CNTs and negatively charged f_4-CNTs. This behavior could be explained through the interaction of positively moieties with the acidic groups of alginate resulting into a ionic interaction. The lower amount of positively moieties on f_5-CNTs obtained through the 1-3-dypolarcycloaddition reaction prevents the interaction with carboxylic groups of alginate seen for CNTs functionalized through the diazonium salt-based arylation reaction (data obtained from TGA and Kaiser Test). On the other hand the strong effect of oxidized f_4-CNTs could be explained through the release of protons from the high amount of carboxylic groups on the carbon surface. In presence of free protons the alginate is able to turn into alginic acid starting a gelation process[28,29].

6.5 Low Field NMR Relaxometry of f-CNTs/alginate hydrogels

In parallel to the rheological experiments, studies of T_2 relaxometry (low field NMR) have been carried out in order to obtain information about the interactions between CNTs and water and between CNT and alginate chains (Figure 11). It has been demonstrated that CNTs functionalized with different types of moieties give shifted picks during NMR studies. That is probably due to the organization of solvent molecules around the carbon nanotubes sidewall[30,31]. Based on these requirements, low field NMR relaxometry is a suitable technique to investigate the behavior of f-CNTs in relation to the solvent molecules and the polymeric chains.

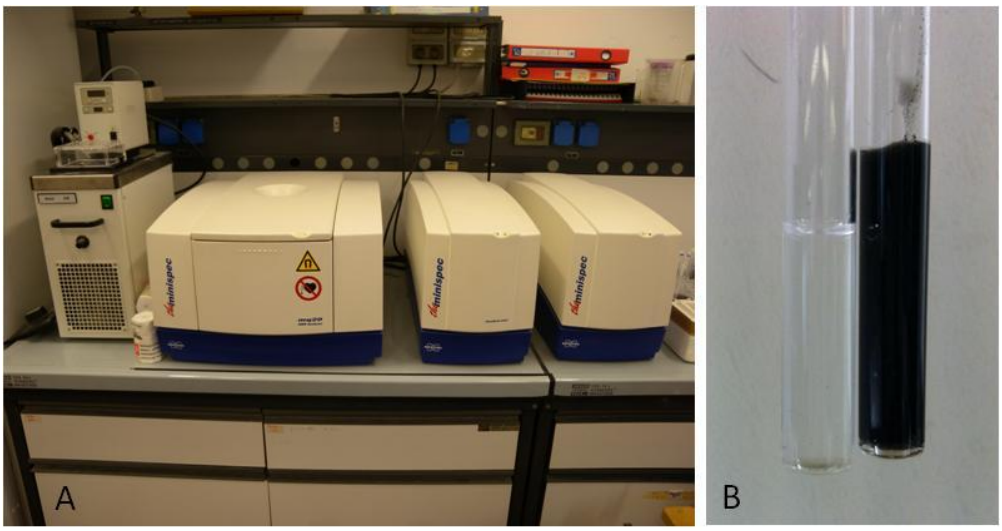

Figure 11. Low field NMR apparatus (A). Alginate and f-CNTs-based alginate hydrogels into the NMR tubes.

Water relaxometry measurements revealed a very interesting variation of the T_2 values depending on the concentration and on the functionalization of CNTs. That behavior suggests that the f-CNTs are able to interact in a specific way with water and could be differently entrapped in the polymer matrix. First of all f-CNTs/alginate hydrogels have been tested in order to evaluate the degree of dispersion of the nanostructures into the polymeric matrix. The presence of f-CNTs 0.1% decreases drastically the relaxation time of water molecules into the matrix. Increasing ten-fold the amount of CNTs, the average relaxation time T_2 (ms) remains almost constant for f_1 and f_2-CNTs whereas it decreases in the case of f_4 and f_5.

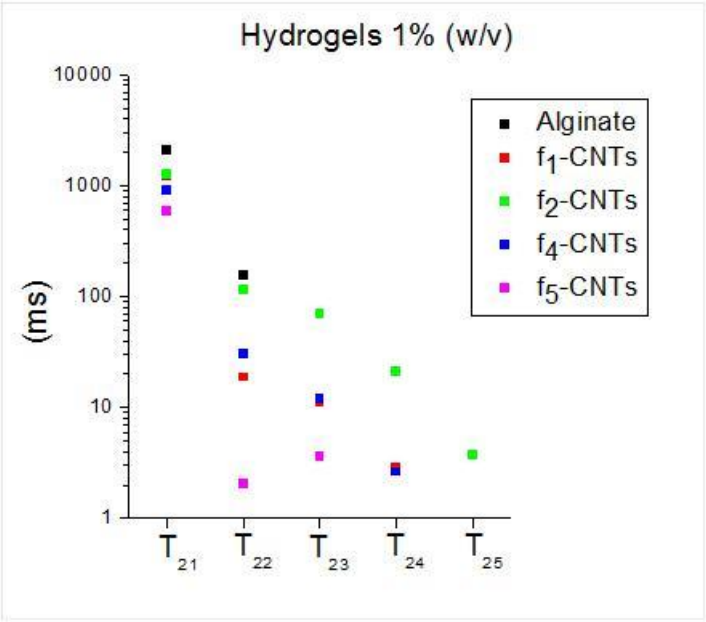

Figure 12. Graphical representation of T_{2x} values for hydrogels containing f-CNTs 1% w/v acquisitions.

The presence of different T_{2x} in comparison to the blank alginate hydrogel indicates a complex organization of water molecules due to the interaction of f-CNTs within the surrounding environment (Figure 12). That effect is particularly evident for f_2-CNTs: the aggregation of nanotubes, confirmed by rheological measurements, produces another species into the polymeric matrix indicating a further value of T_{2x}. The aspect under investigation is also confirmed by the higher values of T_{2x} than f_1, f_4 and f_5-CNTs-based alginate hydrogels. That behavior turns out to be much more evident during the relaxometry tests carried out on f-CNTs/alginate solutions.

6.6 Low Field NMR Relaxometry of f-CNTs/alginate solutions

We decided to evaluate the stability of f-CNTs suspensions both in water and in alginate solution (data not shown). F_1 and f_2-CNTs have been selected to perform the stability studies through the low field NMR technique at the concentrations of 0.01% and 0.1%. Both f_1 and f_2-CNTs in alginate solution showed a stability up to 4 days in terms of constant values of T_2. After 4 days the T2*x* values started increasing. However alginate solutions containing 0.1% of f-CNTs turned out to be more stable than the solution with the lowest amount of carbon nanotubes. Stability studies of f-CNTs suspended in milli-Q water showed a completely different behavior. Indeed f_1-CNTs demonstrated a stability in the course of the time whereas f2-CNTs started aggregating after 40 minutes reaching the T_2 value of the free water.

6.7 *In vitro* evaluation of cytotoxicity and viability

Cytotoxicity and viability have been evaluated for osteosarcoma (MG63) and fibroblast (NIH/3T3) cell lines in 2 different experiments:

1. Directly in contact with scaffolds
2. In presence of different concentration of f-CNTs previously dispersed in water and added to the medium culture.

Cytotoxicity has been evaluated through the lactate dehydrogenase cytotoxicity assay (LDH assay) and the Live/Dead assay, whereas the cell viability has been evaluated through a "modified" LDH assay[32].

The preliminary LDH studies have been carried out on MG63 cells incubated with small fragments of scaffolds (0.1% or 1% w/v f_1-CNTs and f_4-CNTs) for 24 and 72 hours. The results show high variability in the cytotoxicity which doesn't seem related to the f-CNTs concentration inside the polymeric matrix. On the other hand the values are contrasting the observation of the cells at the fluorescence microscopy. These results are probably due to the interference of CNTs with the assay[20]. The cells viability and the cytotoxicity have been also evaluated through the Live/Dead assay in presence of the scaffold fragments. The assay revealed a certain toxicity of the scaffolds with high variability of the results. The high variability is probably due to the direct contact between cells and the scaffolds that could scratch the cells from the wells interfering with their growth. For this reason we need a different test where CNTs-based substrates don't interfere with the tests. Cell proliferation

studies will be carried out incorporating the tritiated timidine in the cells in order to evaluate their proliferation inside the hydrogels and the scaffolds.

The modified LDH assay proposed by Ali-Boucetta *et al.*[32] turns out to be a reliable method to evaluate the viability of the cells in presence of f-CNTs. We evaluated the viability of cells seeded in presence of with different concentrations of f-CNTs in order to avoid the interference noticed in the previous described essays. Briefly, the media have been removed, the cells have been lysed and the cell lysate has been centrifuged in order to precipitate the f-CNTs. The LDH modified assay has been performed on the supernatant. Data show that f-CNTs are non-toxic for these kind of cells at the tested concentrations (Figure 13). After 24 hours the viability of cells seeded in presence of f-CNTs is comparable to the control and after 72 hours the viability of cells seems to be increased in presence of CNTs but further experiments are necessary to confirm the data.

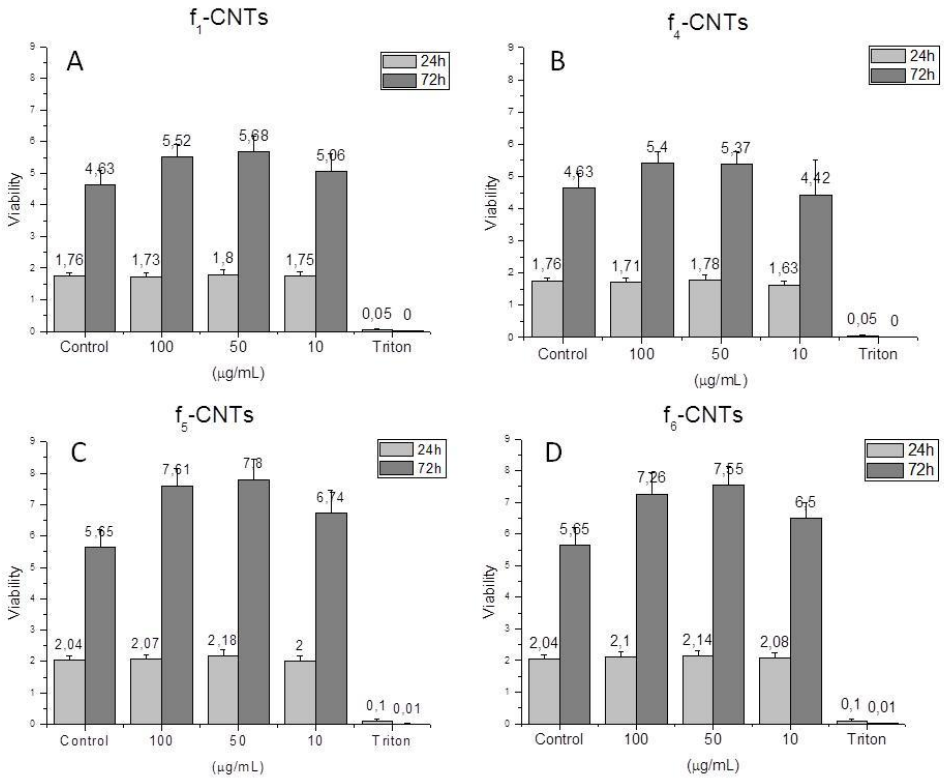

Figure 13. Viability of MG63 cells evaluated through the modified LDH assay.

During the viability tests a new type of functionalization has been introduced in the prospect of developing scaffolds containing hydroxyapatite (Scheme 6).

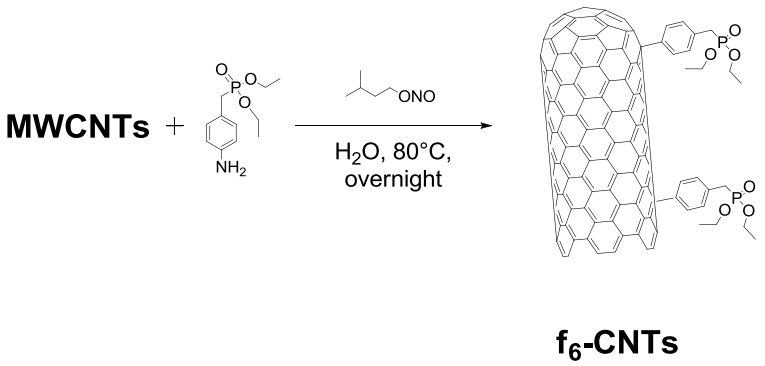

Scheme 6. Diazonium salt-based arylation reaction employed to functionalize CNTs with sulfonate group.

As mentioned in the introduction chapter, bone healing and repair are limited in the treatment of some medical pathologies such as osteoporosis, osteogenesis imperfecta or tumor resection. For these reasons could be appropriate the development of a 3D scaffold able to promote the tissue regeneragion and at the same time able to facilitate the nucleation and growth of hydroxyapatite (HAp), which is the major component of natural bone tissues[33]. It has been demonstrated that functionalization of carbon nanotubes with carboxylic groups or phosphonate groups could promote the HAp mineralization on their surface[34-37]. CNTs has been reacted with diethyl (4-aminobenzyl) phosphonate following the diazonium salt-based arylation reaction. Before testing the scaffolds filled with f_6-CNTs to evaluate the

mechanical properties, it has been useful to evaluate the cellular viability. Viability tests developed on MG63 cells has been evaluated through the modified LDH assay. Also in this case the presence of CNTs suspended in the medium culture has not shown toxicity for the cells.

6.8 Conclusions and future prospective

During this work we studied the interaction of different types of functionalized MWNTs with alginate in the form of hydrogels. Water T_2-relaxometry has been employed as an innovative technique to understand the interactions between f-CNTs and the polymer matrix. It has been possible to obtain precious information about the water molecules organization around the CNTs sidewall and the polymeric chains. On the other hand, through the low field NMR technique it has been possible to evaluate the presence of different type of water, CNTs and polymeric organization into the entirety of the hydrogel entities. This technique has been also useful to evaluate the dispersion capability of the carbon nanotubes into the polymeric structure. The different organization of CNTs into the alginate chains network could be the explanation for the non-linear trend of compression and rheological tests. As we mentioned before, the correlation between the shear (G) and the compression (E) moduli should be E=3G. Concerning hydrogels alg 2% CNTs 1%, the presence of carbon nanotubes the compression modulus is lower than the alginate blank hydrogel whereas the shear modulus is higher for 1% CNTs and comparable for 0.1% CNTs-based alginate hydrogels. That could be due to

the different entities of the applied stress. It is possible that the water organization around the carbon nanotubes could affect the behavior of the systems under compression stress in terms of different water molecules delivery during the compression and consequently different ultimate compression strength.

Cytotoxicity tests confirmed the interference of CNTs on the colorimetric assays used to evaluate influence of f-CNTs in the cell viability. The modified LDH assay demonstrated to be a reliable method to evaluate the viability of the cells in presence of f-CNTs. Tests carried out on f-CNTs showed a lack of cytotoxicity of functionalized carbon nanotubes for osteosarcoma (MG63) and fibroblast (NIH/3T3) cell lines. Cell proliferation studies will be carried out in the next future of the project also on 3D hydrogels and scaffolds through the incorporation of tritiated timidine. Indeed the future studies will be focused on scaffold mechanical and biological aspects. We will undertake the study of hydroxyapatite nucleation in presence of functionalized CNTs on 2D substrated: glass coverslips covered by a layer of nanotubes through the spray coating technique and dipped into phosphate buffer solutions. After the initial step, the mechanical properties of the freeze-dried hydrogels will be

evaluated in terms of compression modulus and ultimate compression strength.

References

1. N.J. Castro *et al*., Recent progress in interfacial tissue engineering approaches for osteochondral defects. *Ann. of Biomed. Eng*. **2012**, 40, 1628-40.
2. E.L. Fong *et al*., Building bridges: leveraging interdisciplinary collaborations in the development of biomaterials to meet clinical needs *Adv. Mater*. **2012**, 24, 4995-5013.
3. J.A. Sanz-Herrera *et al*., On scaffold designing for bone regeneration: a computational multiscale approach. *Acta Biomater*. **2009**, 5, 219-229.
4. D. Puppi *et al*., Polymeric materials for bone and cartilage repair. *Prog. in Polym. Sci*. **2010**, 35, 403-440.
5. R. Dimitriou *et al*., Bone regeneration: current concepts and future directions. *BMC Medicine*, **2011**, 9, 66.
6. R.E. McMahon *et al.,* Development of nanomaterials for bone repair and regeneration. *J. Biomed. Mater. Res. Part B*, **2013**, 101 B, 387-397.
7. M.M. Stevens. Biomaterials for bone tissue engineering. *MaterialsToday*, **2008**,11, 18-25.
8. E. Tejeda-Montes *et al*., Bioactive membranes for bone regeneration applications: Effect of physical and biomolecular signals on mesenchymal stem cell behavior. *Acta Biomater*. **2014**, 10, 134-141.
9. G. Turco et al., Alginate/hydroxyapatite biocomposite for bone ingrowth: a trabecular structure with high and isotropic connectivity. *Biomacromolecules* **2009,** *10,* 1575-1583.

10. K.Y. Lee & D.J. Mooney. Alginate: properties and biomedical applications. *Prog. Polym. Sci*. **2012**, 37, 106-126.
11. K. Sahithi *et al*., Polymeric composites containing carbon nanotubes for bone tissue engineering. *Int. J. Biol. Macromol*. **2010**, 46, 281-283.
12. J. Venkatesan *et al*., Preparation and characterization of chitosan-carbon nanotube scaffolds for bon tissue engineering. *Int. J. Biol. Macromol*. **2012**, 50, 392-402.
13. E.D. Yildrim *et al*., Fabrication, characterization, and biocompatibility of single-walled carbon nanotube-reinforced alginate composite scaffolds manufactured using freeform fabrication technique. *J. Biomed. Mater. Res., Part B*. **2008**, 87, 406-414.
14. R.M. Mendes *et al*., Effects of single-walled carbon nanotubes and its functionalization with sodium hyaluronate on bone repair. *Life Sci*. **2010**, 87, 215-222.
15. H. Ali-Boucetta *et al*., Asbestos-like Pathogenicity of Long Carbon Nanotubes Alleviated by Chemical Functionalization Angew. Chem., **2013**, 52, 1-6.
16. H. Dumortier *et al*., Functionalized Carbon Nanotubes Are Non-Cytotoxic and Preserve the Functionality of Primary Immune Cells. *Nano Lett*. **2006**, 6, 1522-1528.
17. K. Yang & Z. Liu. In Vivo Biodistribution, Pharmacokinetics, and Toxicology of Carbon Nanotubes. *Current Drug Metabolism*, **2012**, 13.
18. K. Kostarelos *et al*., Promises, facts and challenges for carbon nanotubes in imaging and therapeutics. *Nat. Nanotech*. **2009**, 4, 627-633.

19. L. Lacerada *et al*., Tissue histology and physiology following intravenous administration of different types of functionalized multiwalled carbon nanotubes. *Nanomedicine*, **2008**, 3, 149-161.
20. G. Wang *et al*., Understanding and correcting for carbon nanotube interferences with a commercial LDH cytotoxicity assay. *Toxicology* **2012**, *299*, 99-111
21. S.Y. Madani *et al*., A concise review of carbon nanotube's toxicology. *Nano Rev*. **2013**,4.
22. D. Liu *et al*., Different cellular response mechanisms contribute to the length-dependent cytotoxicity of multi-walled carbon nanotubes. *Nanoscale Res. Lett*. **2012**, 7, 361-370.
23. J. Zhang *et al*., Effect of Chemical Oxidation on the Structure of Single-Walled Carbon Nanotubes. *J. Phys. Chem. B* **2003,** 107, 3712-3718.
24. Z. Wang *et al*., The surface acidity of acid oxidised multi-walled carbon nanotubes and the influence of in-situ generated fulvic acids on their stability in aqueous dispersions. *Carbon*, **2009**, 47, 73-79.
25. V. Georgakilas *et al*., Amino acid functionalisation of water soluble carbon nanotubes. *Chem. Comm*. **2002**, 3050–3051.
26. A. Bianco *et al*., Biomedical applications of functionalised carbon nanotubes. *Chem. Comm*. **2005**, 571–577.
27. A. Bianco et al., Making carbon nanotubes biocompatible and biodegradable. *Chem. Comm.* **2011**, 47.
28. K.I. Draget *et al*., Alginic acid gels: the effect of alginate chemical composition and molecular weight. *Carbohydr. Polym*. **1994**, 25, 31-38.

29. K.I. Draget *et al*., Ionic and acid gel formation of epimerised alginates; the effect of AlgE4. *Int. J. Biol. Macromol*. **2000**, 27, 117-122.
30. J.H. Walther et al., Carbon nanotubes in water: structural characteristics and energetics. *J. Phys. Chem. B* **2001,** *105,* 9980-9987.
31. A.R.A. Dezfoli et al., Structural properties of water around uncharged and charged carbon nanotubes. Korean J. Chem. Eng. 2013, 30, 693-699.
32. H. Ali-Boucetta *et al*., Cellular uptake and cytotoxic impact of chemically functionalized and polymer-coated carbon nanotubes. *Small,* **2011**, 7 (22), 3230-8.
33. L.C. Palmer *et al*., Biomimetic systems for hydroxyapatite mineralization inspired by bone and enamel. *Chem. Rev*. **2008,** 108, 4754-4783.
34. C. Cazorla *et al*., Calcium-based functionalization of carbon nanostructures for peptide immobilization in aqueous media. *J. Mater. Chem.* **2012,** 22, (37), 19684-19693.
35. J.D. Kretlow & A.G. Mikos. Review: Mineralization of synthetic polymer scaffolds for bone tissue engineering. *Tissue Engineering* **2007,** 13, (5), 927-38.
36. K. Schöller et al., Biomimetic route to calcium phosphate coated polymeric nanoparticles: influence of different functional groups and pH. *Macromol. Chem. Phys.* **2011,** 212, (11), 1165-1175.
37. S. Liao *et al*., Self-assembly of nano-hydroxiapatite on multi-walled carbon nanotubes. *Acta Biomater*. **2007**, 3, 669-675.

Acknowledgements

I am grateful to my supervisor Prof. Maurizio Prato for giving the opportunity to do a PhD in his research group. A special thanks to Dott.ssa Susanna Bosi, my thesys co-supervisor. Thanks to Claudio Gamboz for TEM analysis and to Dott.ssa Francesca Vita for SEM analysis. I would like to thank also Prof. Ballerini's group, Prof. Paoletti and Prof. Grassi's groups: a special thanks to Dr. Ivan Donati, Dr. Massimiliano Borgogna, Dr. Andrea Travan, Davide Porreli and Michela Abrami.